Information Sciences in Imaging at Stanford

State of the Section

Daniel L. Rubin, MD, MS

My research program develops computational methods to *extract quantitative information from images* and integrate them with clinical and molecular data *to enable discovery* of image biomarkers of disease and decision support applications to *improve clinical effectiveness.*

ISIS LINKS

Home

Projects

Representative Publications

People

Secure Login

INFORMATION SCIENCES IN IMAGING

Our Mission

Our mission is to advance the clinical and basic sciences in radiology, while improving our understanding of biology and the manifestations of disease, by pioneering methods
in the information sciences that integrate imaging, clinical and molecular data.

Our Vision

Our vision is that we gain new knowledge from imaging examinations by integrating and analyzing them with related clinical and molecular data. ISIS aims to achieve this goal by exploring the full spectrum of information-intensive activities in imaging (e.g., image management, storage, retrieval, processing, analysis, understanding, visualization, navigation, interpretation, reporting, and communications) and in non-

ISIS NEWS

2011 ISIS Seminar Series:
The ISIS group hosts a monthly seminar series about a wide ranging field of topics.

Course Offerings:
Computational Methods for Biomedical Image Analysis and Interpretation (BMI 260)

Computational Methods for Biomedical Image Analysis and Interpretation: Lectures (BMI 261)

ISIS: Mission Statement

To advance the clinical and basic sciences in radiology, while improving our understanding of biology and disease by pioneering methods in the information sciences that integrate imaging with clinical, genomic and proteomic data.

ISIS Goals (1 of 2)

- To develop tools for:
  - Collecting, annotating and integrating imaging, clinical, and molecular data
  - Analyzing integrated databases

- To generate scientific discoveries linking molecular and imaging phenotypes

- To translate our findings into clinical care through decision support systems related to improving the value of images for personalized, less-invasive approaches to detection and treatment.

ISIS

Information Sciences in Imaging at Stanford

ISIS Goals (2 of 2)

To achieve these goals requires engagement in:

- the full spectrum of information-intensive activities in imaging (*e.g.,* image management, storage, retrieval, processing, analysis, understanding, visualization, navigation, interpretation, reporting, and communications), and

- non-imaging domains (e.g., pathology, genomic and proteomic markers, family history, prior medical reports, and clinical outcomes).

Core Faculty

Sandy Napel, PhD
Professor
Radiology
Co-Section Chief

Sylvia Plevritis, PhD
Professor
Radiology
Co-Section Chief

Curt Langlotz, MD PhD
Professor
Radiology, Assoc Chair for Information Technology

Daniel Rubin, MD
Assistant Professor
Radiology

ISIS **Information Sciences in Imaging at Stanford**

Beyond ISIS

David Paik, PhD
Scientific Director
Elucid Bioimaging

Information Sciences in Imaging at Stanford

Affiliated Faculty

Chris Beaulieu, M.D., Ph.D
Professor, Radiology, Chief of Musculoskeletal Imaging

Bao H. Do, MD
Clinical Assistant Professor (Affiliated) Radiology

Olivier Gevaert, PhD
Acting Assistant Professor, Medicine - Biomedical Informatics Research

Robert J. Herfkens, M.D.
Professor of Radiology, Associate Chair for Clinical Technology.

R. Brooke Jeffrey, M.D.
Professor, Radiology, Associate Chair for Academic Affairs

Nishita Kothary, MD
Associate Professor, Radiology

David Larson, MD
Associate Professor, Pediatric Radiology Associate Chair of Performance Improvement, Department of Radiology

Parag Mallick, M.D.
Assistant Professor, Radiology

Ann Leung, M.D.
Professor, Radiology, Diagnostic Radiology, Chief of Thoracic Imaging

Jafi Lipson, MD
Assistant Professor, Radiology

Killian M. Pohl, Ph.D.
Senior Scientist, SRI International

iSiS

Information Sciences in Imaging at Stanford

Administrative Staff

Danae Barnes
Program Manager, ISIS

Maggie Bos
Administrative
Assistant

Lauren Miller
Admin Assistant:
Daniel Rubin
Dept of Radiology

Elizabeth Colvin
Admin Assistant:
Sandy Napel,
3DQ Lab

Administrative Staff

AAd

Fuad Nijim
CCSB Program
Manager

Margaret Murphy
Student Services
Coordinator

ISIS Researchers

- 8 Scientific Staff

- 10 Postdoctoral fellows

- 8 Graduate students

- 1 Visiting scholar

- 1 Visiting Professor

ISIS Space
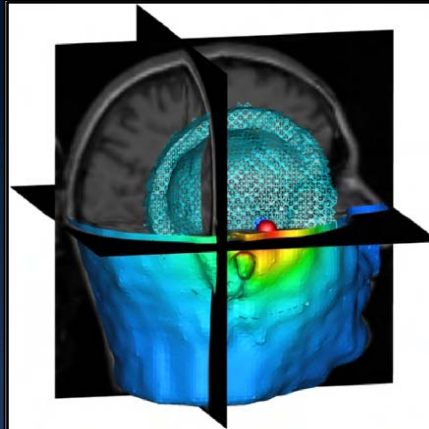
Lucas Center

Clark Center

+Porter Avenue

September 11th, 2014

Arrillaga Alumni Center, 326 Galvez

9am- 4pm

Please join us for the Annual ISIS Retreat

Keynote:

Chris Johnson, *Professor,*
University of Utah

"**Visualizing the Future of Biomedicine**"

Agenda:

- 9:00- 9:15   Introduction, welcome
- 9:15- 9:45   Affiliated Faculty intro
- 9:45-10:45   Keynote Speaker
- 10:45-11:00 Break
- 11:00-12:30   Electronic Poster Session
- 12:30-1:30   Lunch, McColl Plaza
- 1:30-3:00   Breakout Groups
- 3:00- 4p   Close and Social Hour

Afternoon Breakout Groups

Students:
- Career planning, *Stanford Strategic Initiatives*
- "**Life after Stanford,**" *Dan Golden, CellScope, Inc.*

Faculty and Affiliated Faculty:
- *Research Overlap*
- *Synergies/Opportunities*
- *Future of ISIS: name, direction*
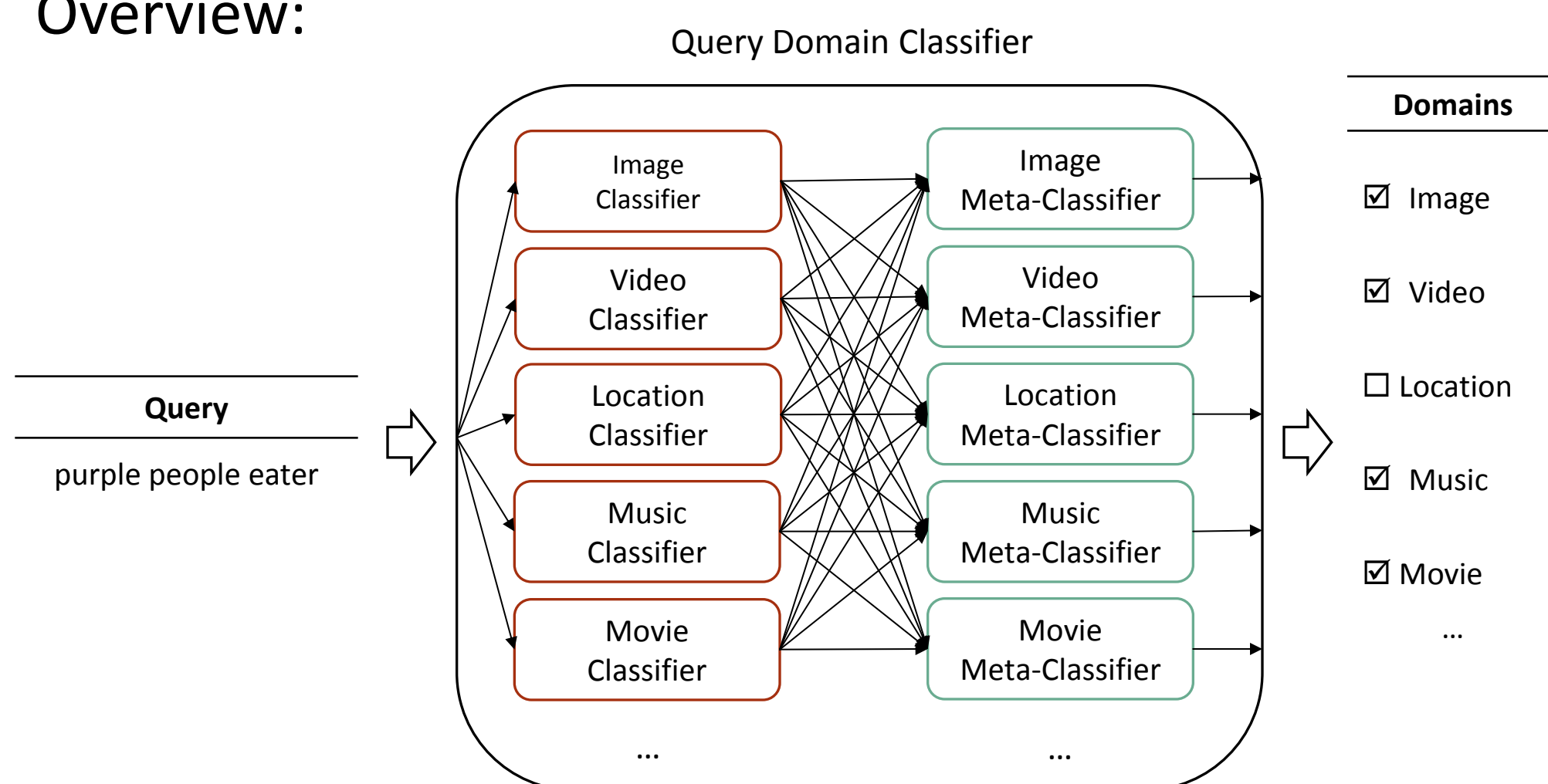
Semantic Text Analysis

Saeed Hassanpour

Objectives

Build computational methods and tools for extracting and organizing knowledge from text to assist users to comprehend unstructured text and find the information they are looking for:

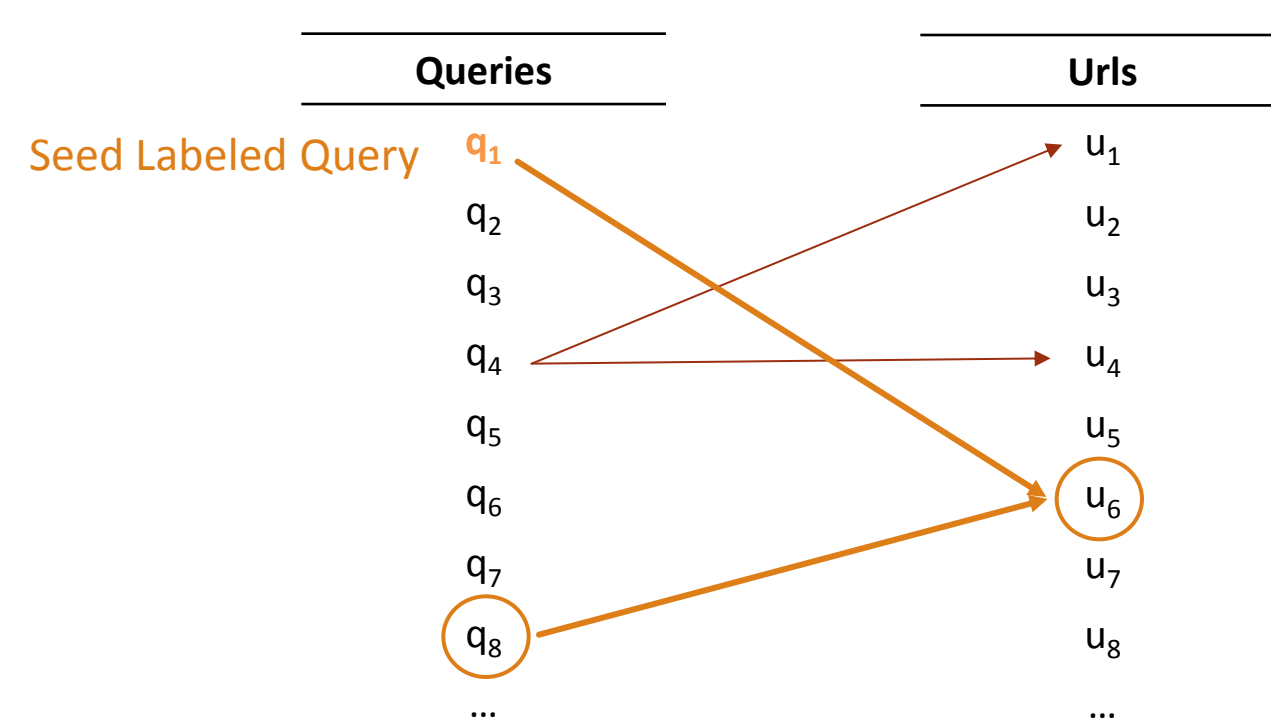- Semantic query classification
- Semantic query annotation

Semantic Query Classification

Overview:

Query Domain Classifier

Query: purple people eater

Domains: ☑ Image ☑ Video ☐ Location ☑ Music ☑ Movie …

Gathering Labeled Data: Semi-Supervised Learning

- Unlabeled data: Search log
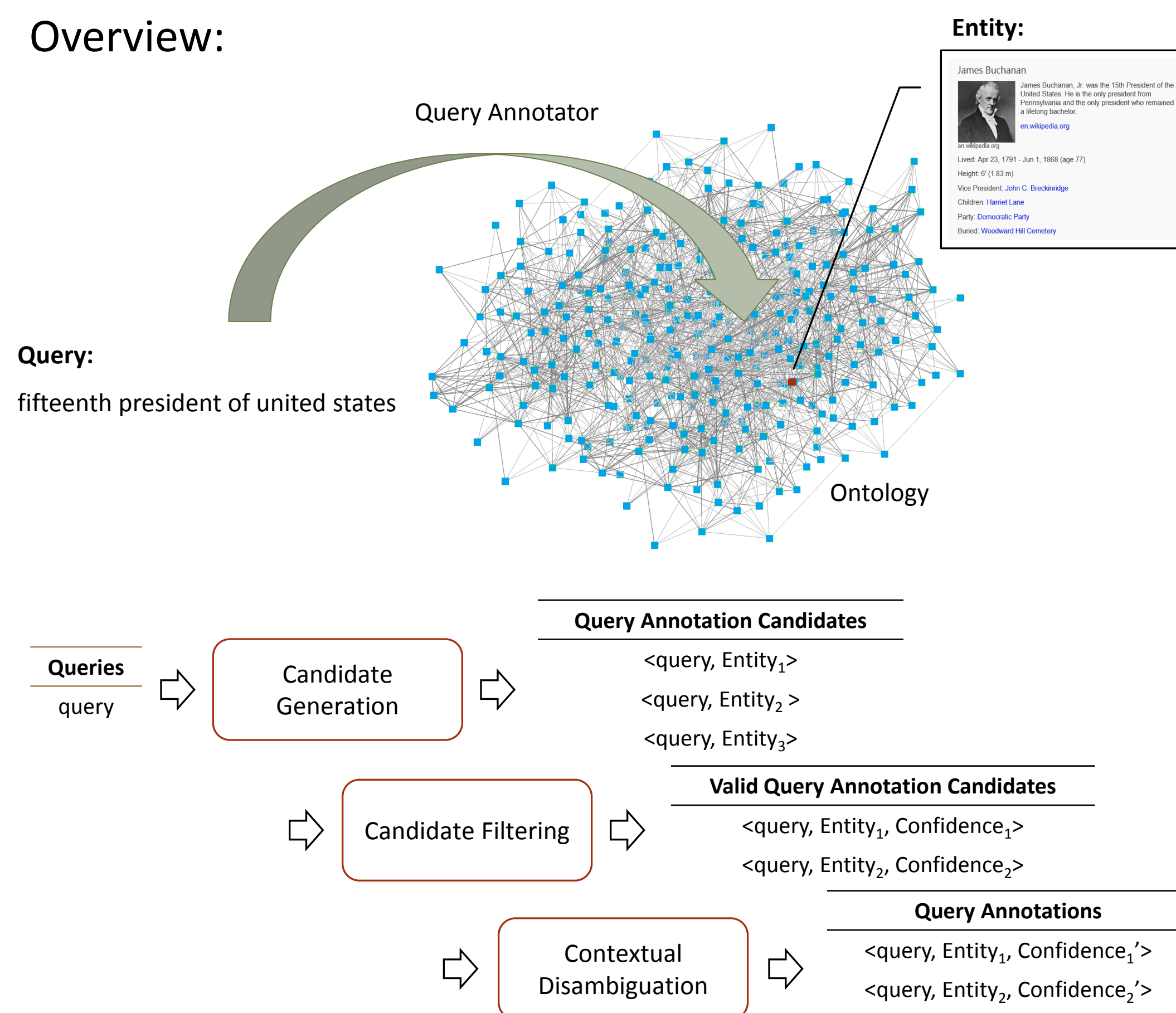- Labeled data: Seed labeled queries

Model Training:

- Extract features from labeled data
  - N-gram Frequencies: Use uni, bi, tri- gram frequencies
  - N-gram Types: Use proper name dictionaries
- Train SVMs for the first layer classifiers
- Train MARTs for the second layer classifiers

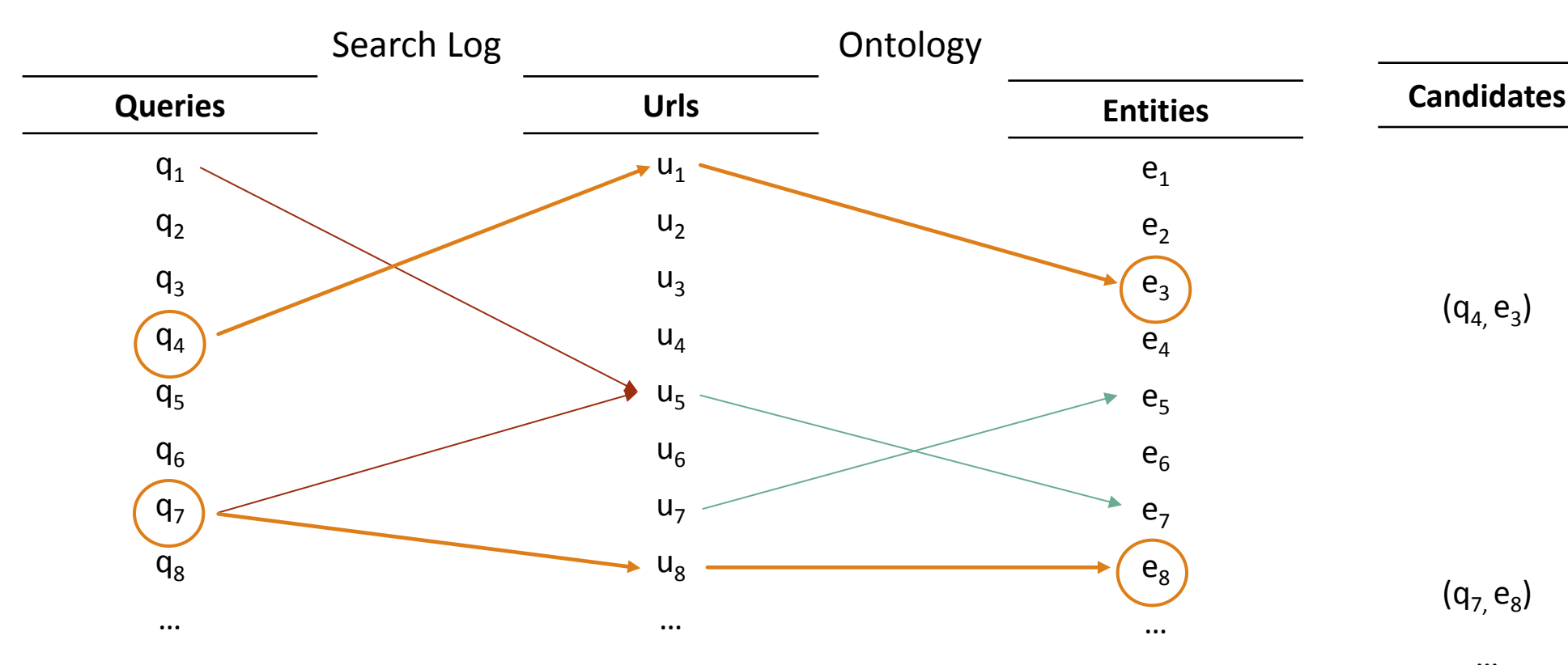**Evaluation and Results:** Based on 1,000 test query judgments:

- Precision: 92% (12% increase compared to the baseline)
- Recall: 83% (22% increase compared to the baseline)
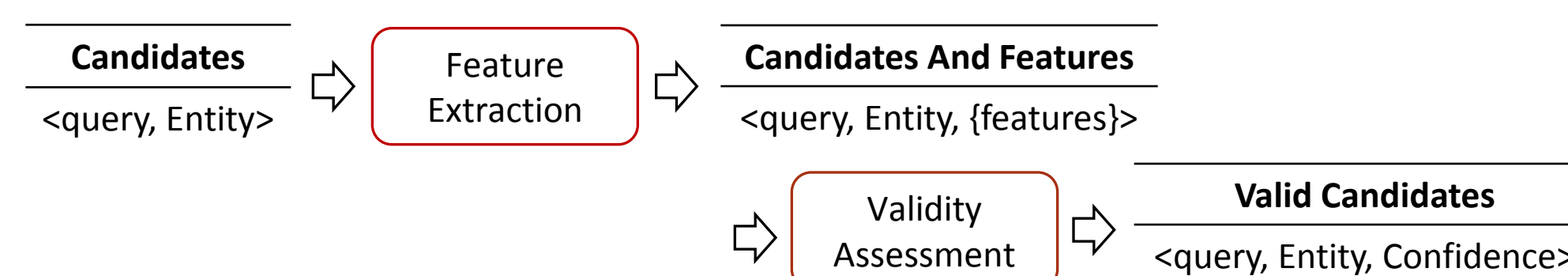
Semantic Query Annotation

Overview:

Query Annotator

Entity:

Query: fifteenth president of united states

Ontology

Queries → Candidate Generation → **Query Annotation Candidates**
<query, $Entity_1$>
<query, $Entity_2$>
<query, $Entity_3$>

Candidate Filtering → **Valid Query Annotation Candidates**
<query, $Entity_1$, $Confidence_1$>
<query, $Entity_2$, $Confidence_2$>

Contextual Disambiguation → **Query Annotations**
<query, $Entity_1$, $Confidence_1'$>
<query, $Entity_2$, $Confidence_2'$>

Candidate Generation

Search Log | Ontology

Queries   Urls   Entities   Candidates

(q_4, e_3)

(q_7, e_8)

Candidate Filtering

Candidates
<query, Entity>
→ Feature Extraction →
Candidates And Features
<query, Entity, {features}>
→ Validity Assessment →
Valid Candidates
<query, Entity, Confidence>

Validity Assessment Evaluation and Results: 1,000 labeled annotation candidates are used as a test set

- Precision: 91%
- Recall: 78%

**Contextual Disambiguation:** Consider contextual information in query annotation:

- Temporal information and patterns
- Location information and patterns

Temporal Disambiguation: Use a short recent search log window to generate candidate features

News about Francis Bacon
bing.com/news
Francis Bacon painting auctioned for more than $142 million, breaks record
CNN
(CNN)— A painting by artist Francis Bacon sold for $142,405,000 on Tuesday, breaking the record as the most expensive piece of art ever auctioned, according...
Francis Bacon's 'Lucian Freud' triptych breaks auction price records
Los Angeles Times
An Idiot's Guide To Francis Bacon, The Man Behind The World's Most Expensive Painting
The Huffington Post

Francis Bacon Philosopher (1561 − 1626)
Francis Bacon Painter (1909 − 1992)

Evaluation and Results: Applied to 500 test queries and their annotating entities. DCG@1 14% increased (p-value < 0.01)

Location-Based Disambiguation:

- Model annotating entities' locations of interest distributions (GMM)
- Extract location sensitive queries through KL-divergence comparison
- Adjust location sensitive queries' annotation confidence scores

Query: giants — San Francisco Giants GMM

Query: giants — New York Giants GMM
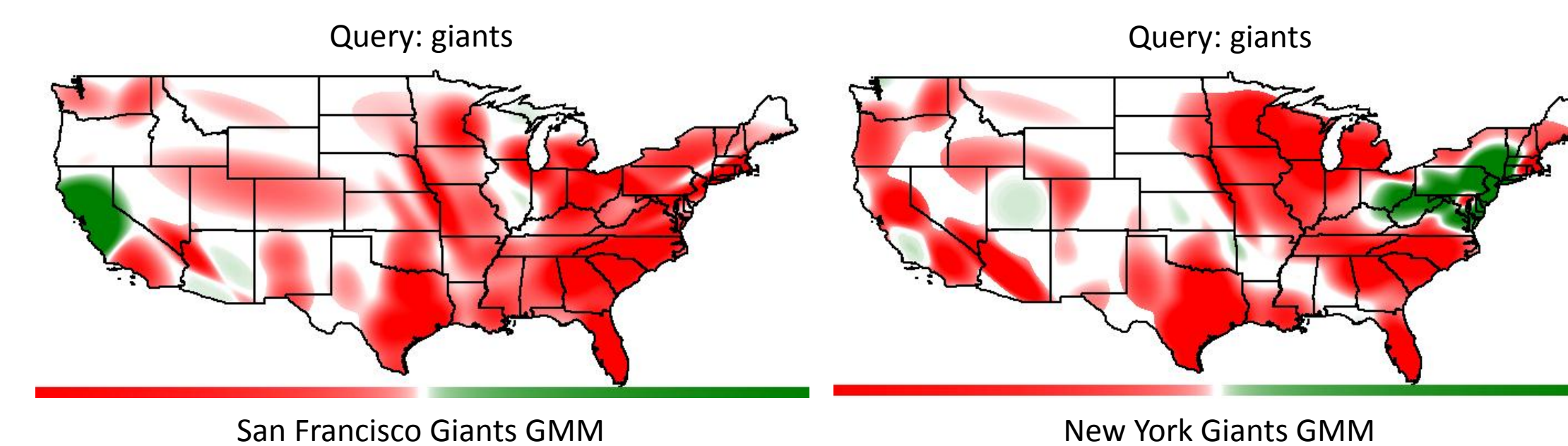
Evaluation and Results: Applied to 1,000 ambiguous queries:

- Precision: 85%
- Recall: 98%

References

Direct Answer Triggering in Search, US Patent Filed, 2014.
Temporal Context Aware Query Entity Intent, US Patent Filed, 2014.

DRUGMNEM: An optimization strategy for targeted combination of drugs using single- drug screening single cell data

Benedict Anchang, Harris Fienberg, Sean Bendall, Rob Tibshirani and Sylvia Plevritis

isis
Information Sciences
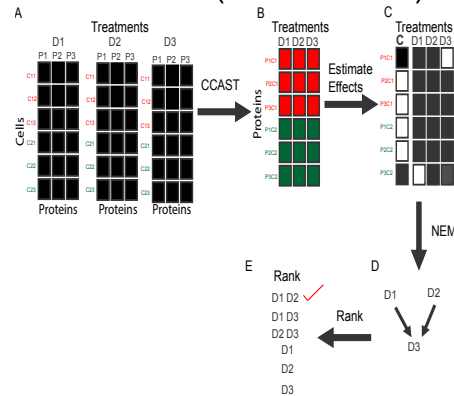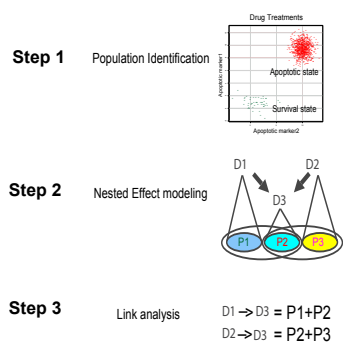in Imaging at Stanford

OBJECTIVES

Accumulating evidence implicates intratumor heterogeneity as an important challenge to cancer treatment. Standard drug combinations do not kill all tumor cells. We need to optimize drug combination for each patient separately. We rationalize that targeting multiple key pathways across different cell types or cell states will decrease the likelihood of emerging resistant populations.

Our objective is to develop an optimized framework for effective combination therapy using cell population data that reveals heterogeneity in inter and intra-cellular signaling at the level of single cells within a single patient

Standard therapy

D1
D2

Before treatment

tumor 1   tumor 2   tumor 3

After treatment

drug
Normal cells
Sensitive cells
Non sensitive cells

Optimal therapy

D1
D2
D3

Before treatment

tumor 1   tumor 2   tumor 3

After treatment

drug
Normal cells
Sensitive cells

METHODS

DRUG Mixture Nested Effects Models (DRUGMNEM)

Step 1 Population Identification

Drug Treatments

Apoptotic state

Survival state

Apoptotic marker1
Apoptotic marker2

Step 2 Nested Effect modeling

D1   D2
D3
P1   P2   P3

Step 3 Link analysis

D1 → D3 = P1+P2
D2 → D3 = P2+P3

A
Treatments
D1   D2   D3
P1 P2 P3 P1 P2 P3 P1 P2 P3

Cells

Proteins   Proteins   Proteins

CCAST →

B
Treatments
D1 D2 D3
P1C
P2C
P3C

Proteins

Estimate Effects →

C
Treatments
C   D1 D2 D3
P1C
P2C
P3C
C1C
P1C2
P2C2

NEM ↓

E Rank
D1 D2 ✓
D1 D3
D2 D3
D1
D2
D3

Rank ←

D
D1   D2

D3

Scoring drug combinations

$$Regimen_{best} = \underset{\underset{r}{\cup} S_r^*}{argmax} \left(Max \left\{ \left(\sum_{i \in \underset{u}{\cup} T_{k_u}} P_{cik} \right) \mid k \in c \right\} \right)$$

where S_r^* corresponds to the set of all r drug combinations

P_{cik} corresponds to the probability of where S_r^* co

all the targets across DRUGMNEM netwo under each T_{k_u}.
be a combination set
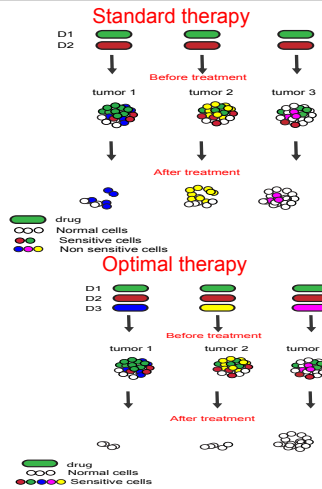
RESULTS

DRUGMNEM predicts pP38 MAPK inhibitor(SB) as an important drug for combination therapy for HeLa cells

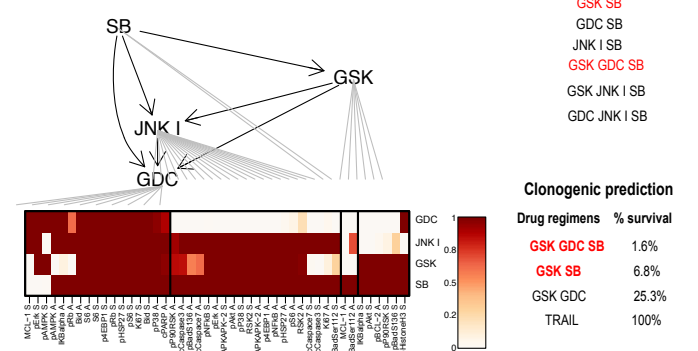**Inhibitors**: JNK 1(JnK), GDC(PI3K), GSK(Mek), SB(pP38 MAPK)

Stimulation: TRAIL (Base line treatment)

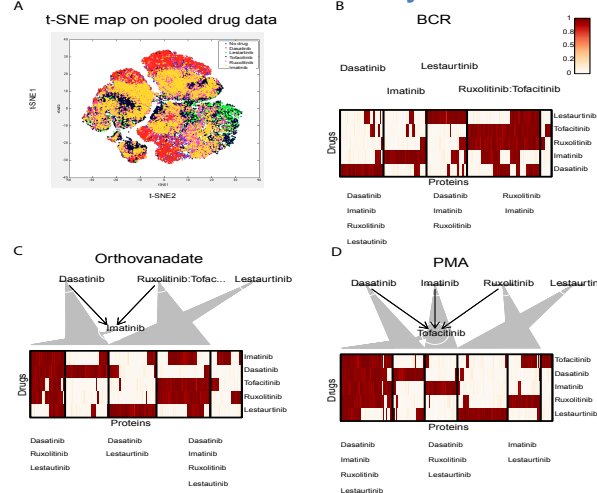**Cell states** : Apoptotic and survivor from cPARP/cCaspace3

Intracellular markers:
MCL1,pBCL2,pP90RSK, pHistoneH3, pBadS136, Bid, pP38, cCaspase7, pBadSer112, cCaspase3, pRb, Ki67, pAMPK, cPARP, IKBalpha, S6, pS6, pErk, pHSP27, pAkt, pNFkB, pMAPKAPK2, RSK2, p4EBp1

DRUGMNEM Network

SB → GSK
JNK I
GDC

DRUGMNEM prediction
GSK SB
GDC SB
JNK I SB
GSK GDC SB
GSK JNK I SB
GDC JNK I SB

Clonogenic prediction

Drug regimens	% survival
GSK GDC SB	1.6%
GSK SB	6.8%
GSK GDC	25.3%
TRAIL	100%

DRUGMNEM results on normal PBMC drug response under BCR, Pervanadate and PMA ionomycin stimulations

A t-SNE map on pooled drug data

B BCR
Dasatinib   Lestaurtinib
Imatinib   Ruxolitinib:Tofacitinib

Drugs

C Orthovanadate
Dasatinib Ruxolitinib:Tofac... Lestaurtinib
Imatinib

Drugs

D PMA
Dasatinib Imatinib Ruxolitinib Lestaurtinib
Tofacitinib

Drugs

Inhibitors: Ruxolitinib(Jak1-2), Tofacitinib(Jak3), Lestauritinib(Jak2), Dasatinib(BCR/Abl), Imatinib(BCR/Abl)

Dose level: max 10uM
Time lag for inhibition: 15 mins
Time lag for stimulation: 30mins

REFERENCES

1. Anchang et al. (2014) *CCAST: A model–based gating strategy to isolate homogeneous subpopulations in a heterogeneous population of single cells. PloS Computational Biology.*
2. Markowetz et al. (2005) *Non-transcriptional pathway features reconstructed from secondary effects of RNA interference. Bioinformatics* 21, 4026-4032, 2005.
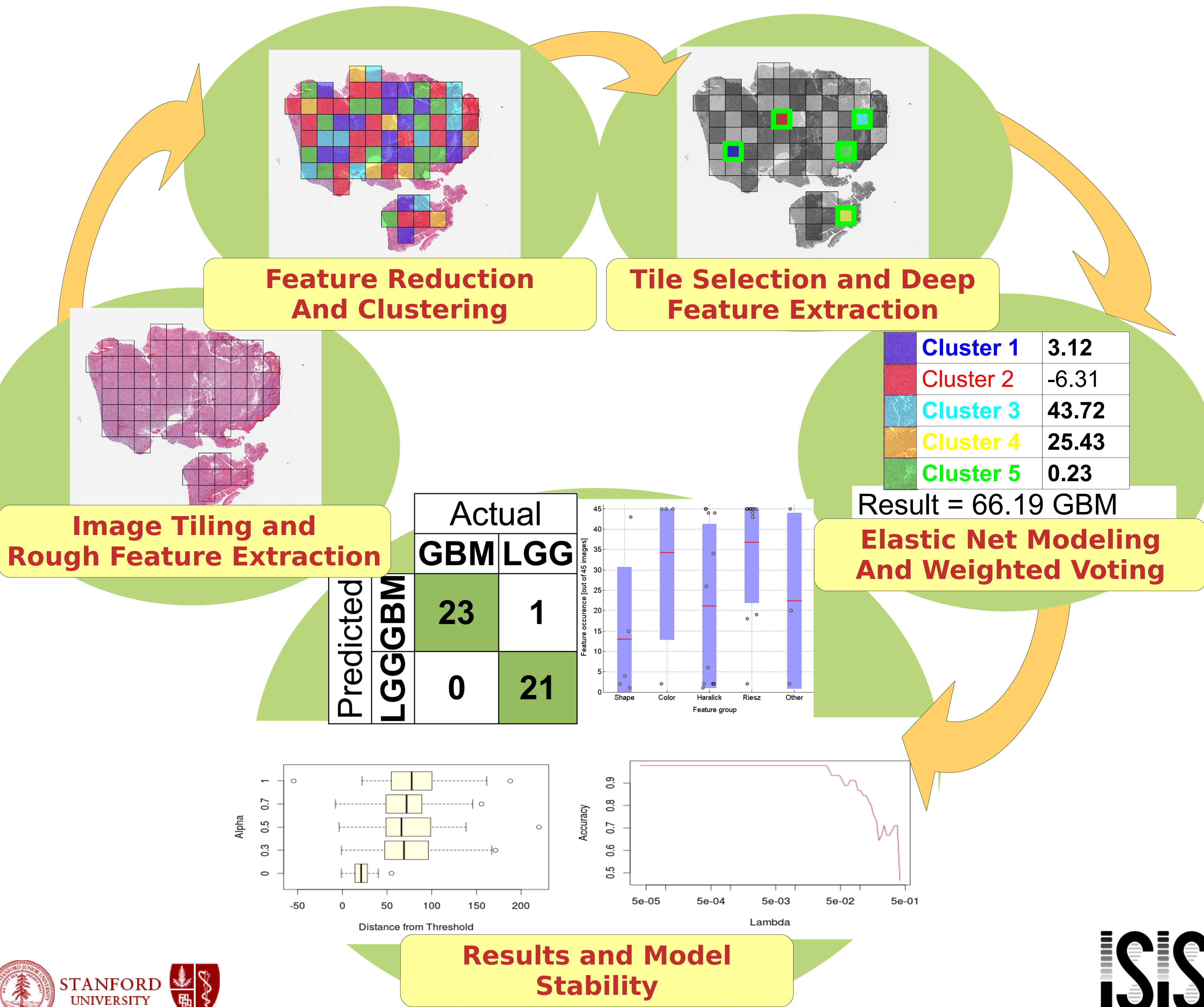
ACKNOWLEDGEMENTS

Automated Classification of Brain Tumor Type in Digital Pathology Images Using Local Patches

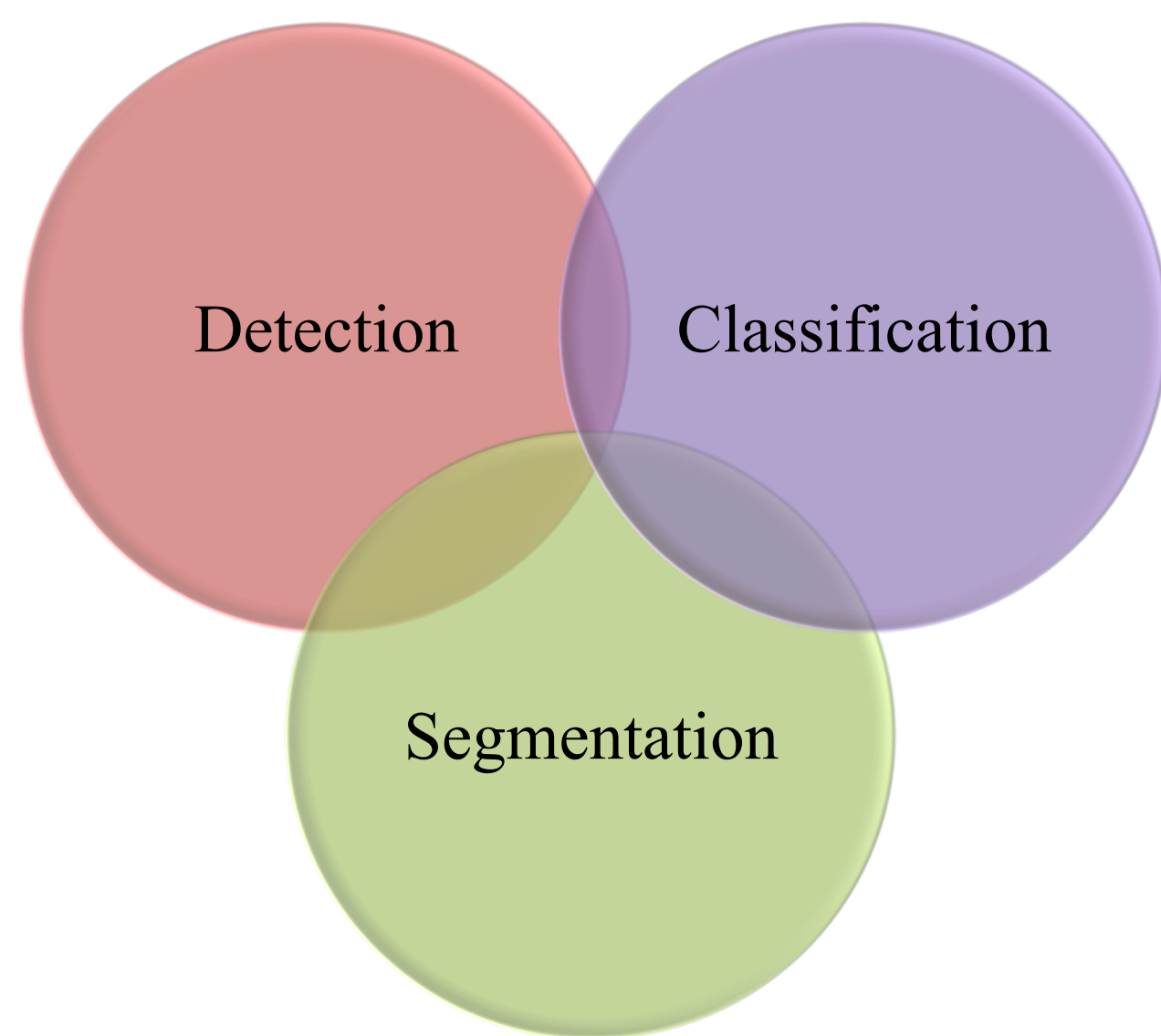Jocelyn Barker[a], Assaf Hoogi[a], Adrien Depeursinge[a,b], and Daniel L. Rubin[a]

[a]Department of Radiology, Stanford University School of Medicine, CA, USA.

[b]eHeatlh Unit, University of Applied Sciences Western Switzerland, Sierre (HES-SO)

Feature Reduction And Clustering
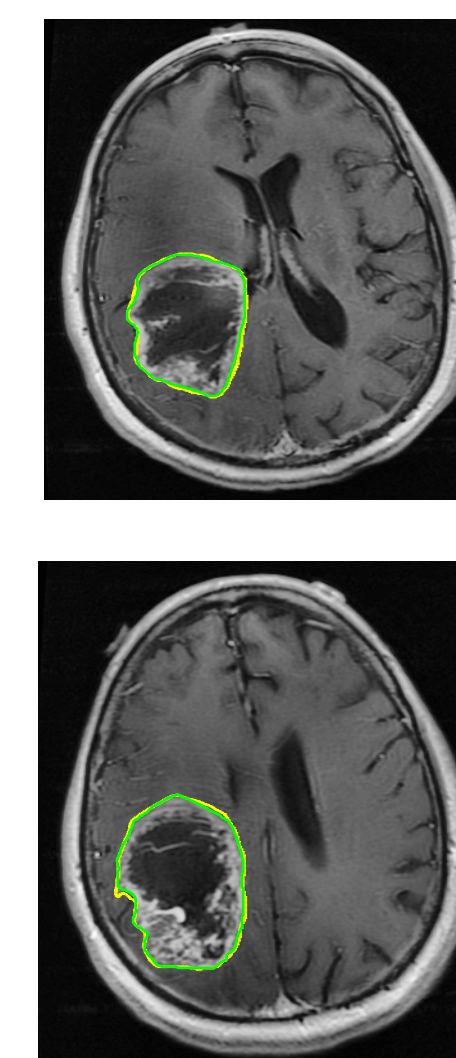
Tile Selection and Deep Feature Extraction

Image Tiling and Rough Feature Extraction

Cluster 1	**3.12**
Cluster 2	-6.31
Cluster 3	**43.72**
Cluster 4	**25.43**
Cluster 5	**0.23**

Result = 66.19 GBM

Elastic Net Modeling And Weighted Voting

		Actual	
		GBM	**LGG**
Predicted	**GBM**	**23**	**1**
	LGG	**0**	**21**

Results and Model Stability

Segmentation and Classification of abnormal lesions

Assaf Hoogi, Daniel L. Rubin

Information Sciences in Imaging at Stanford

OBJECTIVE

Detection — Classification — Segmentation

METHODS

Detection
Input – Raw data + liver borders	Output – Detected lesions

Segmentation
Input – Detected lesions masks	Output – Lesion segmentation

Classification
Input – Segmented lesions	Output – Lesions classification

Detection + Classification

monkey?

Histogram — Classification — [monkey, dog, tree, ...]

Feature extraction — Clustering

BOW with 2 different dictionaries – one for the intra-lesion areas and second for the lesion's boundaries

Segmentation

- Level set segmentation
- Local framework
- Spatial features for optimal:
  1. Localization
  2. Curve evolution direction
  3. Cost function
- Different models for different challenges

RESULTS

Detection

True negative
False negative
True positive
False positive

Segmentation

MRI liver lesions

MRI brain tumors | **CT breast cancer** | **CT liver lesions** | **Mammography**
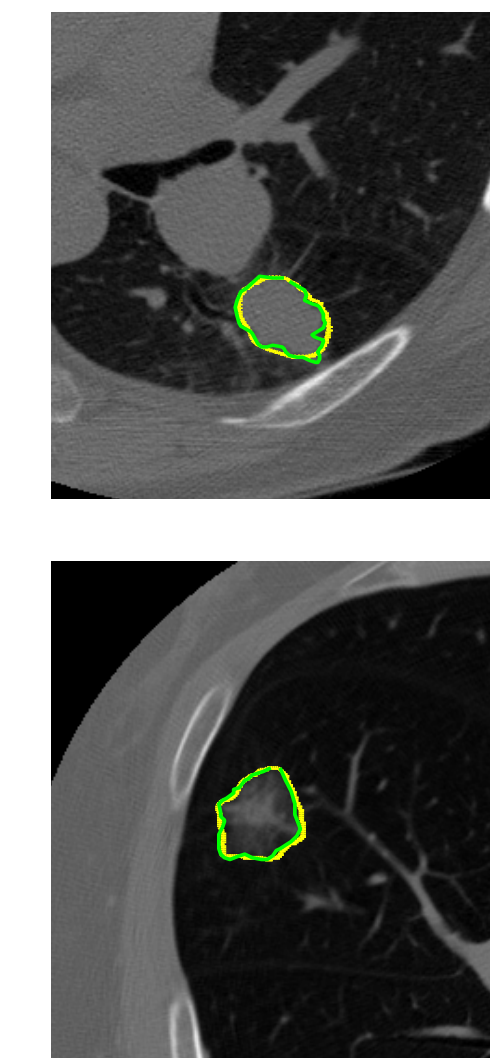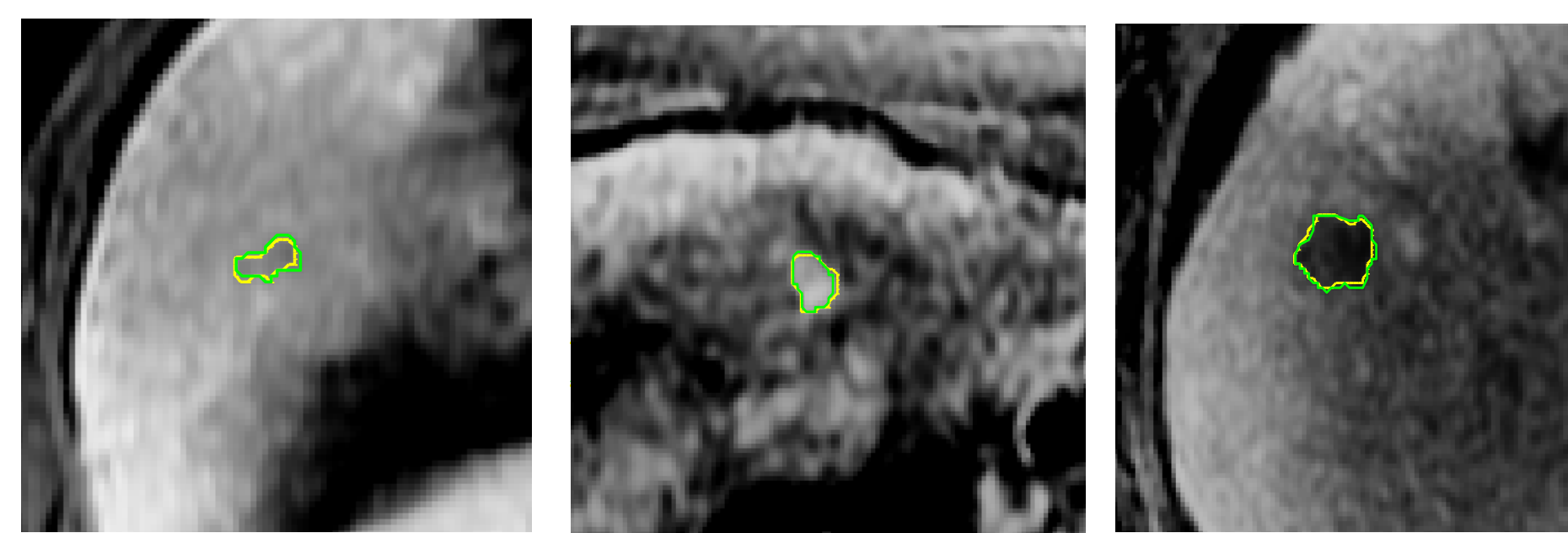
Statistics for liver lesions
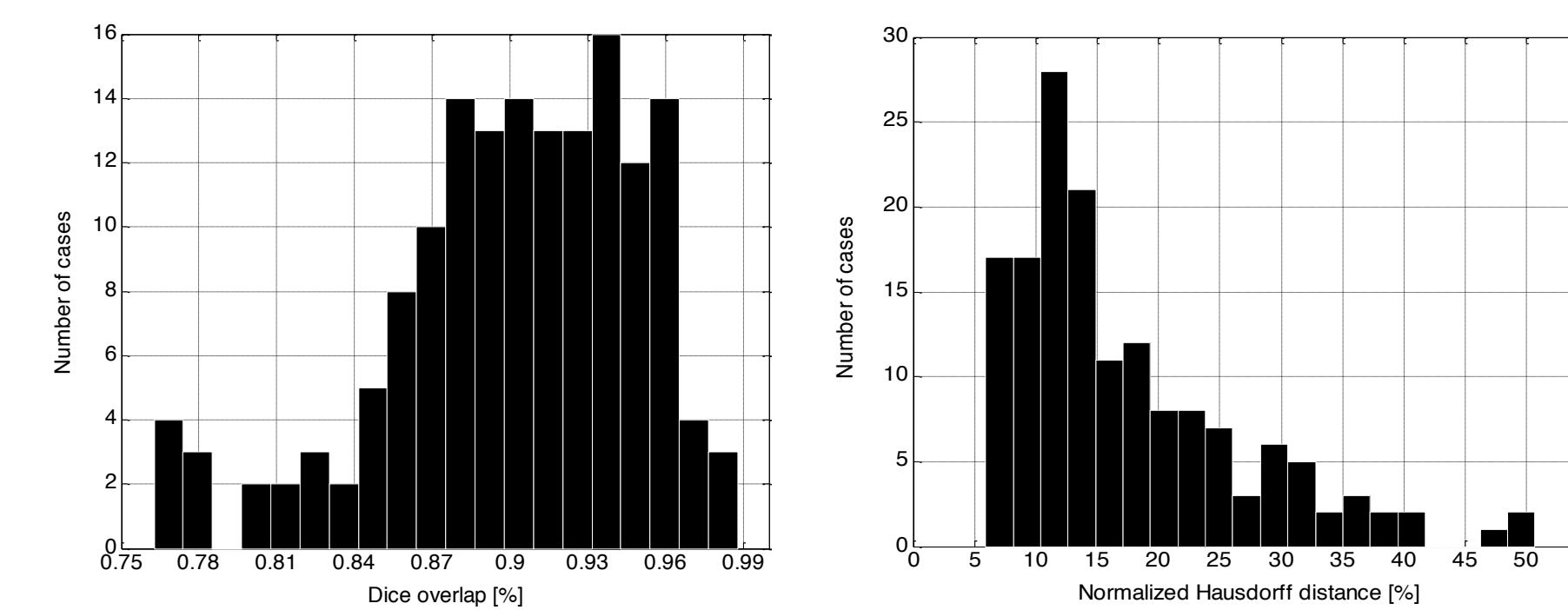
Classification

Method	Accuracy
Our method	**99.08%**
GLCM	89.91%
Gabor	90.83%

True\ Auto	Cyst	Met	Hem	Sensitivity
Cyst	39	0	0	100%
Met	0	46	0	100%
Hem	0	1	23	95.8%
Specificity	100%	98.4%	100%	
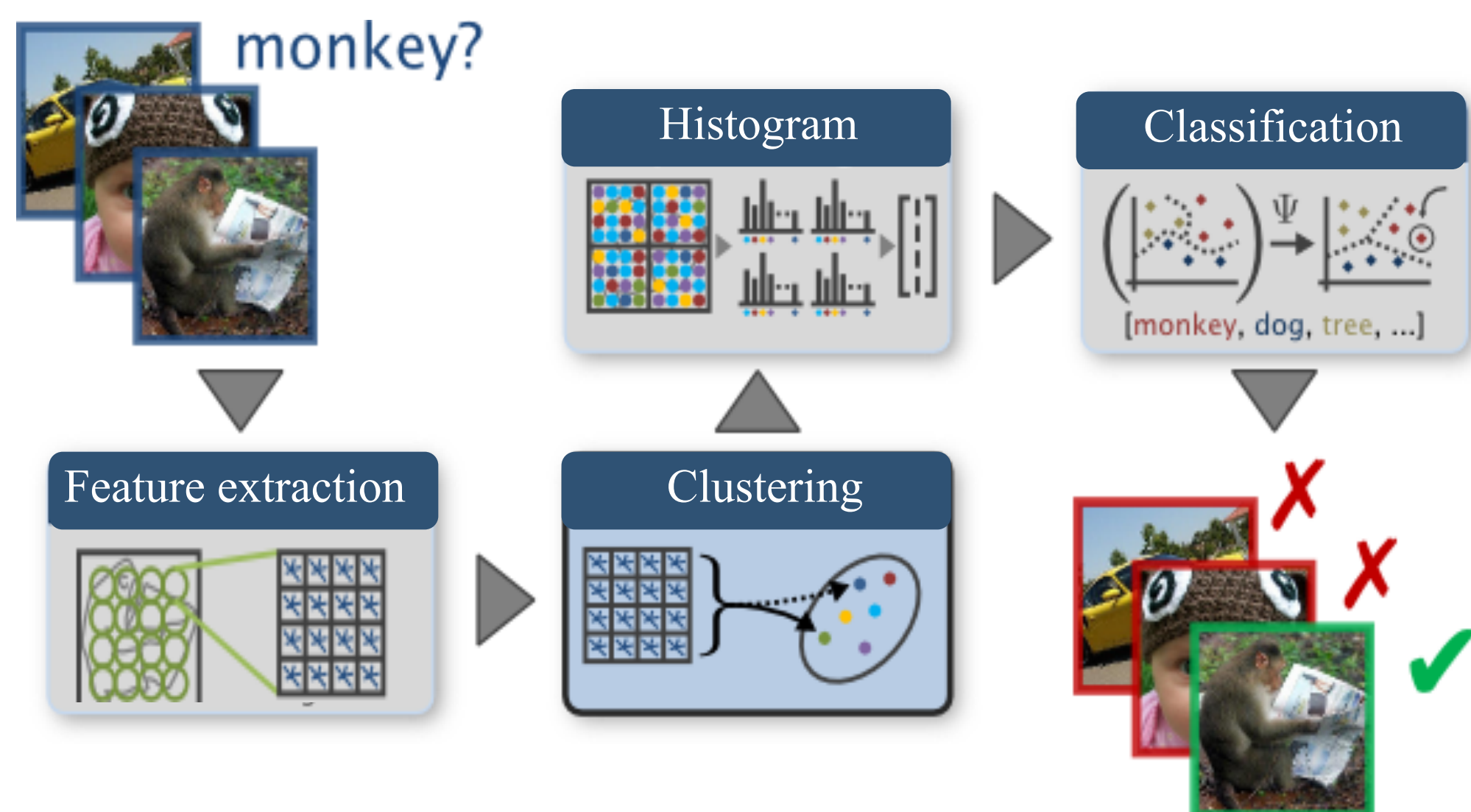
References

- T. Chan and L. Vese, "Active contours without edges," IEEE Trans. Image Process., vol. 10, no. 2, pp. 266–277, Feb. 2001
- S. Lankton, A. Tannenbaum, Localizing region-based active contours, IEEE Trans.Image Process. 17 (11) (2008) 2029–2039.
- G. Csurka, C. Dance, C. Bray, L Fan, "Visual categorization with bags of keypoints, " in *Proceedings Workshop on Statistical Learning in Computer Vision*, (2004).

Meta-analytical methods for imaging genomics

Mapping genes and brain to neurological disorder

Problem

We are terrible at diagnosis and treatment of neuropsychiatric disorder

Why?

The Gold Standard DSM-V
- No biological validity
- Heterogeneous categories
- High comorbidity

Who is suffering?
- 61.5 million Americans (1 in 4 adults)
- 60% of whom receive no treatment
- Lost earnings per year

DIAGNOSTIC AND STATISTICAL MANUAL OF MENTAL DISORDERS
FIFTH EDITION
DSM-5
AMERICAN PSYCHIATRIC ASSOCIATION

$193.2 billion

How to fix?

Meta-analytical methods that integrate genes, brain, and behavior can

A) recapitulate known knowledge about disorders, and
B) provide a signature that predicts behavior.
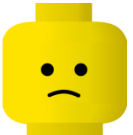
behavior → brain map → genes

Isn't that just imaging genomics?
There is no work that brings meta-analysis to this domain.

Aim 1: summarize behavioral phenotypes as brain maps and gene sets

1. Associating behavioral terms to brain regions

behavior → brain map

Select term, "anxiety"
Select term frequency threshold > 0.001
Text mine the literature, and count!

What does the neuroscience literature have to say about the experience of anxiety?

NEUROSYNTH
100,953 results
3,489 studies
Top 17 journals

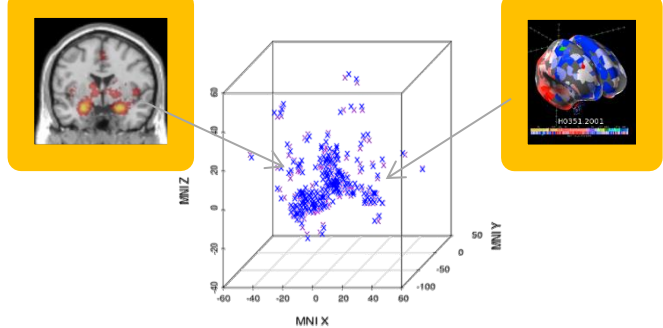| anxiety present activation present | anxiety present activation absent |
| anxiety absent activation present | anxiety absent activation absent |

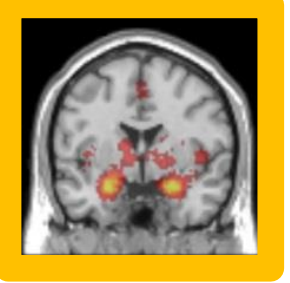### 2. Find regulatory patterns within brainterm maps

brain map → genes

ALLEN BRAIN ATLAS
~4000 coordinates
60K probes

Match points (<3mm)
Define gene sets: Shapley Value Regression

3. Brainterm...

MAPS

GENE SETS
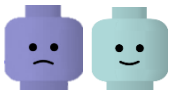CIITA
NFE2
PPARA
HIST1H4G
SLC22A14
...

Aim 2: test brain maps and gene sets against neuropsychiatric disorder

1. Gene Set Enrichment Analysis

Enrichment Score: the degree to which a gene set S is overrepresented at the extremes of a ranked list of differential expression between two phenotypes.

PHENOTYPES
49 disorders (GEO)

GENE SETS
525 behavioral terms
Up /down regulated sets
Total N=1050

LAMP1
RPSA
LDHB
EIF3E
LGALS1

CIITA
NFE2
PPARA
HIST1H4G
SLC22A14

Enriched for anxiety?

A Significant Result Means
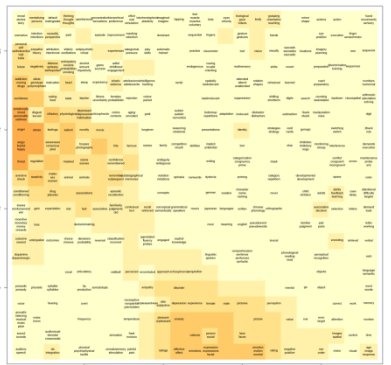
AUTISM SPECTRUM DISORDER

| BRAINTERMS | BRAINTERM MAPS | CORE GENES |
| mood vision | | CIITA HIST1H4G SLC22A14 ... |

2. Novel Visualization Strategy

1. Summary image of disorder
2. Match to SOM nodes
3. Color by score

"Brain Lattice" self-organizing map (SOM)

Aim 3: validate brain maps and gene sets

1. Recapitulate Known Knowledge

DISORDER
- genes
- behavior
- brain map

Disorder	known	Our genes	Intersect
Autism Spectrum Disorder	826	26	0
Alzheimer	1586	411	44
Lupus	795	62	7
Multiple Sclerosis	1010	178	12
Parkinson	945	9	0
Post Traumatic Stress Disorder		10	
Rett Syndrome	116	21	0
Schizophrenia	1455	11	1

2. Predict Behavioral Phenotype

genes → behavior

1 In diseases: exome > SNPs > behavior
2 In normal: Duke Neurogenetics Study

Functional Annotation for ASD-RETT

A novel meta-analytical approach for imaging genomics

behavior → brain map → genes → behavior

Informed by imaging | genetic signatures of behavior

Vanessa Sochat
vsochat@stanford.edu

The Wall Lab
wall-lab.stanford.edu

Stanford University School of Medicine
Funded by NSF, SGF, Microsoft Research

PROJECT WEB INTERFACE

Evaluating the Impact of Varied Compliance to Lung Cancer Screening Recommendations using a Microsimulation Model

Summer S. Han, S. Ayca Erdogan, Ann Leung and Sylvia K. Plevritis

Information Sciences in Imaging at Stanford

BACKGROUND

- National Lung Screening Trial (NLST) showed low-dose computed tomography (LDCT) reduces lung cancer (LC) mortality[1].
- Recently, the U.S. Preventive Services Task Force (USPSTF) recommended a heavy smoker aged 55 to 80 be screened annually by LDCT, thereby extending the stopping age from 74 to 80 compared to NLST [2].
- This decision was made partly with model-based analyses from consortium Cancer Intervention and Surveillance Modeling Network (CISNET)[3].
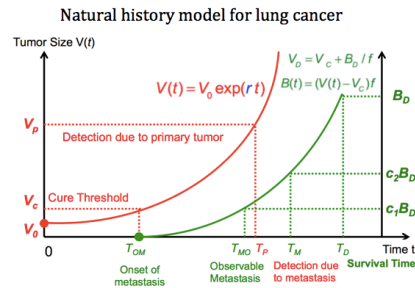
OBJECTIVES

- As part of CISNET lung group, we develop a microsimulation model that simulates lung cancer initiation, progression, detection and survival
- We calibrate our model to NLST data using and validated it using data from the Prostate, Lung, Colorectal, and Ovarian (PLCO) trial.
- We evaluate the impact of varying compliance levels to the USPSTF screening recommendations in the U.S. population.

METHODS
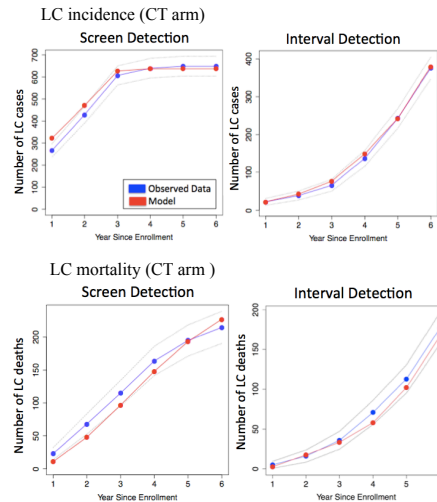
Microsimulation Model

- The purpose of our microsimulation model is to evaluate the population-level impact of an intervention or health policy recommendation related to lung cancer.
- We simulate individual-level lung cancer history including incidence age in the absence of screening, tumor growth rate and progression to lethal metastases and histologic subtype.
- We then impose a specific screening intervention to each individual and estimate individual-level outcomes.
- To estimate the population-level outcomes of the given strategy, individual-level outcomes are aggregated.

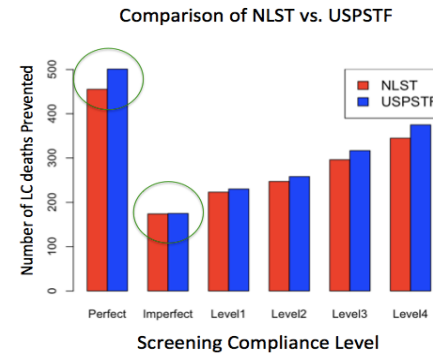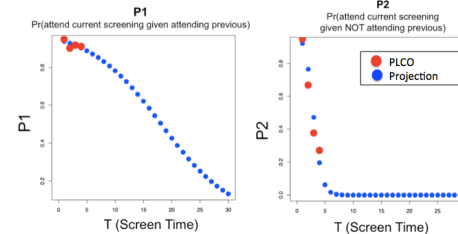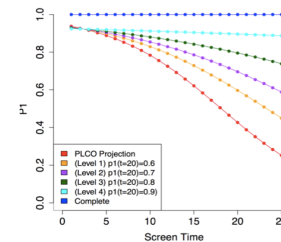### Natural history model for LC as a main component of the microsimulation model

Natural history model for lung cancer

Tumor Size $V(t)$

$V(t) = V_0 \exp(r\,t)$

$V_D = V_C + B_D / f$
$B(t) = (V(t) - V_C)f$

Detection due to primary tumor

Cure Threshold

V_P, V_C, V_0, B_D, $c_2 B_D$, $c_1 B_D$

T_{OM} Onset of metastasis, T_{MO} Observable Metastasis, T_P, T_M Detection due to metastasis, T_D, Time t, Survival Time

RESULTS

Calibration to the NLST data

LC incidence (CT arm)

Screen Detection / Interval Detection

Number of LC cases vs Year Since Enrollment

Observed Data / Model

LC mortality (CT arm)

Screen Detection / Interval Detection

Number of LC deaths vs Year Since Enrollment

Comparison of NLST vs. USPSTF Under varying compliance levels

Comparison of NLST vs. USPSTF

Number of LC deaths Prevented vs Screening Compliance Level (Perfect, Imperfect, Level1, Level2, Level3, Level4)

NLST / USPSTF

Observed compliance transition probability from the PLCO data and projections

P1 — Pr(attend current screening given attending previous) vs T (Screen Time)

P2 — Pr(attend current screening given NOT attending previous) vs T (Screen Time)

PLCO / Projection

Varying the levels of transition probabilities P_1 in Markov model for compliance

P1 vs Screen Time

- PLCO Projection
- (Level 1) p1(t=20)=0.6
- (Level 2) p1(t=20)=0.7
- (Level 3) p1(t=20)=0.8
- (Level 4) p1(t=20)=0.9
- Complete

Compliance Probability of NLST and USPSTF

Compliance probability over screen time

[NLST-ish] / [USPSTF]
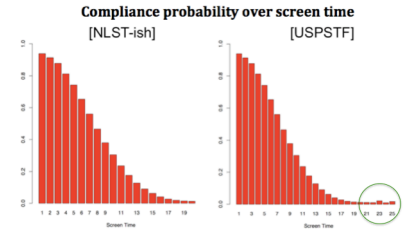
Conclusions

- Our simulation model reproduce the outcomes of the NLST and the PLCO data very closely
- We predict that perfect compliance to the USPSTF recommendation saves 501 LC deaths per 100,000 persons (compared to 455 in NLST)
- However, assuming compliance behaviors extrapolated from PLCO yields 175 LC deaths-avoided per 100,000 persons (compared to 174 in NLST) , demonstrating that the benefit for extending the stopping age substantially decreases.
- The implementation of the USPSTF recommendation is expected to contribute to a reduction in LC deaths, but the magnitude of the reduction will be heavily influenced by screening compliance.

REFERENCES

1. Aberle D, Adams A, Berg C, et al. Reduced lung-cancer mortality with low-dose computed tomographic screening. The New England journal of medicine 2011;365(5): 395.
2. Moyer VA. Screening for lung cancer: US Preventive Services Task Force recommendation statement. Annals of internal medicine 2014.
3. de Koning HJ, Meza R, Plevritis SK, et al. Benefits and harms of computed tomography lung cancer screening strategies: a comparative modeling study for the US Preventive Services Task Force. Annals of internal medicine 2014.

Saliency based Ulcer Detection in Wireless Capsule Endoscopy Images

Yixuan Yuan, Jiaole Wang and Max Q.-H. Meng

ISIS
Information Sciences
in Imaging at Stanford

OBJECTIVES

- Wireless capsule endoscopy (WCE) is a revolutionary devise that provides direct, noninvasive visualization of the small bowel.
- The ulcer is one of the most common lesions that affects approximately 10% of the people in the world.
- Our objectives are to automatically detect the ulcer frames in the WCE images.

METHODS

Step 1: Propose a saliency detection method based on multilevel superpixel representation to outline the ulcer candidates.
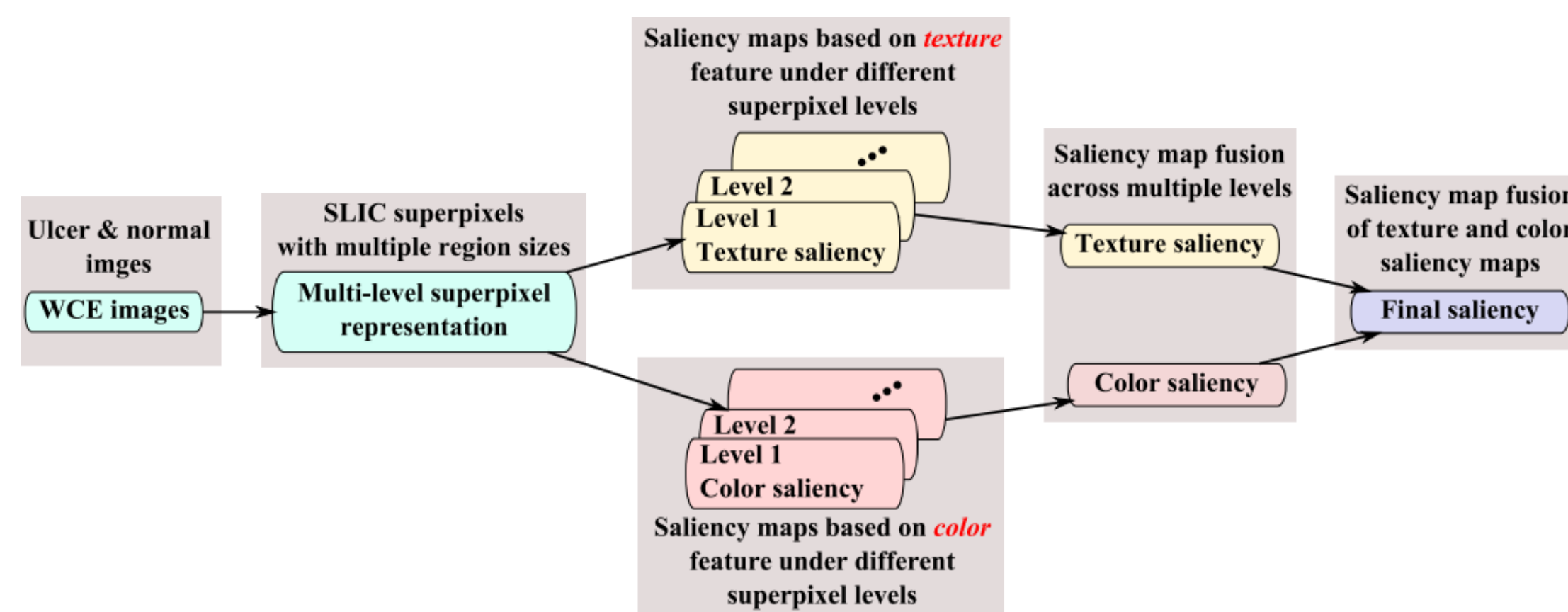
Step 2: propose a modified Locality-constrained linear coding (LLC) method to encode the image based on the saliency map.
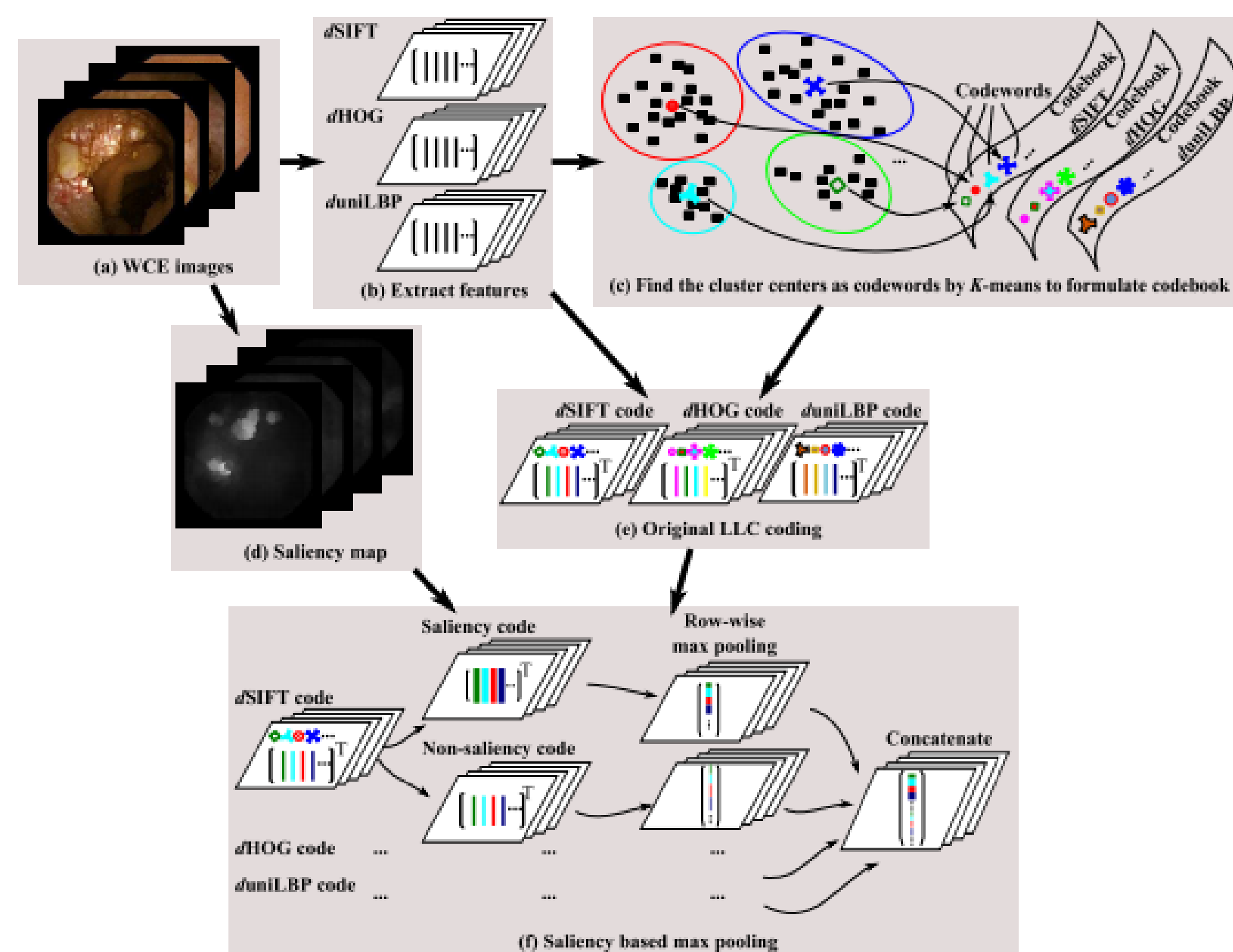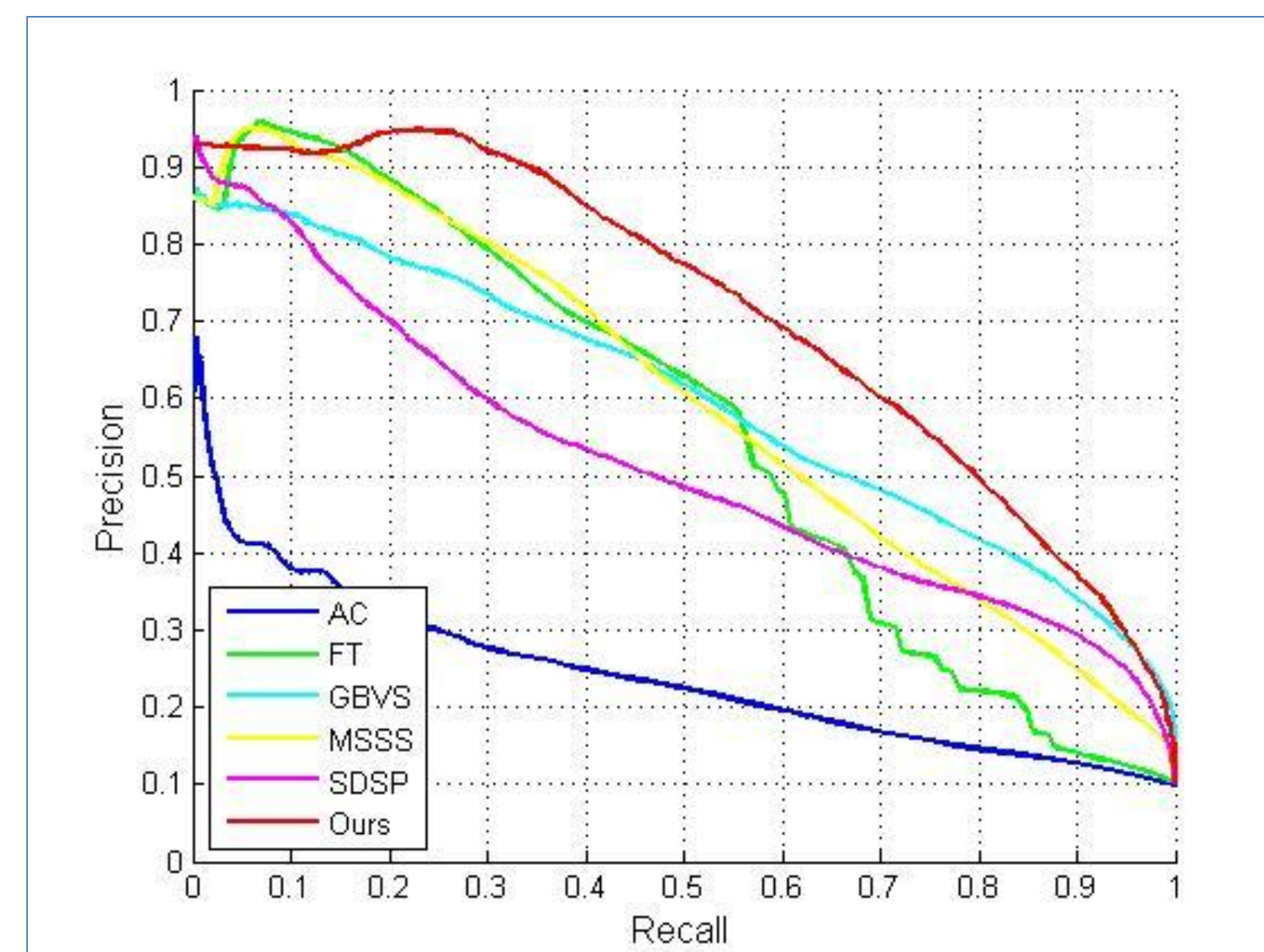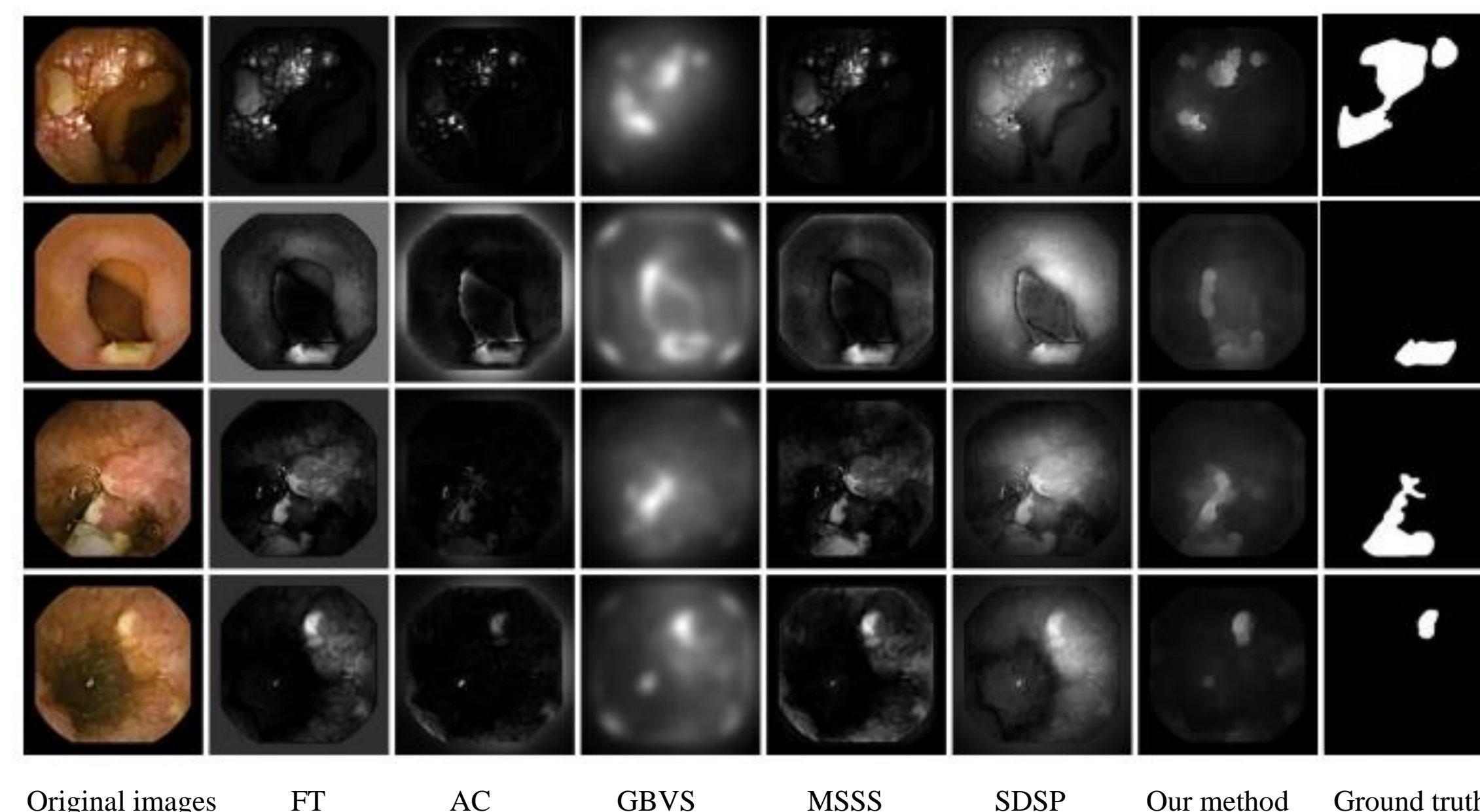

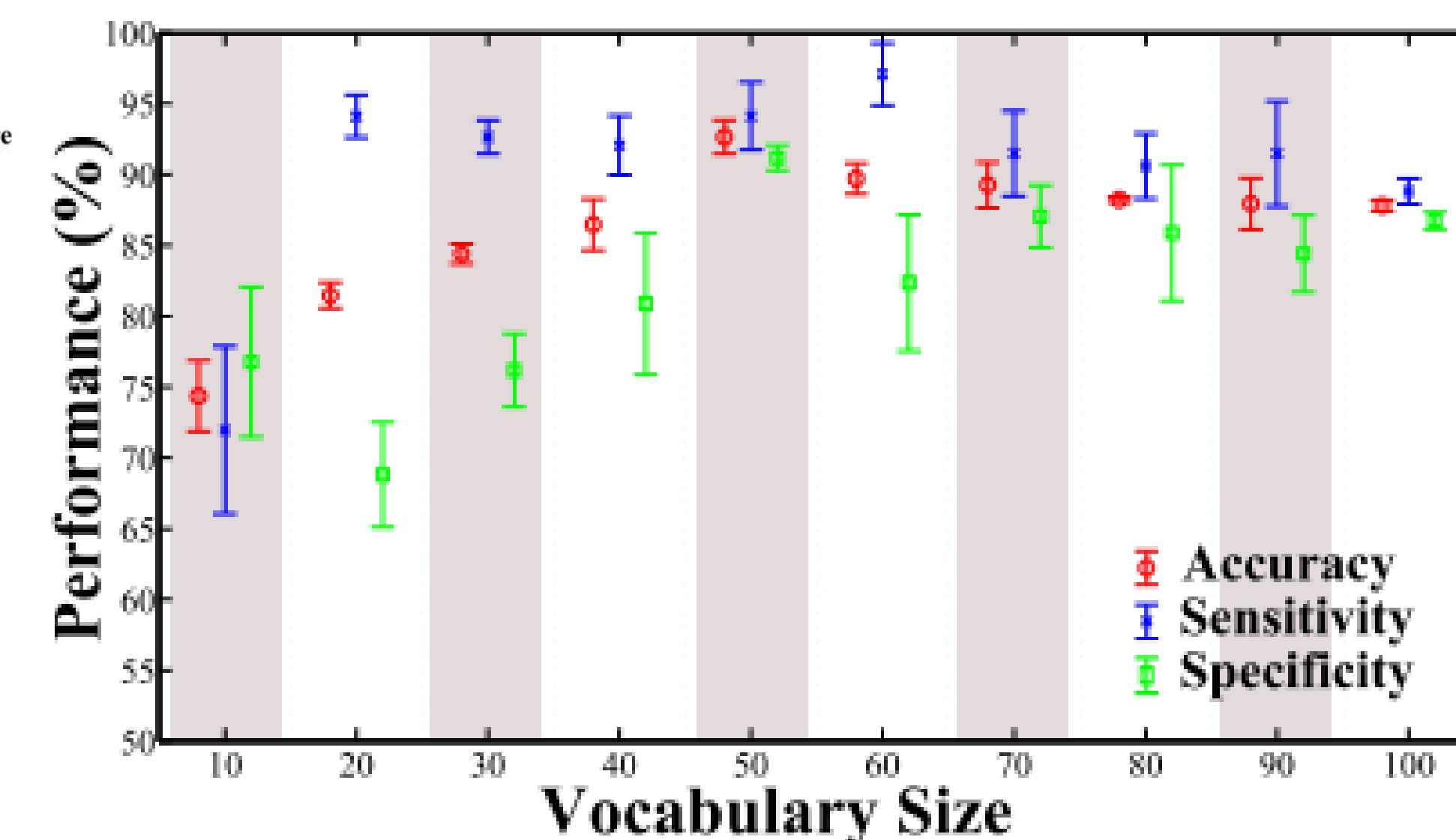## RESULTS

Step1.1, Results of saliency extraction.
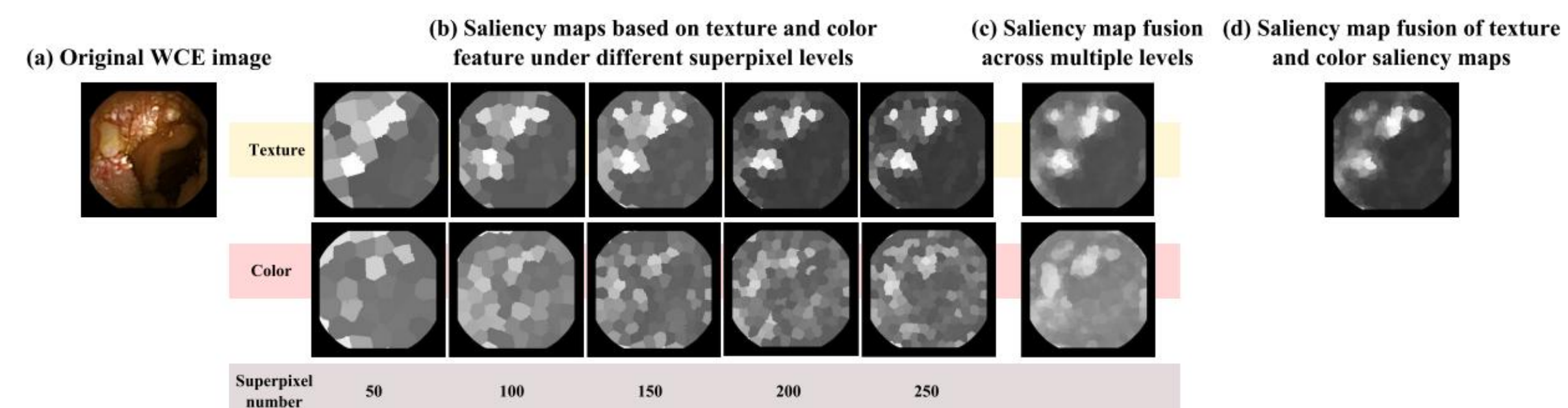
Step1.2, Comparison results qualitatively and quantitatively.

Original images   FT   AC   GBVS   MSSS   SDSP   Our method   Ground truth
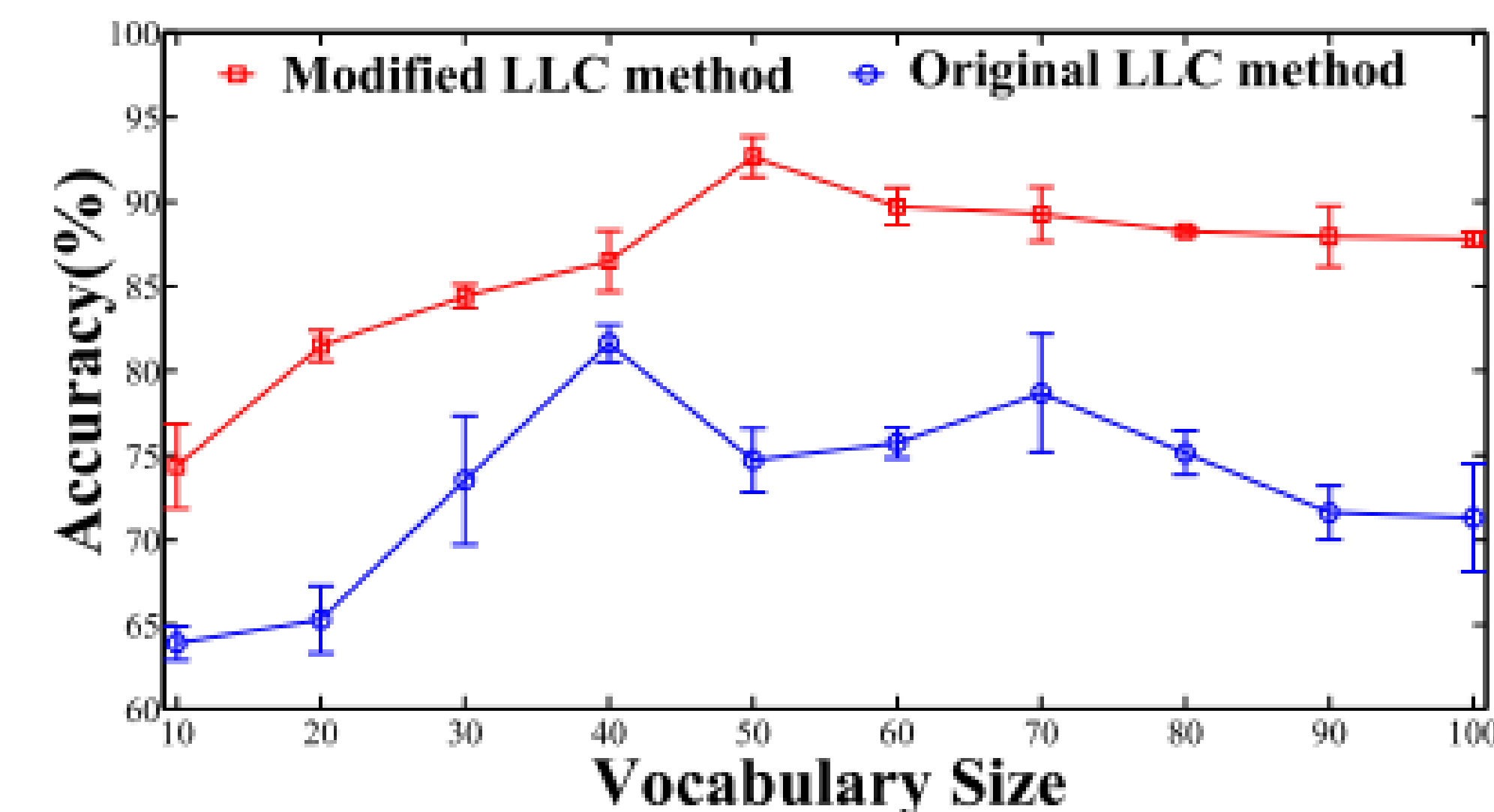

- Precision corresponds to the ratio of saliency pixels correctly assigned to all the pixels of extracted regions.
- Recall is defined as the percentage of detected salient pixels in relation to the ground truth number.

Step2.1, Results of Classification Performance.

Step2.1, Results of comparison on the original LLC method and our modified one.


REFERENCES

1. J. Wang, J. Yang, K. Yu, F. Lv, T. Huang, and Y. Gong, "Locality constrained linear coding for image classification," in Computer Vision and Pattern Recognition (CVPR), 2010 IEEE Conference on. IEEE, 2010, pp. 3360–3367.
2. R. Achanta, A. Shaji, K. Smith, A. Lucchi, P. Fua, and S. Susstrunk, "Slic superpixels compared to state-of-the-art superpixel methods," Pattern Analysis and Machine Intelligence, IEEE Transactions on, vol. 34, no. 11, pp. 2274–2282, 2012.

ACKNOWLEDGEMENTS
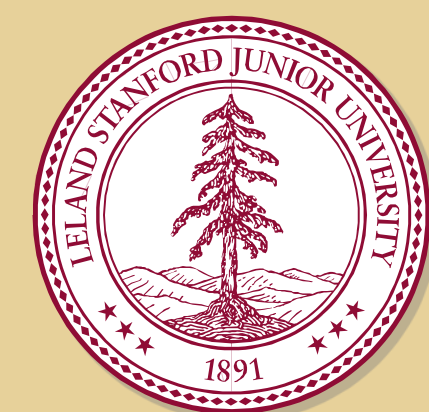
Annotation Imaging Markup API & Semantic Information Extraction From Free Text Mammography Reports

Hakan Bulu, PhD, Daniel L. Rubin, MD, MS

ISiS
Information Sciences
in Imaging at Stanford

Annotation Imaging Markup (AIM) project defines an information model for image annotation and markup in health care. It can be used to annotate images for clinical and teaching purposes, standardized image annotation and markup is most critical in clinical trials.

The AIM API is a Java library which provides developers a framework that will enable them to adopt AIM in their applications.

```xml
<?xml version="1.0" encoding="UTF-8" standalone="no"?>
<ImageAnnotationCollection xmlns="gme://caCORE.caCORE/4.4/edu.north
    <uniqueIdentifier root="qz4v4pltldlynrrsl6oedex40qgrjup3mfijwkg
    <dateTime value="2014-06-20T12:38:43"/>
    <user>
        <name value="admin"/>
        <loginName value="admin"/>
        <roleInTrial/>
    </user>
    <equipment>
        <manufacturerName value="GE MEDICAL SYSTEMS"/>
        <manufacturerModelName value=""/>
        <softwareVersion value="LightSpeedApps308I.2_H3.1M5"/>
    </equipment>
    <person>
        <name value="AJB-1-265-338089^^^^"/>
        <id value="338089146142790150429846112194538233781"/>
        <birthDate value="1978-01-16T00:00:00"/>
        <sex value="M"/>
        <ethnicGroup/>
    </person>
    <imageAnnotations>
        <ImageAnnotation>
```

```java
// Creating new intance of
// ImageAnnotationCollection class
ImageAnnotationCollection iac =
        new ImageAnnotationCollection();
// Creating new intance of
// Equipment class
Equipment equ =
        new Equipment();
//*** Setting properties of the equipment
equ.setManufacturerName(
        new ST("GE MEDICAL SYSTEMS"));
equ.setManufacturerModelName(
        new ST(""));
equ.setSoftwareVersion(
        new ST("LightSpeedApps308I.2_H3.1M5"));
// Setting Equipment of
// the ImageAnnotationCollection
iac.setEquipment(equ);
```

INTRODUCTION

In radiology reports, there is a huge amount of medical data in unstructured text format. Therefore there is a need to use NLP methodologies to discover important information from this data.

METHODS

- Converting unstructed free-text mammography reports to srtuctred format (XML).
- Calculating similarity score between the abnormalities.
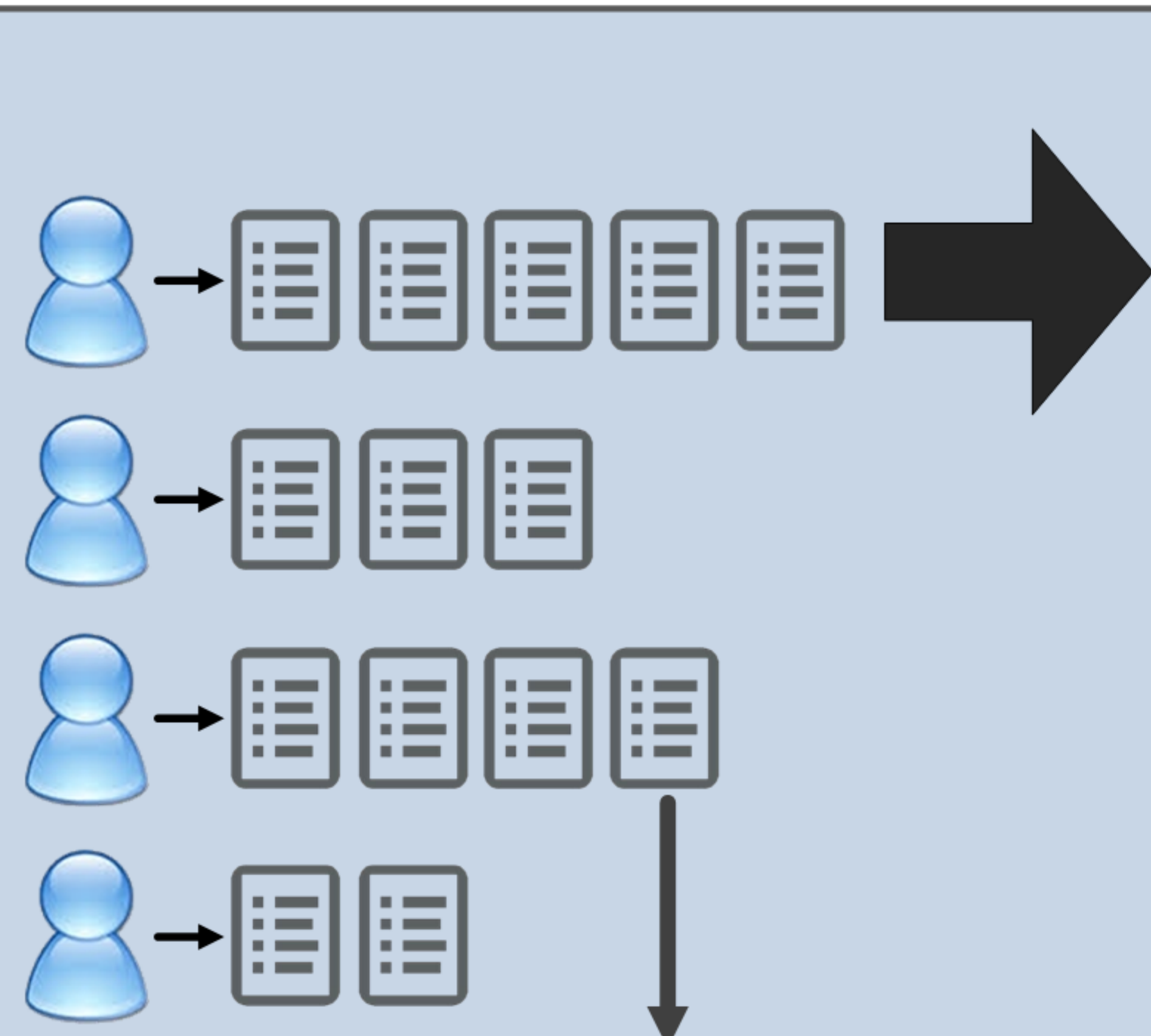- Connecting the abnormalities according to their similarity scores.

RESULTS

From free-text mammography reports, we extract type of the abnormalities with their characteristic (i.e. shape, density, margin etc.), size and anatomic locations.

With these information;

- We can query the huge free-text repositories, i.e. "Find all irregular and high density masses."
- We can follow-up any particular abnormality, i.e. "Size of the mass is decreased from 1.1 cm to 7 mm during the past 3 years."
- We can run data mining algorithms and can find new relationships between the abnormality characteristics.

#70A BILATERAL DIAGNOSTIC MAMMOGRAM: 7/15/1999 CLINICAL: Nodules daughter had premenopausal breast cancer Comparison is made to exam dated: 7/16/1997 Froedtert Memorial Lutheran Hospital. There are scattered fibroglandular elements in both breasts that could obscure a lesion on mammography. Scattered benign appearing calcifications scattered benign appearing ...

04.28.1999 — Scattered_Fibroglandular_Densities

*** Left Breast ***

Calcification
Category Benign
Laterality Left

Calcification
Type Punctate
Laterality Left
ClockFace 12
Depth Anterior

Spacial Case
Type Lymph_Node
Laterality Left
Quadrant Upper_Outer

Associated Finding
Type Architectual_Distortion
Laterality Left
ClockFace 12
Depth Anterior

05.17.2000 — Heterogeneously_Dense

*** Left Breast ***

Calcification
Category Benign
Laterality Left

Calcification
Type Punctate
Laterality Left
ClockFace 1
Depth Anterior

Spacial Case
Type Lymph_Node
Laterality Left

Associated Finding
Type Architectual_Distortion
Laterality Left
ClockFace 1
Depth Anterior

*** Right Breast ***

Mass
Shape Oval
Margin Circumscribed
Size 1.5 cm
Laterality Right
ClockFace 10
Depth Posterior

Mass
Shape Oval
Margin Obscured
Size 1.5 cm
Laterality Right
ClockFace 10
Depth Middle
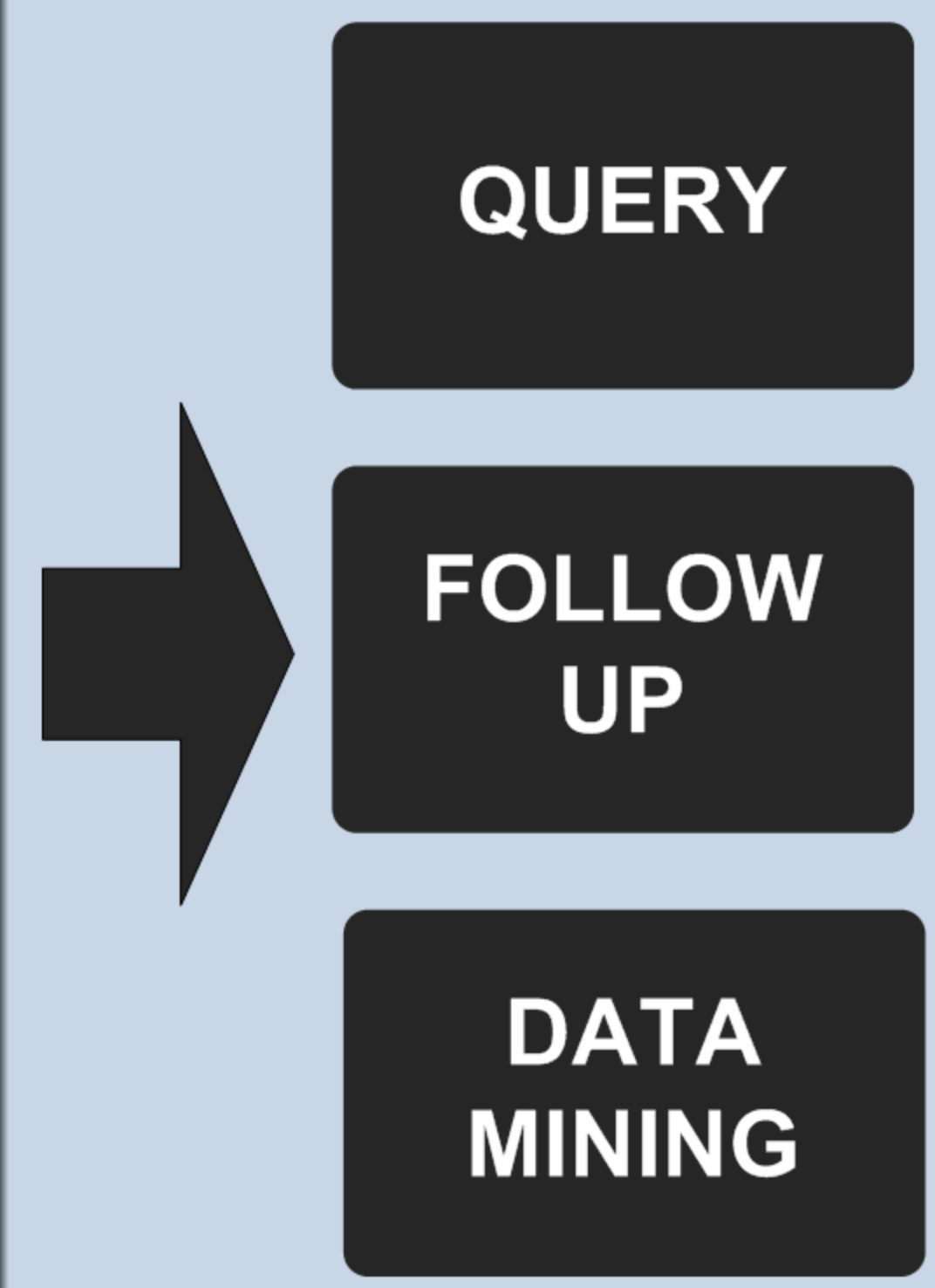
Calcification
Category Benign
Laterality Right

12.05.2000 — Heterogeneously_Dense

*** Right Breast ***

Mass
Shape Oval
Margin Circumscribed
Size 1.9 cm
Laterality Right
ClockFace 7
Depth Middle

Mass
Shape Oval
Margin Circumscribed
Size 1.7 cm
Laterality Right
ClockFace 8
Depth Posterior

Calcification
Distribution Diffuse_Scattered
Laterality Right

08.27.2001 — Heterogeneously_Dense

*** Left Breast ***

Mass
Shape Oval
Margin Circumscribed
Size 1.1 cm
Laterality Left
ClockFace 7
Depth Anterior

Calcification
Category Benign
Laterality Left

Calcification
Type Punctate
Laterality Left
ClockFace 1
Depth Anterior

Spacial Case
Type Lymph_Node
Laterality Left

Associated Finding
Type Architectual_Distortion
Laterality Left
ClockFace 1
Depth Anterior

*** Right Breast ***

Mass
Shape Oval
Margin Circumscribed
Size 2 cm
Laterality Right
ClockFace 10
Depth Posterior

Mass
Shape Oval
Margin Obscured

04.29.2002 — Heterogeneously_Dense

*** Left Breast ***

Mass
Shape Oval
Margin Circumscribed
Size 9 mm
Laterality Left
ClockFace 7
Depth Anterior

Calcification
Category Benign
Laterality Left

Calcification
Category Benign
Type Punctate
Laterality Left
ClockFace 1
Depth Anterior

Spacial Case
Type Lymph_Node
Laterality Left

Associated Finding
Type Architectual_Distortion
Laterality Left
ClockFace 1
Depth Anterior

*** Right Breast ***

Mass
Shape Oval
Margin Circumscribed
Size 1.8 cm
Laterality Right
ClockFace 10
Depth Posterior

Mass
Shape Oval

05.29.2003 — Heterogeneously_Dense

*** Left Breast ***

Mass
Shape Oval
Margin Circumscribed
Size 7 mm
Laterality Left
ClockFace 7
Depth Anterior

Calcification
Category Benign
Laterality Left

Calcification
Type Punctate
Laterality Left
ClockFace 1
Depth Anterior

Spacial Case
Type Lymph_Node
Laterality Left

*** Right Breast ***

Mass
Shape Oval
Margin Circumscribed
Size 1.8 cm
Laterality Right
ClockFace 10
Depth Middle

Mass
Shape Oval
Margin Obscured
Size 1.8 cm
Laterality Right
Depth Anterior
Region Central

Calcification

QUERY

FOLLOW UP

DATA MINING

Automated Methods for retinal Disease Quantification and Prediction of Progression

Luis de Sisternes, PhD,[1] Theodore Leng, MD, MS,[2] Daniel L. Rubin, MD, MS[1]

[1] Departments of Radiology and Medicine (Biomedical Informatics Research), Stanford University School of Medicine, Stanford, CA, USA

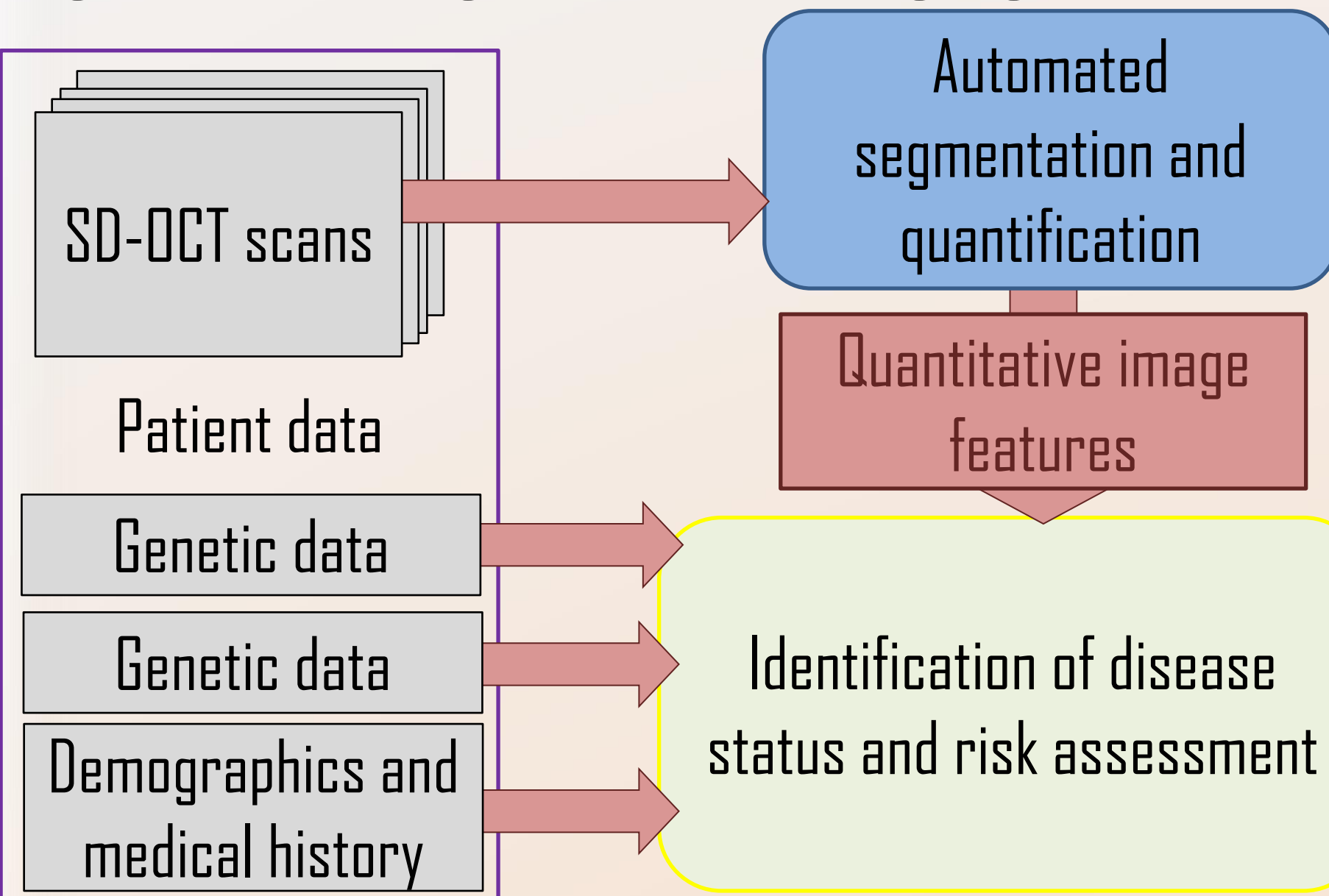[2] Byers Eye Institute at Stanford, Stanford University School of Medicine, Palo Alto, CA, USA

PURPOSE

Characterization of retinal disease typically based on the inspection of 2D color fundus photographs. SD-Optical Coherence Tomography (SD-OCT):

- Possibility of axial characterization of sub-retinal structures in a few micro-meter scale.
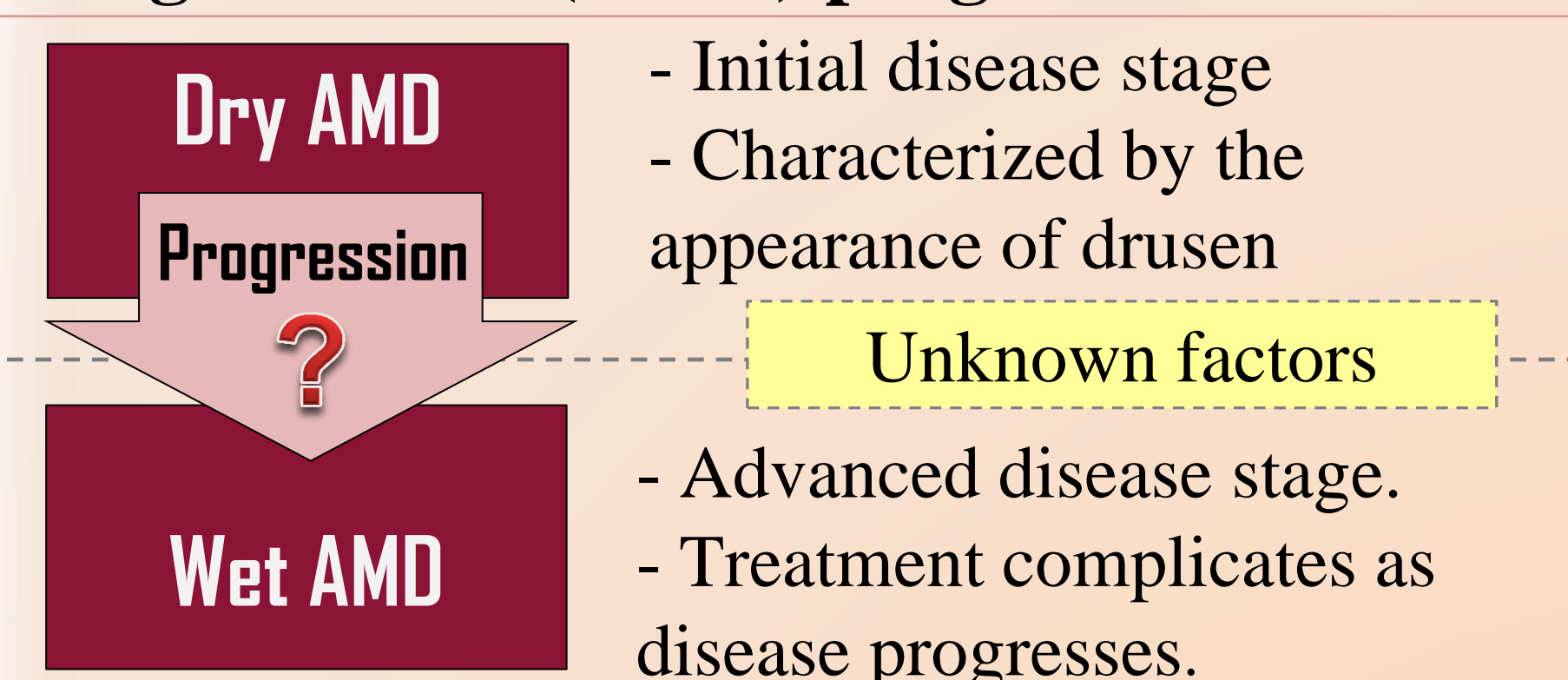- Manual segmentation extremely tedious.

SD-OCT cube / B-scan / A-scan / azimuthal / lateral / axial (depth)
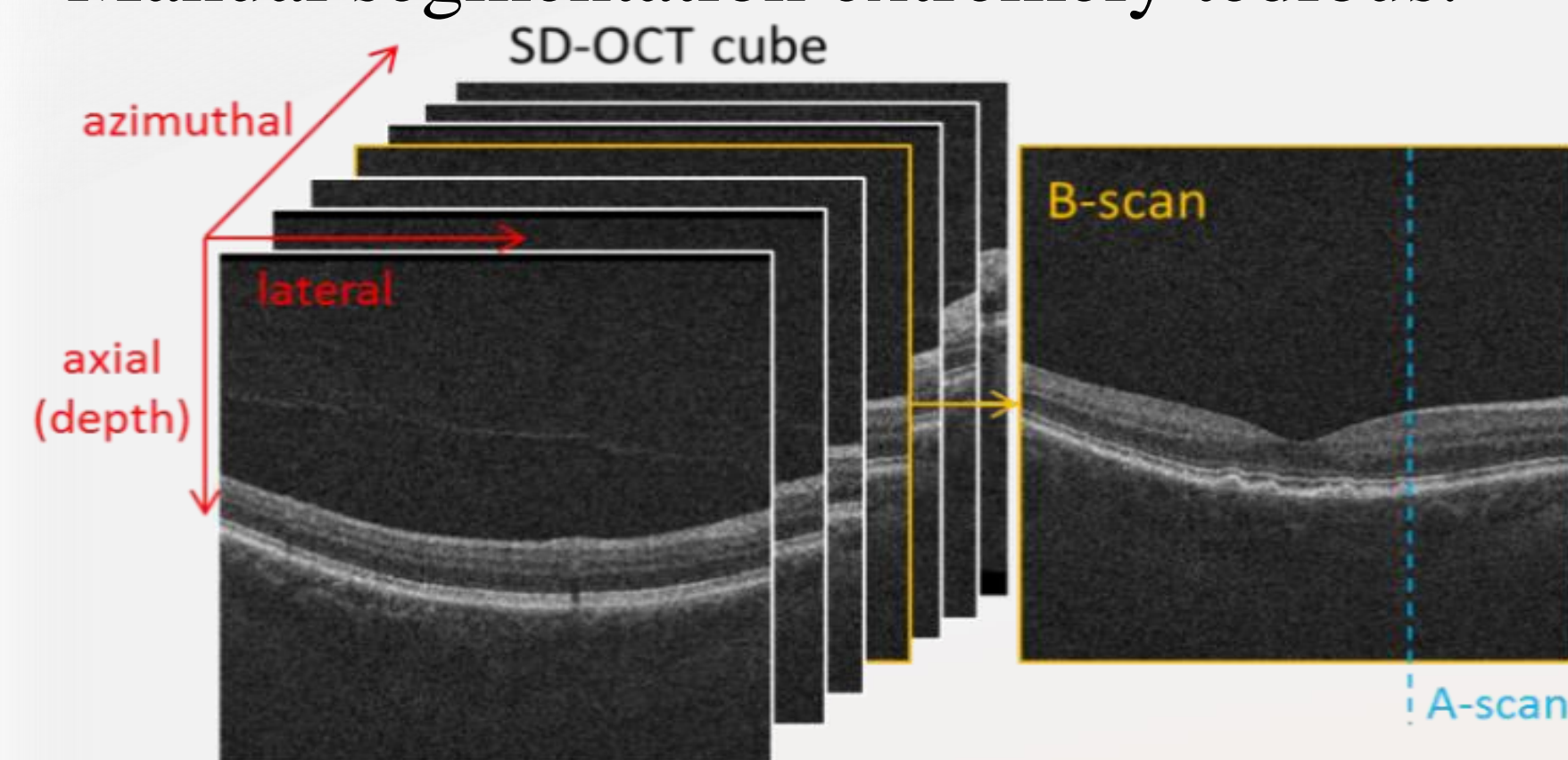
We propose fully automated methods to quantitatively assess disease and predict progression using SD-OCT imaging

SD-OCT scans → Automated segmentation and quantification → Quantitative image features

Patient data: Genetic data, Genetic data, Demographics and medical history → Identification of disease status and risk assessment

APPLICATIONS

- Focus: **Prediction of Age-related macular degeneration (AMD) progression**.

Dry AMD
- Initial disease stage
- Characterized by the appearance of drusen

Progression ? — Unknown factors

Wet AMD
- Advanced disease stage.
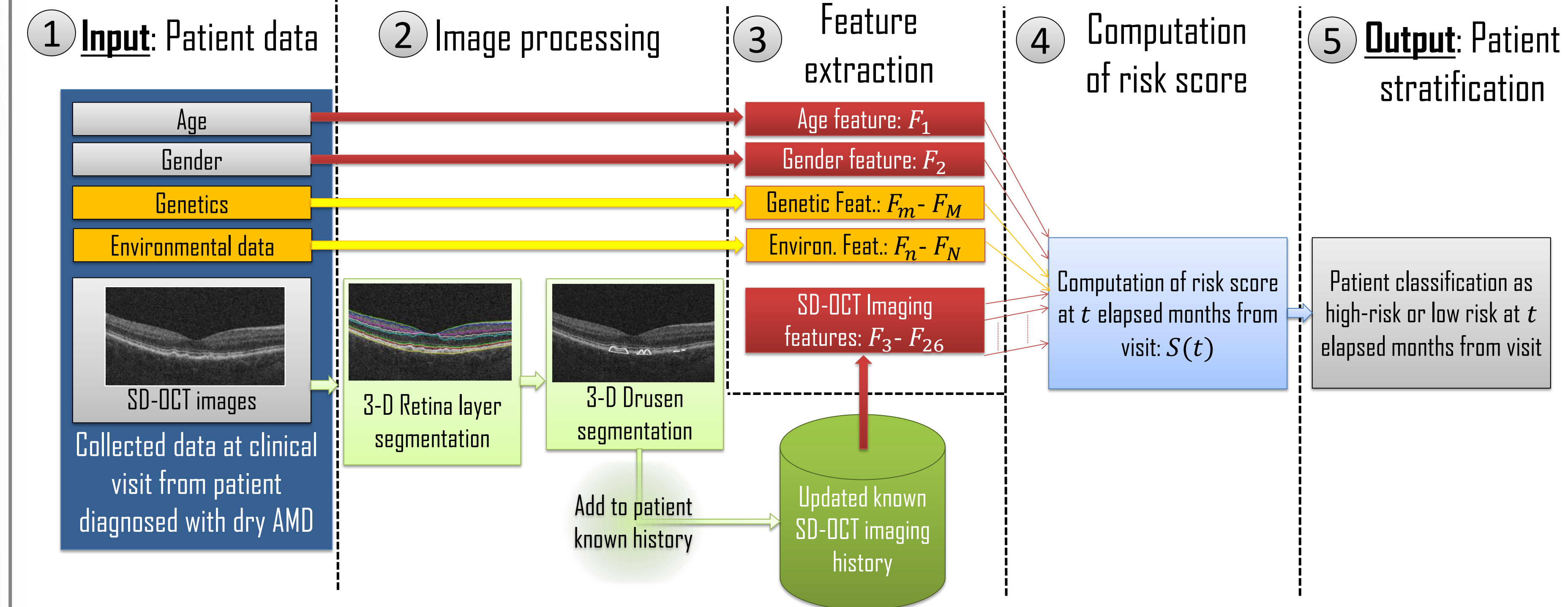- Treatment complicates as disease progresses.

Prompt intervention can greatly improve visual outcome. High-risk patients should have more follow-up visits than low-risk patients.
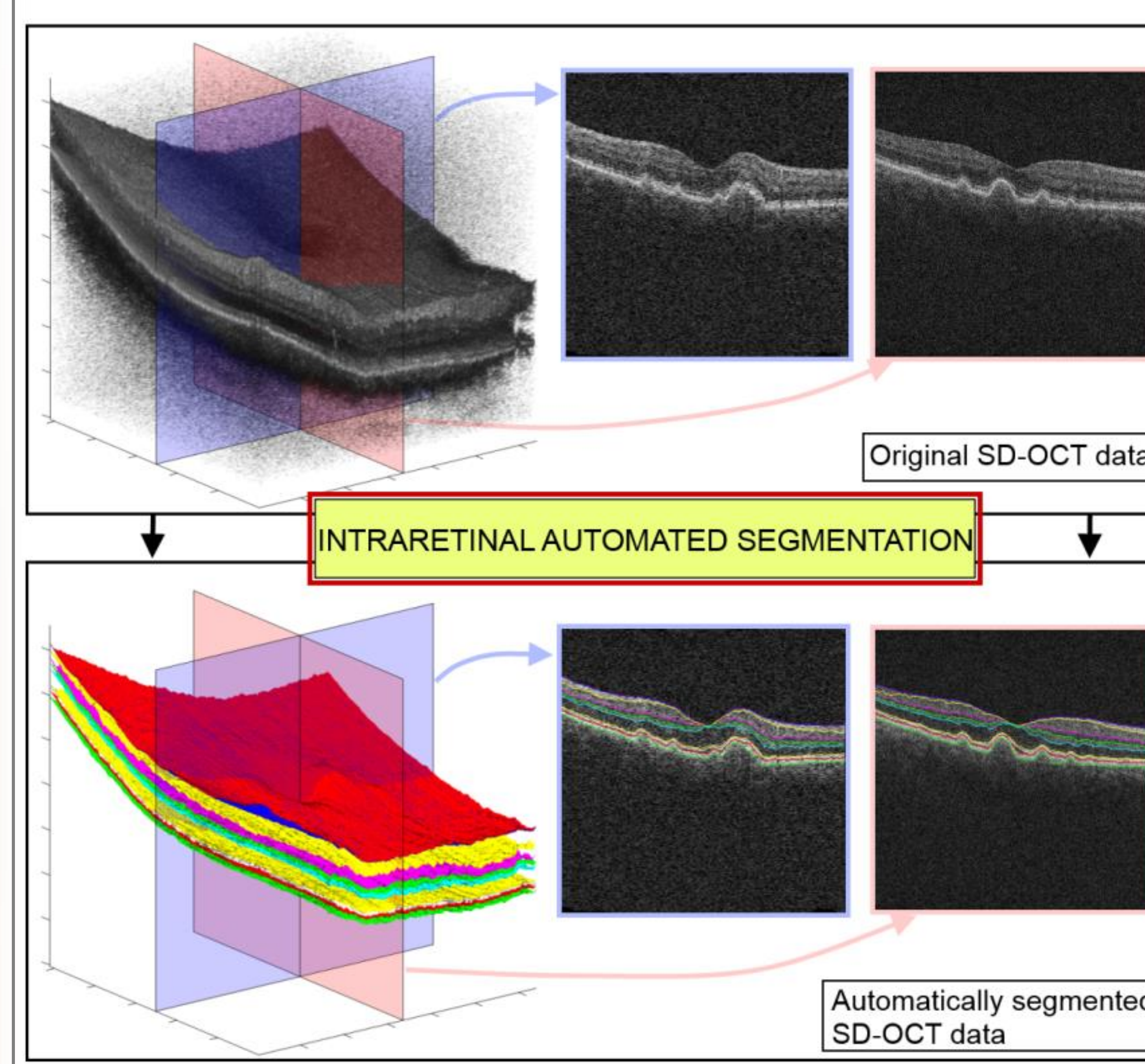
- **GA** quantification and prediction.
- **HQC toxicity** severity assessment.
- **Macular hole** recovery assessment.
- **Retinitis pigmentosa** characterization.
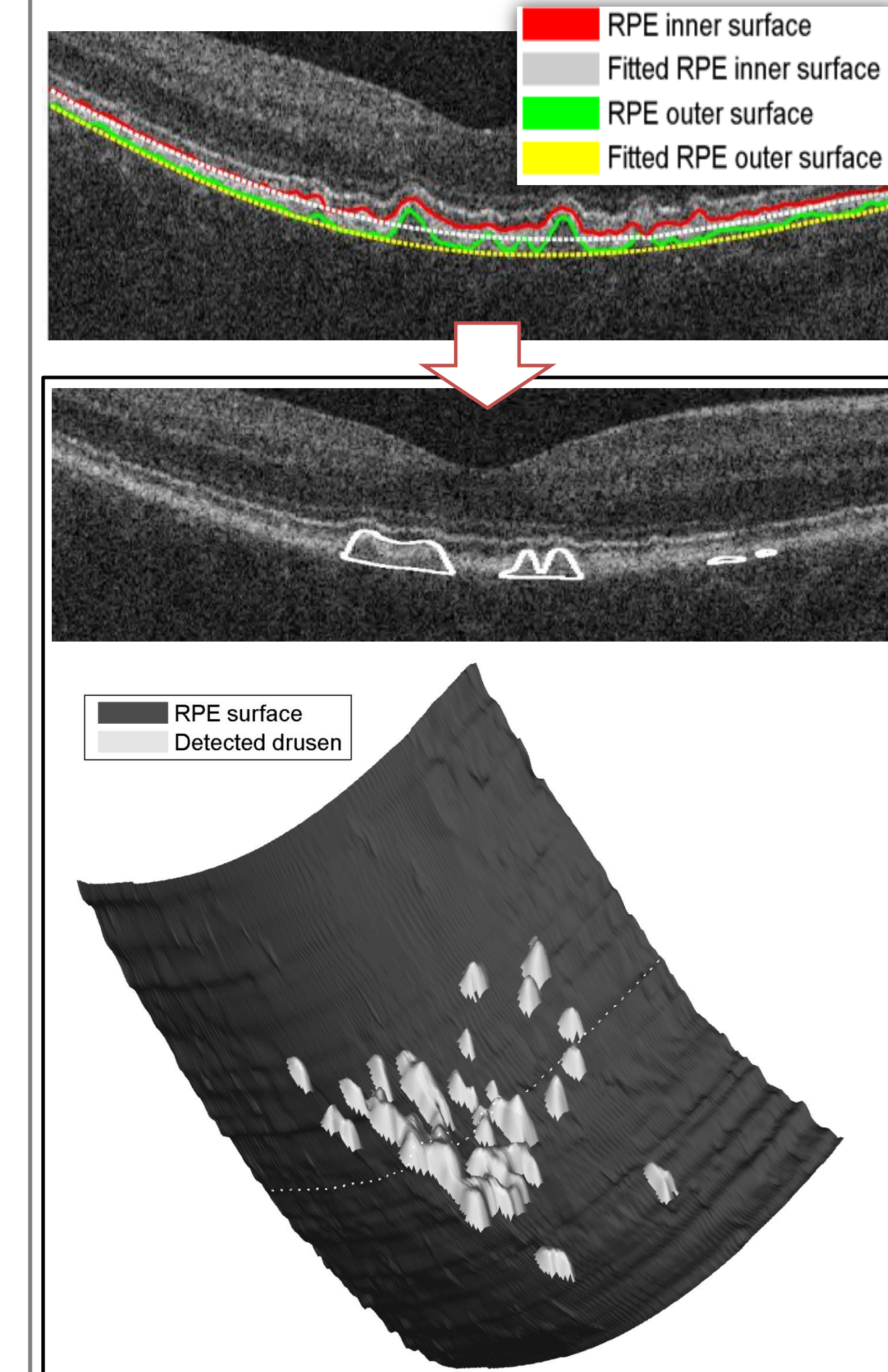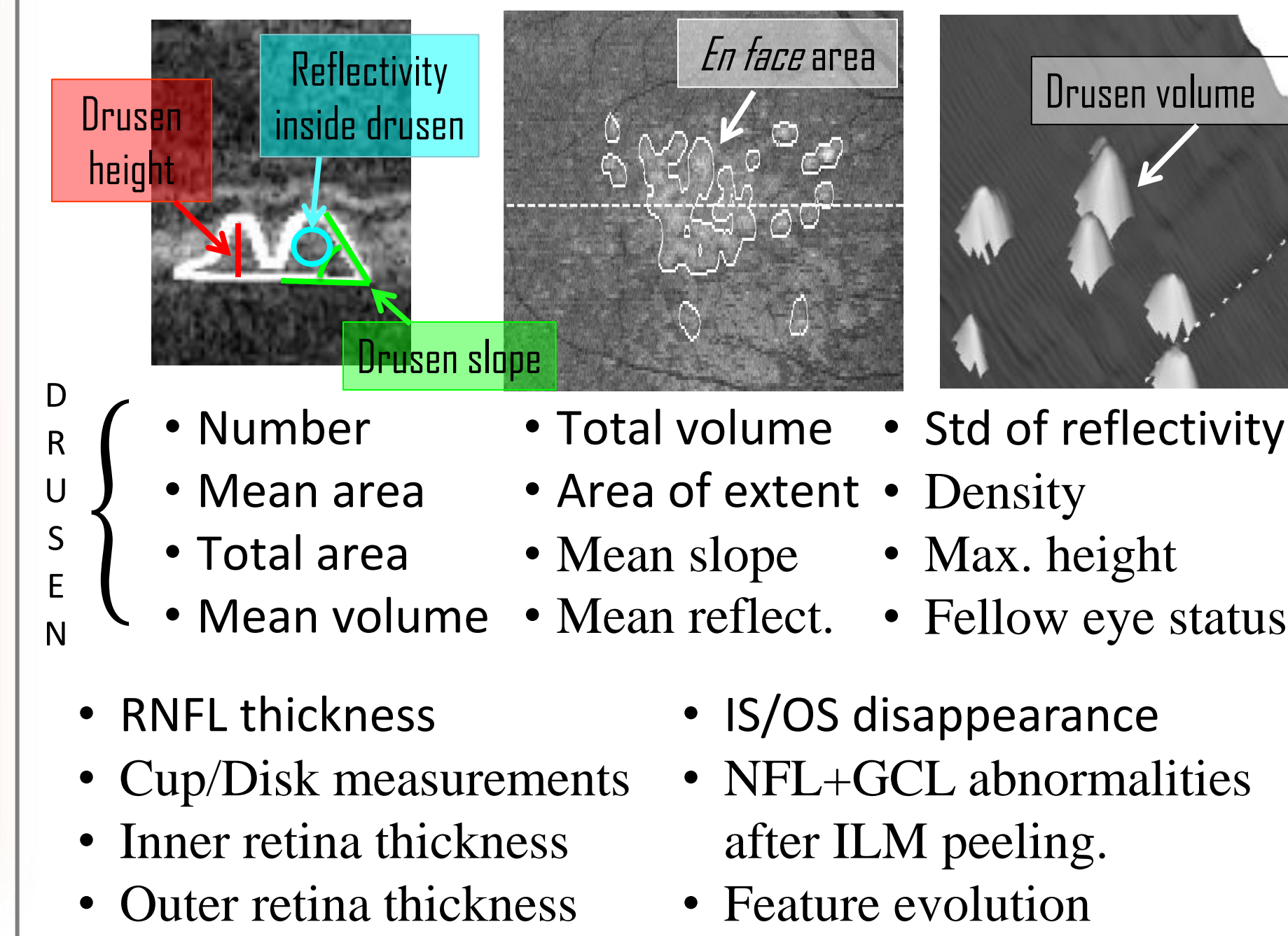- **Glaucoma** characterization and assessment.

METHODS

OVERVIEW

1. **Input**: Patient data
2. Image processing
3. Feature extraction
4. Computation of risk score
5. **Output**: Patient stratification

Age → Age feature: F_1
Gender → Gender feature: F_2
Genetics → Genetic Feat.: $F_m - F_M$
Environmental data → Environ. Feat.: $F_n - F_N$
SD-OCT images → 3-D Retina layer segmentation → 3-D Drusen segmentation → SD-OCT Imaging features: $F_3 - F_{26}$

Computation of risk score at t elapsed months from visit: $S(t)$

Patient classification as high-risk or low risk at t elapsed months from visit

Collected data at clinical visit from patient diagnosed with dry AMD

Add to patient known history → Updated known SD-OCT imaging history

3-D RETINAL LAYER SEGMENTATION

INTRARETINAL AUTOMATED SEGMENTATION

Original SD-OCT data

Automatically segmented SD-OCT data

3-D DRUSEN SEGMENTATION

- RPE inner surface
- Fitted RPE inner surface
- RPE outer surface
- Fitted RPE outer surface

- RPE surface
- Detected drusen

FEATURE EXTRACTION: QUANTIFICATION

Drusen height / Reflectivity inside drusen / En face area / Drusen volume / Drusen slope

DRUSEN:
- Number
- Mean area
- Total area
- Mean volume
- Total volume
- Area of extent
- Mean slope
- Mean reflect.
- Std of reflectivity
- Density
- Max. height
- Fellow eye status

- RNFL thickness
- Cup/Disk measurements
- Inner retina thickness
- Outer retina thickness
- IS/OS disappearance
- NFL+GCL abnormalities after ILM peeling
- Feature evolution

COMPUTATION OF RISK SCORE

Progression score at time t based in a Poisson distribution given α predictors

$$P(t, \alpha) = e^{(\beta_0 + \beta_1\alpha_1 + \beta_2\alpha_2 + \ldots + \beta_K\alpha_K)\cdot t}$$

- $[\beta_1, \ldots, \beta_K]$ found by generalized linear regression for increasing number of features.

PATIENT STRATIFICATION
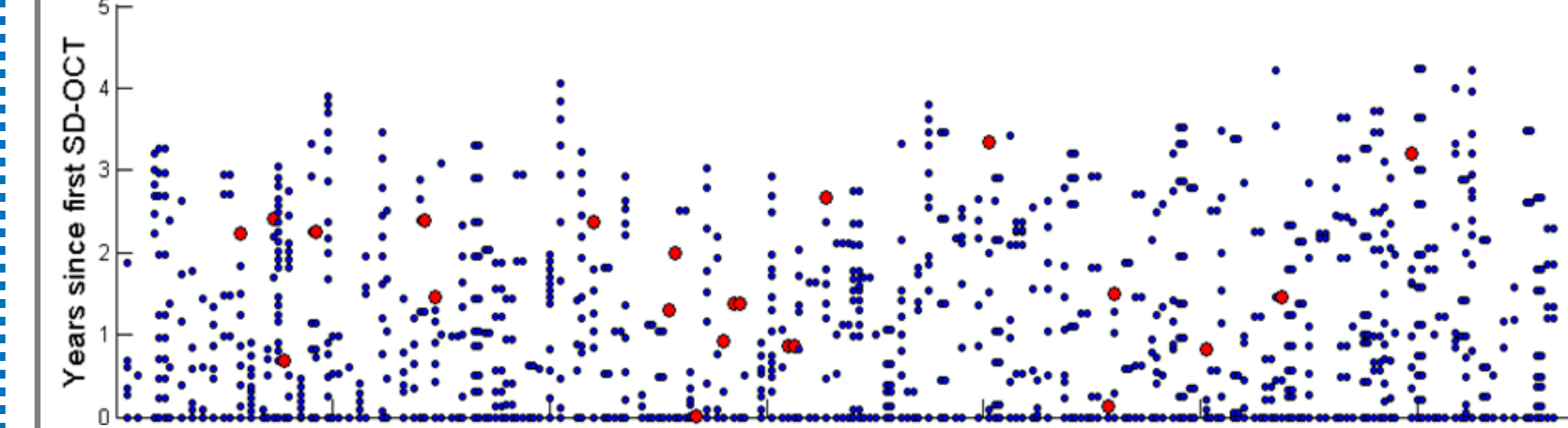
Eye classified at time t since clinical visit:

$$Category(t) \begin{cases} High-risk & if\ S(t) \geq T \\ Low-risk & if\ S(t) < T \end{cases}$$

Threshold T determined by desired sensitivity/specificity.
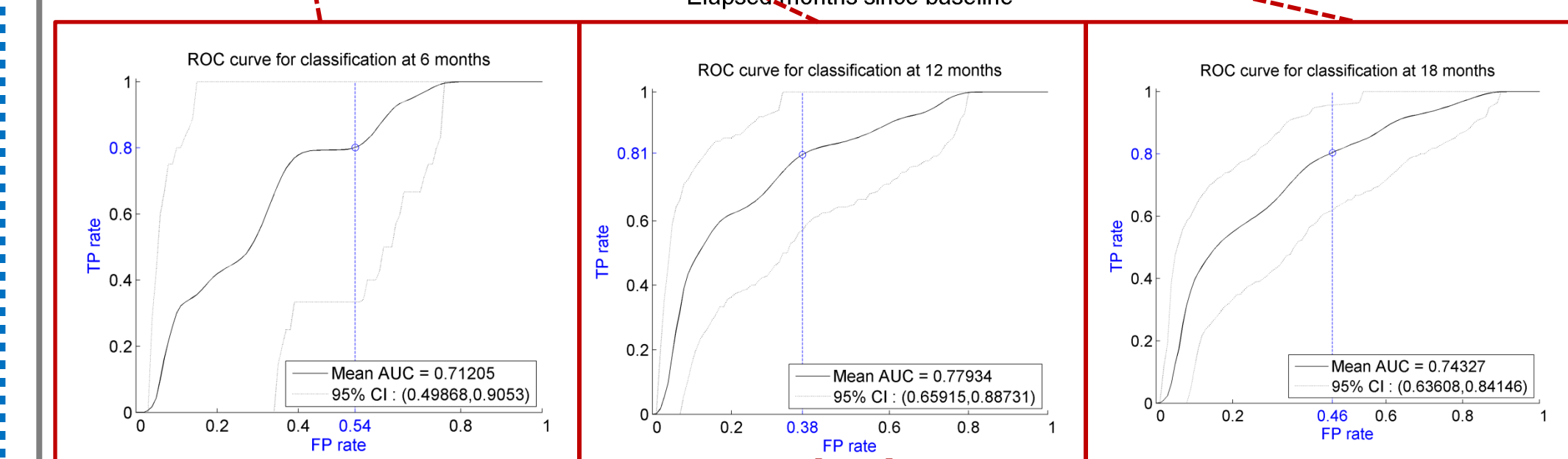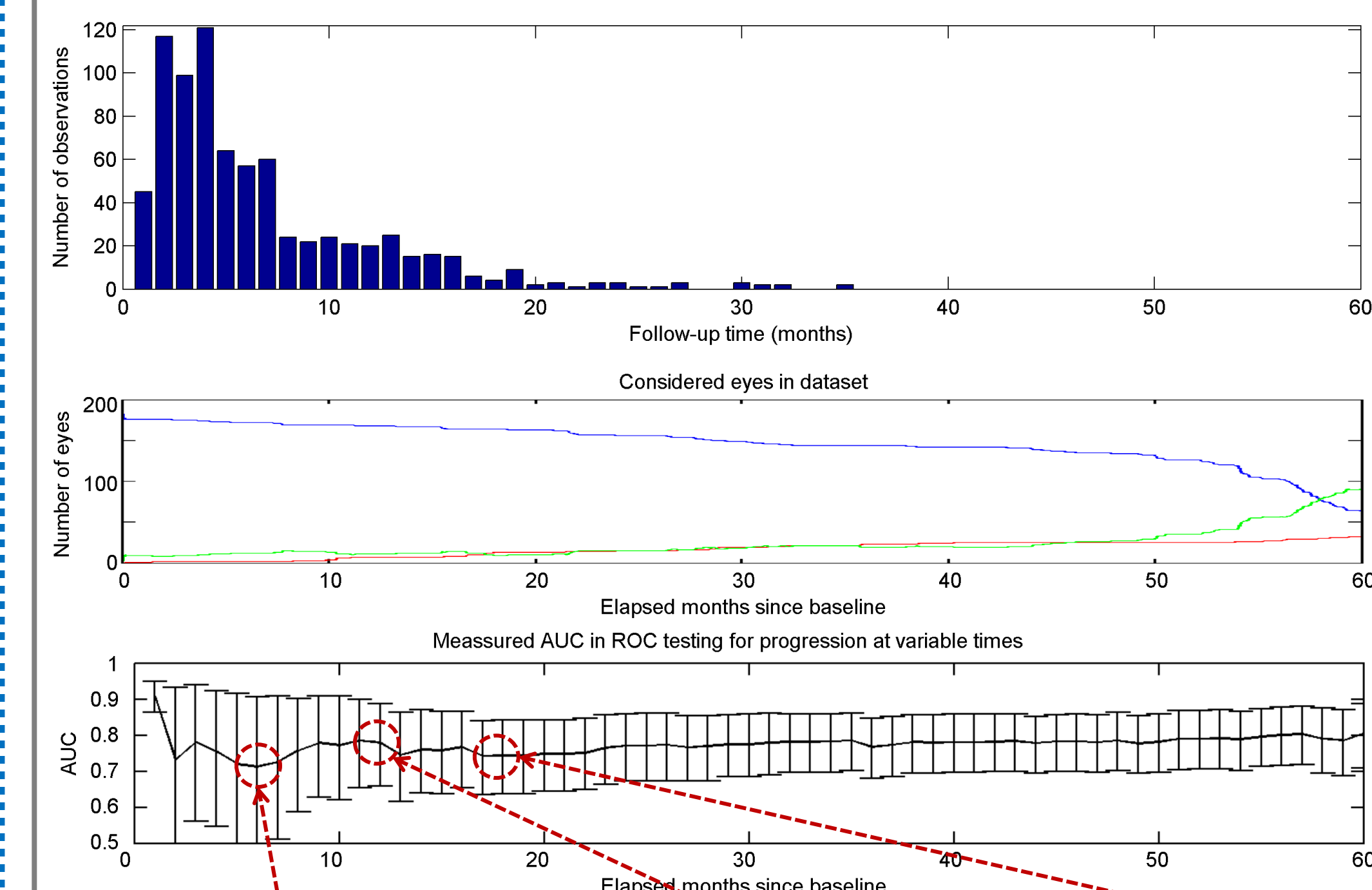
RESULTS

COLLECTED DATA / EVALUATION DESIGN

- 186 AMD eyes (128 patients) over a period of 5 years.
- 36 eyes showing progression during clinical follow-up.
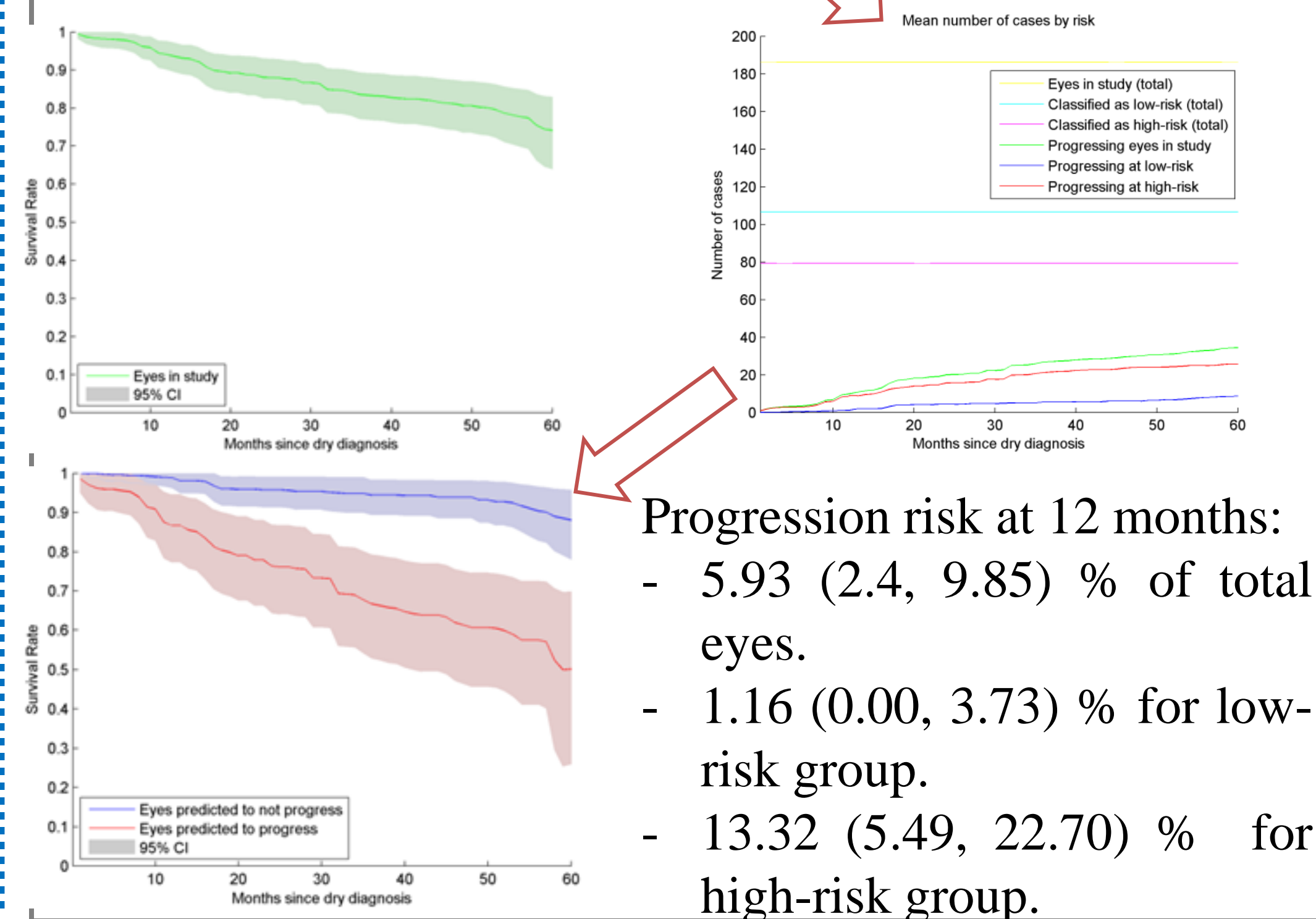

- Training on 790 observations: Pairs of feature set at dry AMD clinical visit and known outcome at follow-up.
- Patient based 10-fold cross validation.
- Confidence intervals by 10^6 bootstrap resampling with replacement.

PERFORMANCE AT GIVEN ELAPSED TIME SINCE CLINICAL VISIT

ROC curve for classification at 6 months: Mean AUC = 0.71205, 95% CI (0.49868,0.9053)
ROC curve for classification at 12 months: Mean AUC = 0.77934, 95% CI (0.69915,0.88731)
ROC curve for classification at 18 months: Mean AUC = 0.74327, 95% CI (0.59008,0.84146)

SURVIVAL AT 12 MONTHS CLASSIFICATION

Progression risk at 12 months:

- 5.93 (2.4, 9.85) % of total eyes.
- 1.16 (0.00, 3.73) % for low-risk group.
- 13.32 (5.49, 22.70) % for high-risk group.

ePAD: Enabling routine imaging assessment of cancer treatment response in the clinical workflow

Daniel L. Rubin, MD, MS[1] Debra Willrett, MS[1] Martin O'Connor, MS[1] Cleber Hague[2] Dilvan A. Moreira, PhD[2] and Camille Kurtz, PhD[3]

[1]Department of Radiology, Stanford University   [2]Department of Computer Science, University of São Paulo, Brazil   [3]University Paris Descartes, France

OBJECTIVES

Quantitative assessment of images of cancer patients is crucial to provide clinicians with objective information about treatment response needed for decision making. Making lesion measurements is laborious and error-prone. The electronic Physician Annotation Device (ePAD) is a Web-based tool to assist radiologists in viewing and measuring cancer lesions. Though presently geared to research settings, it could ultimately be adopted in routine clinical practice. Moreover, through its modular design, it is a platform which the community can adapt and extend to meet the needs of quantitative imaging practice.

SYSTEM

ePAD is a rich Web client workstation providing image viewing and annotation features. The ePAD client communicates with a server-side component which queries an existing PACS and stores ePAD image annotations in an AIM database. These resources are searchable in applications such as content based image retrieval and cancer lesion tracking.

Image viewing and reporting with ePAD

ePAD Web Client

Image Viewing and Semantic Annotation
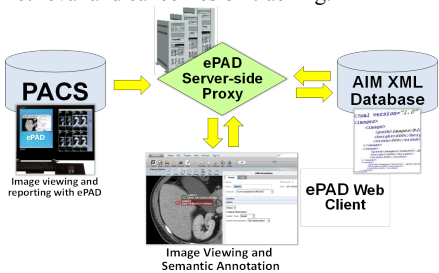
ePAD SUPPORTS AIM TEMPLATES

AIM provides a structured representation of image metadata in computer-readable format. AIM templates provide customizable structured reporting forms. A radiologist views images, makes measurements, and describes their features, while ePAD seamlessly records all data in AIM format, stored in the ePAD AIM database.
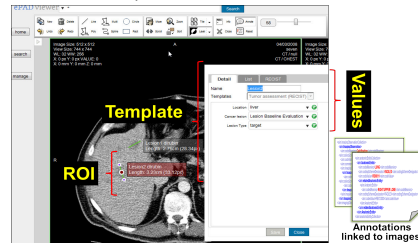
The ePAD AIM database produces automated summaries of target lesions and aggregate measures indicating treatment response.

Automated lesion tracking and summary

EPAD INTEGRATES XNAT

ePAD uses the XNAT platform for managing projects, users, and non-DICOM images to improve interoperability. The ePAD GUI organizes imaging studies under projects.

EPAD API AND PLUGINS

ePAD provides an API and plugin mechanism so that developers can extend the ePAD platform.
API:
1. Java-based programming interface
2. Methods to read/write AIM to AIM database
Plugins:
1. Front-end plugins to extend the user interface
2. Back-end plugins to add quantitative image analysis and processing capabilities

Quantitative Image Feature Plugin

IMAGE ANALYSIS WORKFLOWS

We are developing a pipeline mechanism for automated analysis of quantitative imaging biomarkers directly from the annotated images.
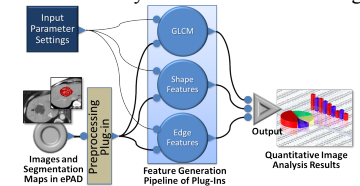
Automated segmentation of PET images

APPLICATIONS

Decision support: ePAD can leverage prior measurements in AIM to prompt the radiologist to annotate all target lesions (and to recognize missing measurements). It can also help the oncologist by producing patient response graphs and waterfall plots automatically from AIM-annotated images.

Auditing and quality assurance: AIM enables linking the lesion measurements to the actual annotations on images for rapid audit and quality assurance on quantitative assessments of images.

Lesion tracking: ePAD can query historical annotations in a patient who had several follow up studies, automatically generating a quantitative imaging summary report.

ACKNOWLEDGEMENTS

Rapid learning with primary healthcare data

Marina Bendersky, Samuel Finlayson, Balasubramanian Narasimhan, Philip W. Lavori, Daniel L. Rubin

Automated assessment of clinical images

Marina Bendersky, Daniel L. Rubin

ISIS — Information Sciences in Imaging at Stanford

OBJECTIVES

- Develop a **rapid learning** system for **cancer decision** support
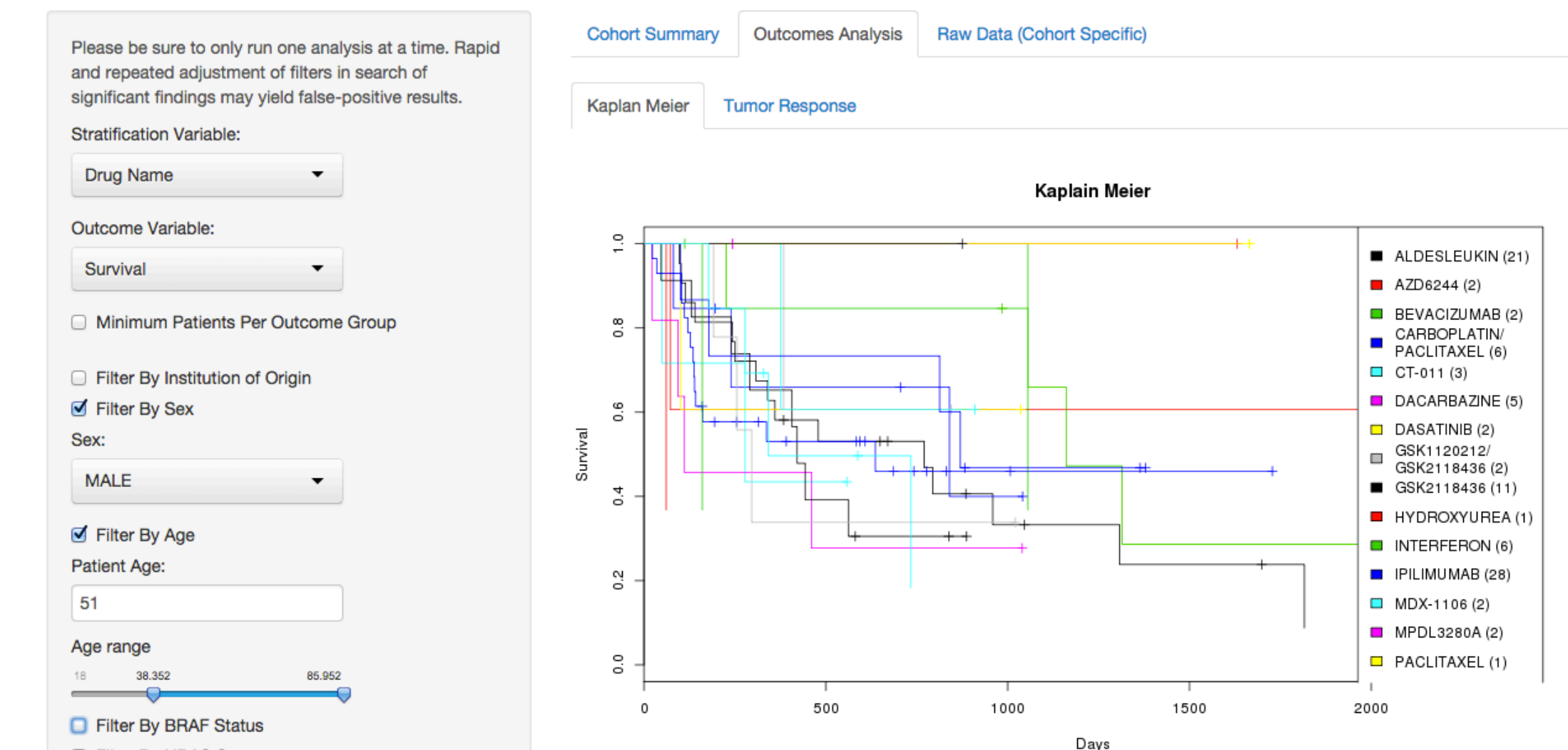- **No data sharing required** since the computation of the models is **distributed**

METHODS / PRELIMINARY RESULTS

Develop a method prototype using **R** and **R 'Shiny'** applications

Front end requires three main processes (**'Shiny'** apps) to:

propose a new distributed computation, set up a master process, and instantiate a slave site.
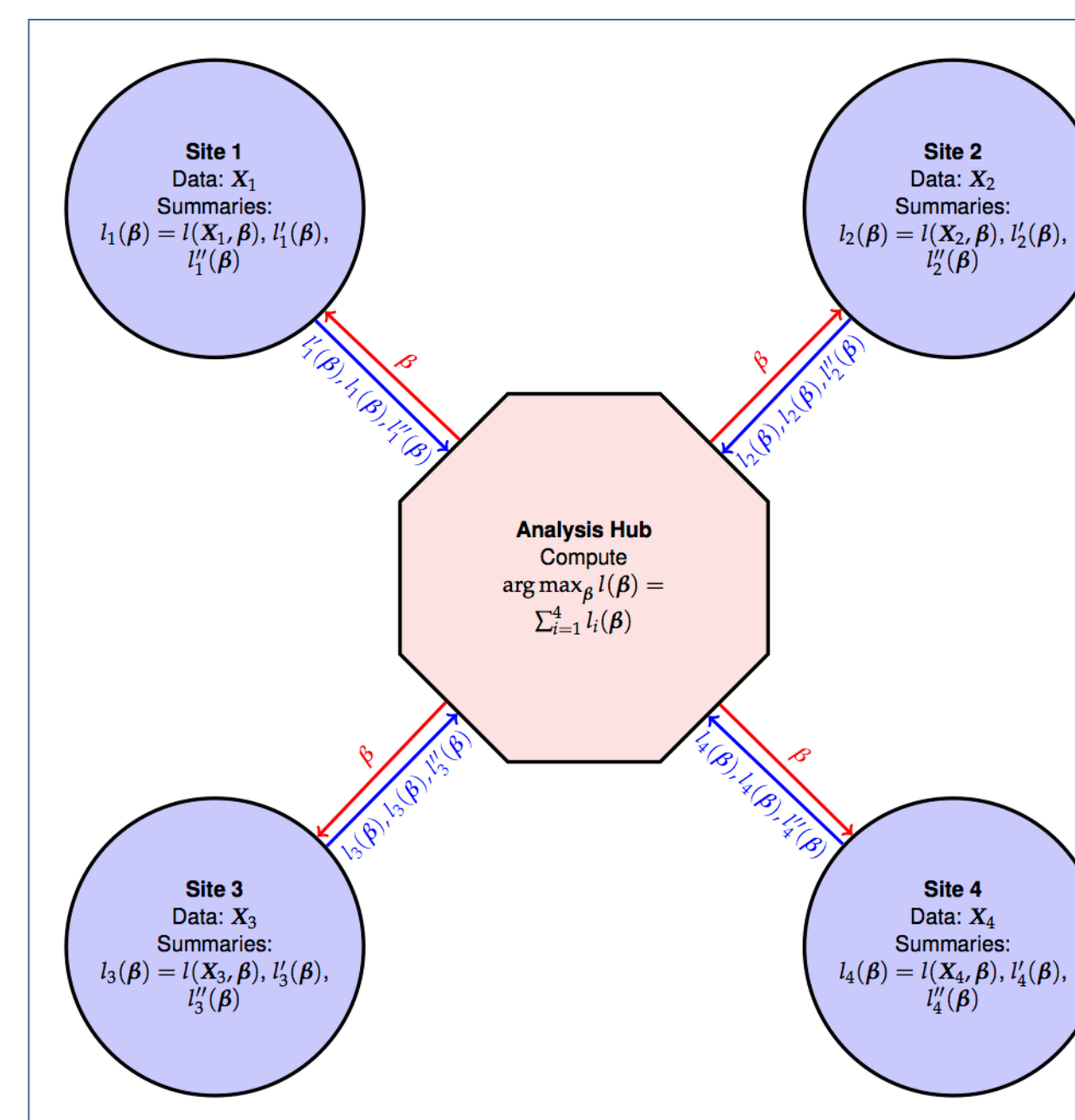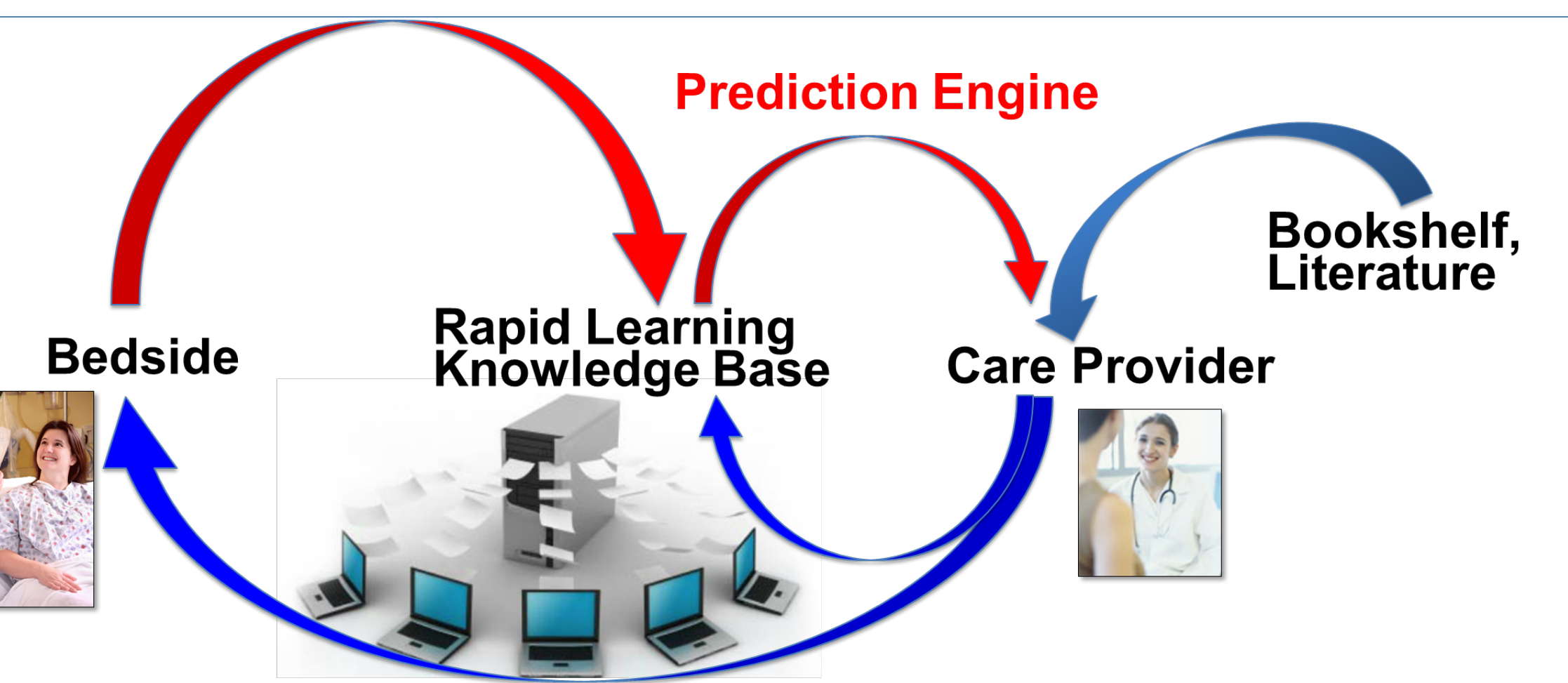

Melanoma Rapid Learning Utility

REFERENCES

- W. Jiang, P. Li, S. Wang, Y. Wu, M. Xue, L. Ohno-Machado, X. Jiang. WebGLORE: a web service for Grid Logistic Regression. Bioinformatics 2013, 29(24):3238-3240

- Y. Wu, X. Jiang, J. Kim, L. Ohno-Machado. Grid Binary Logistic Regression (GLORE): building shared models without sharing data. JAMIA 2012, 19(5):758-764.

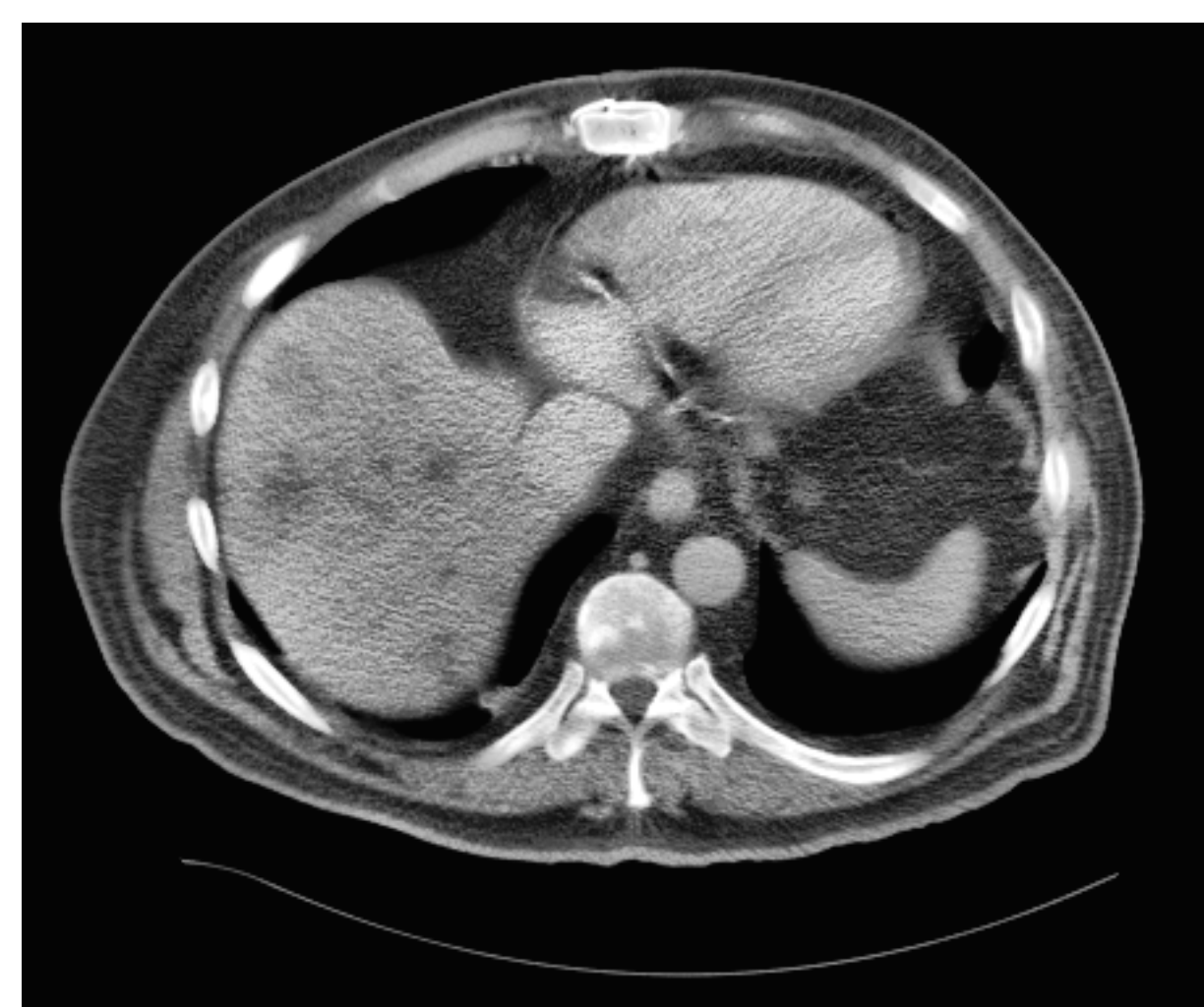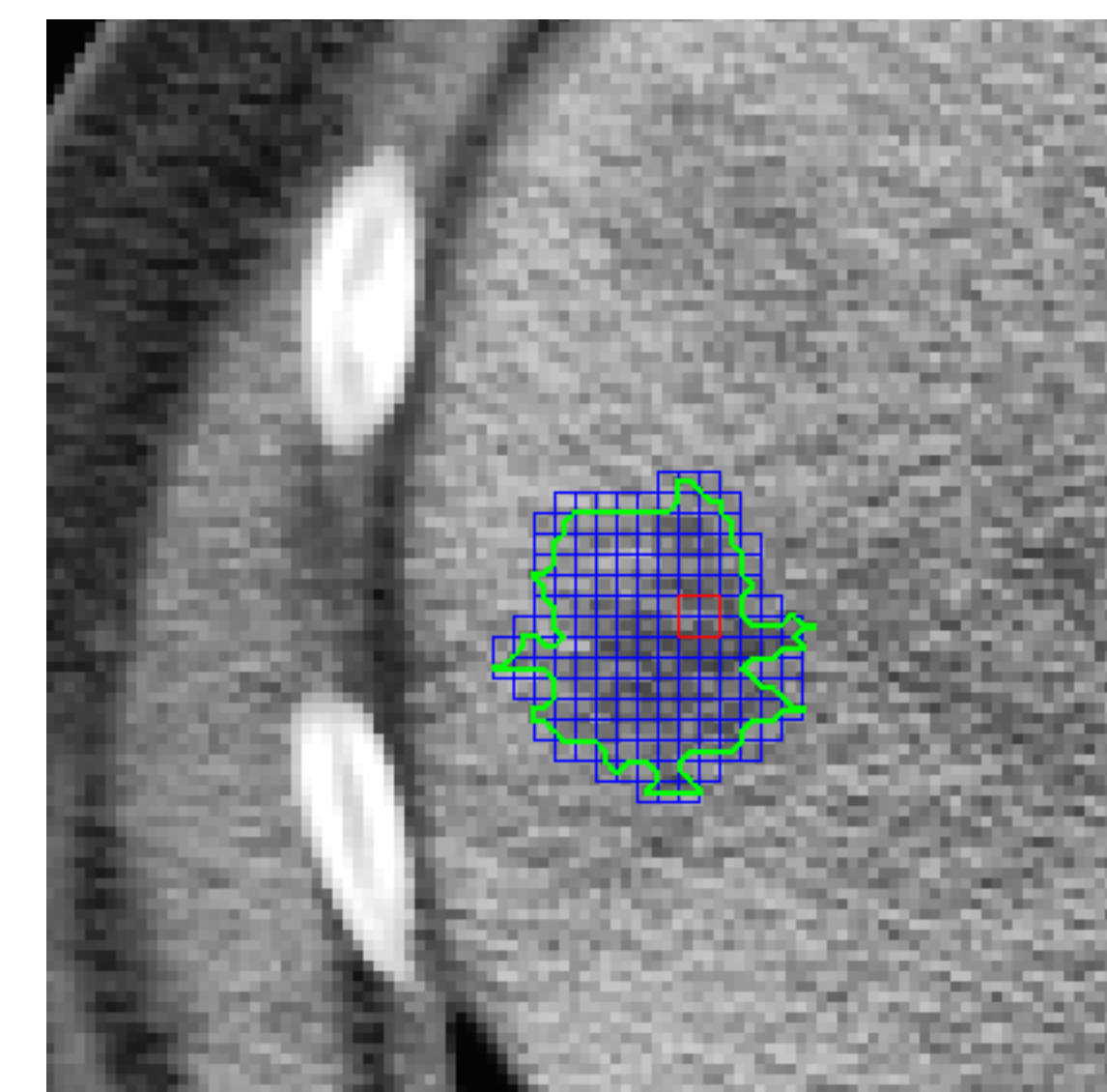# Tools for automatic tumor assessment

Input un-annotated images

Automatic Segmentation

### Computation of features

1) **Lesion tracking: Identify same lesions at different time points**

2) **Automated RECIST summary of lesions and treatment response**

3) **Discover new quantitative imaging biomarkers of cancer response by correlating them with clinical covariates (e.g., overall survival)**
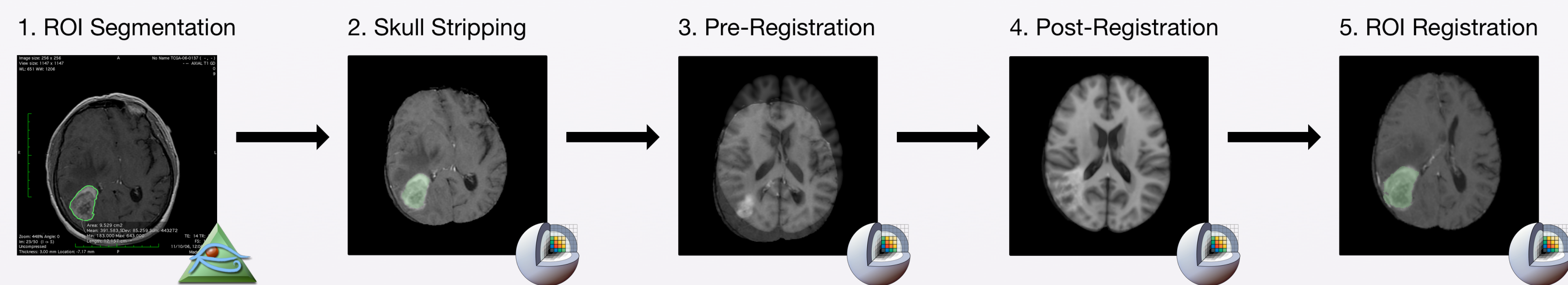
Automated computational identification of anatomical tumor location associated with survival in two large cohorts of human primary glioblasotmas
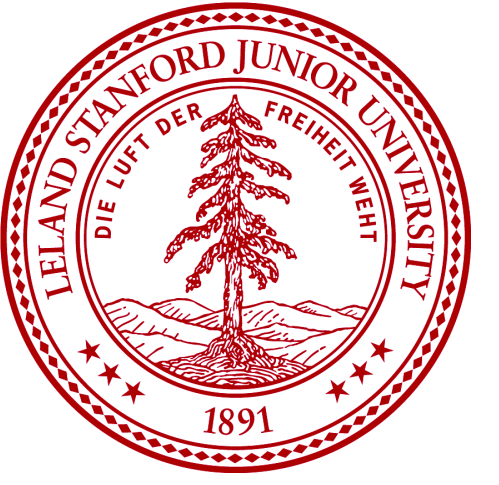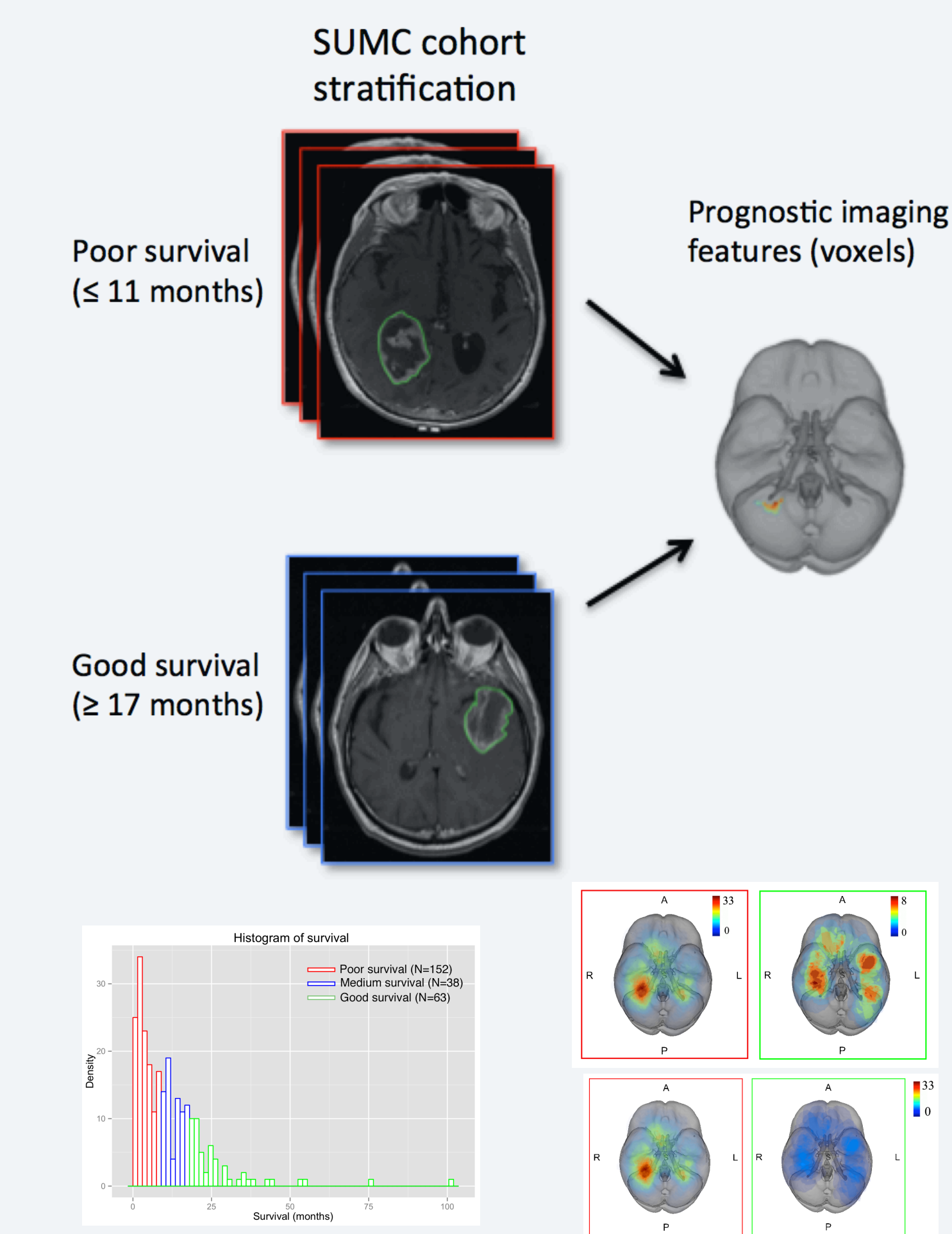
Tiffany Ting Liu[1,2], Achal S. Achrol[3,4,5], Lex A. Mitchell[2], William Du[2], Joshua J. Loya[5], Scott Rodriguez[5], Abdullah Feroze[5], Josh Stuart[6], Griffith R. Harsh IV[5], Daniel L. Rubin[1,2]
[1]Stanford Center for Biomedical Informatics Research and Biomedical Informatics Training Program; [2]Department of Radiology; [3]Stanford Institute for Neuro-Innovation and Translational Neurosciences; [4]Institute for Stem Cell Biology and Regenerative Medicine, and [5]Departments of Neurosurgery, Stanford University Medical Center, Stanford, CA.
[6]Biomolecular Engineering, UC Santa Cruz, Santa Cruz, CA
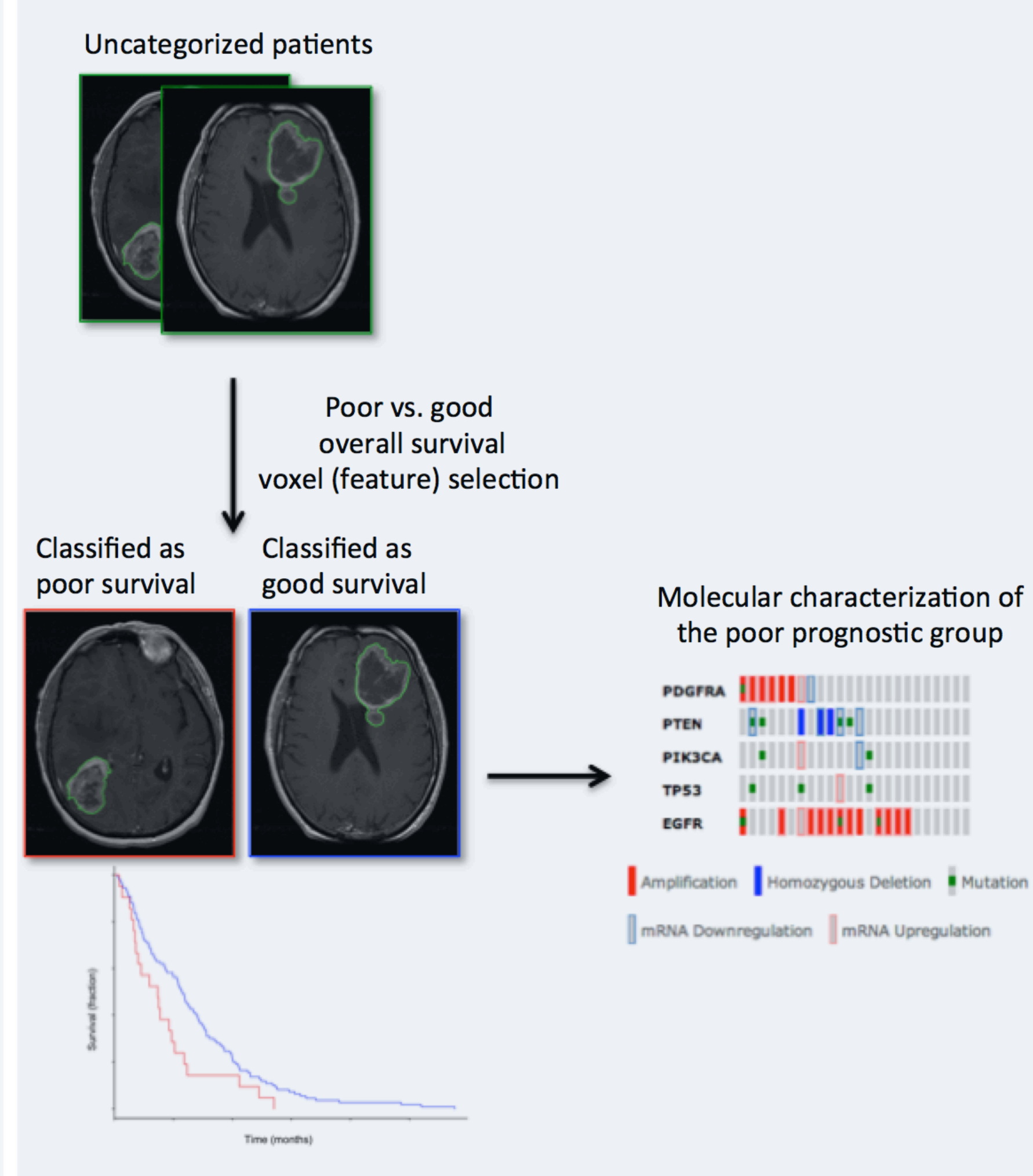
Overview analysis workflow

Figure 1. (a) Automated image processing pipeline

1. ROI Segmentation → 2. Skull Stripping → 3. Pre-Registration → 4. Post-Registration → 5. ROI Registration

(b) Algorithm training on SUMC cohort

SUMC cohort stratification

Poor survival (≤ 11 months)

Good survival (≥ 17 months)

Prognostic imaging features (voxels)

(c) Algorithm validation using TCGA cohort

Uncategorized patients

Classified as poor survival

Classified as good survival

Poor vs. good overall survival voxel (feature) selection

Molecular characterization of the poor prognostic group

PDGFRA
PTEN
PIK3CA
TP53
EGFR

Amplification | Homozygous Deletion | Mutation
mRNA Downregulation | mRNA Upregulation

Methods

Anatomical structures associated with poor survival

Statistical analysis to identify area of differential involvement (ADIFFI) consisted of first constructing a contingency table comparing 2 differential phenotypes (e.g. poor survival versus good survival) and presence of tumor versus no tumor involvement for each image voxel with a 2-tailed Fisher exact test performed on a voxel wise basis.

Permutations with the threshold-free cluster enhancement (TFCE) method previously described were applied to correct for multiple comparisons and a family-wise error rate to ensure an FDR < 0.05.

Results

Univariate and multivariate cox analysis of clinical variables in the training data set. Numbers in parentheses are 95% confidence intervals. GTR: gross total resection; STR: subtotal resection

	Univariate cox		Multivariate cox	
	HR (95% CI)	p-value	HR (95% CI)	p-value
Age	1.02 (1.007, 1.03)	0.00093	1.02 (1.01, 1.03)	0.001
Gender	0.93 (0.72, 1.20) (M)	0.567	-	-
Multicentric/Solitary	0.46 (0.33, 0.64) (S)	2.37e-06	0.66 (0.47, 0.93) (S)	0.019
CEL tumor volume	1.001 (0.997, 1.006)	0.58	-	-
Surgical resection	0.1992 (0.1378, 0.2880) (GTR) 0.4991 (0.3731, 0.6675) (STR)	1.11e-16	0.22 (0.15, 0.32) (GTR) 0.56 (0.41, 0.76) (STR)	5.88e-15 (GTR) 0.000254 (STR)

Fig. 2. Axial, sagittal and coronal slice views of the region associated with poor survival in the training SUMC cohort (p-value < 0.05)
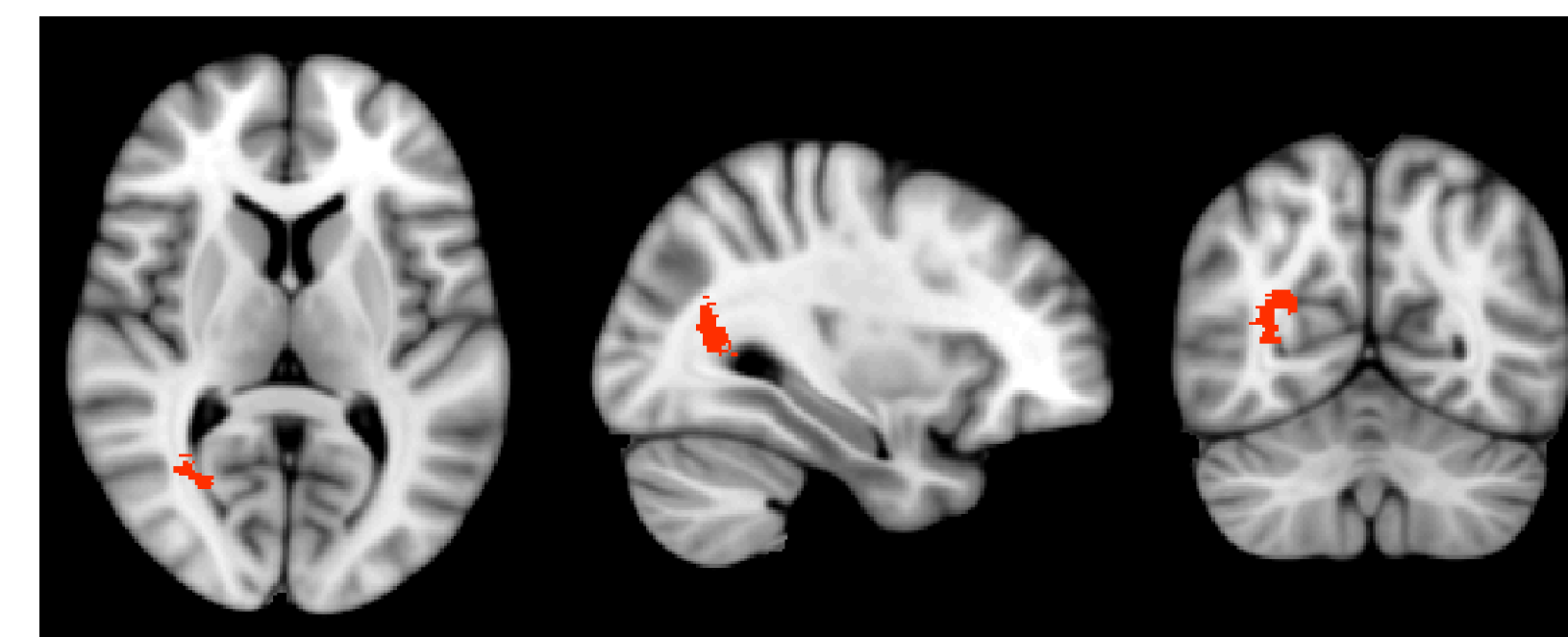

Cerebrum	Lobe	Gyrus	Tissue and cell type	% Significant voxels
Right	Temporal	Sub-gyral	White matter	41.1
Right	Sub-lobar	Lateral ventricle	Cerebro-Spinal Fluid	30.7
Right	Sub-lobar	Extra-nuclear	White matter	11.3
Right	Limbic	Posterior Cingulate	White matter	10.5
Right	Occipital	Sub-Gyral	White Matter	4.7

Fig. 3. Kaplan-Meier survival curves of patients with GBMs depict decreased overall survival in patients with an overlap (Group I) vs. non-overlap (Group II) with the prognostic voxels identified from the training data set (log-rank test p = 0.0341) in the test TCGA cohort
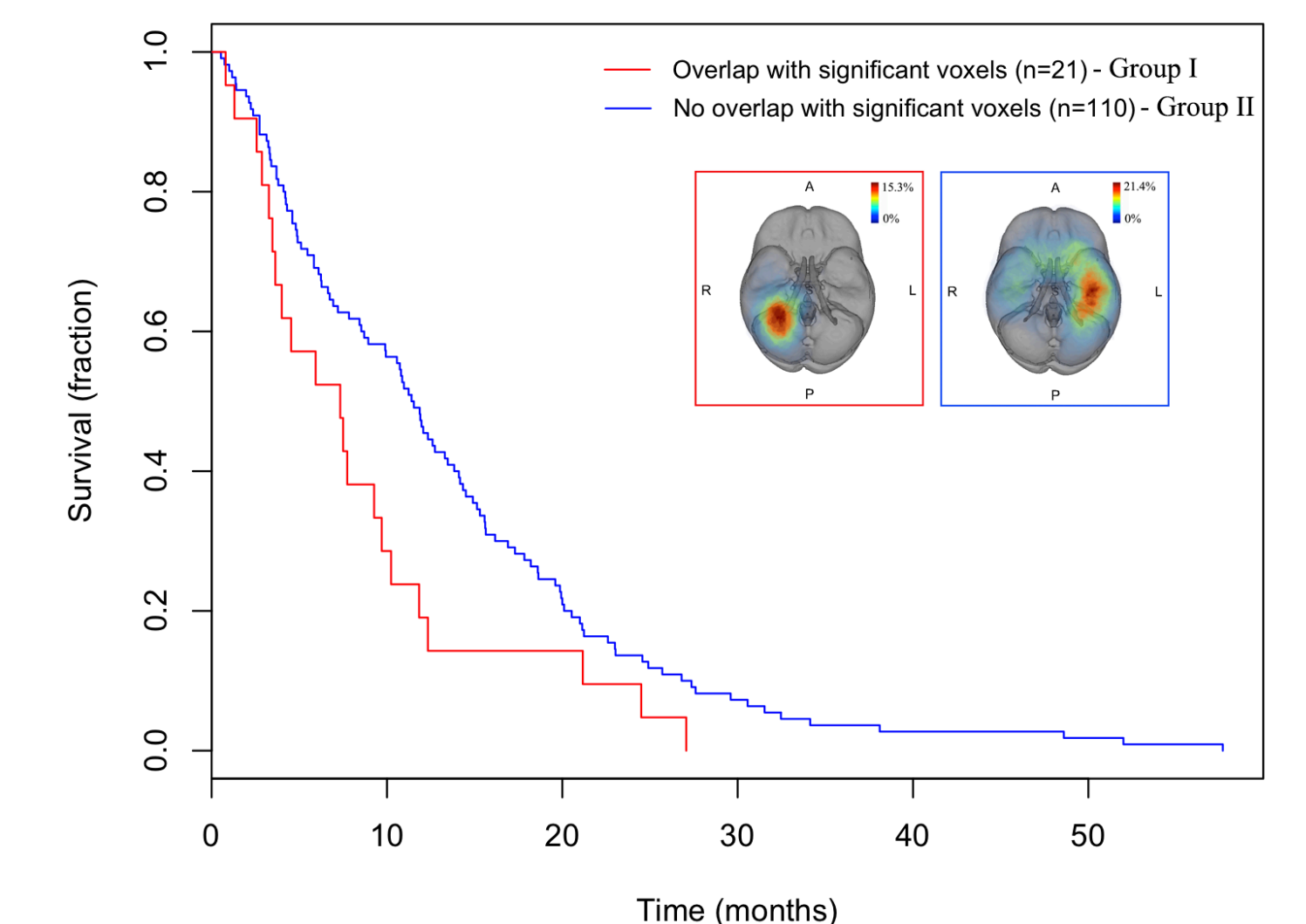
Molecular characterization of the poor prognostic group

	Molecular Subtypes					
	G-CIMP	Non-GCIMP Proneural	Neural	Classical	Mesenchymal	Total
Group I – overlapping	0	7	2	5	6	20
Group II – non-overlapping	4	22	21	25	31	103
% in molecular subtype	0	24.1	8.7	16.7	16.2	16.3

Early neural differentiation module
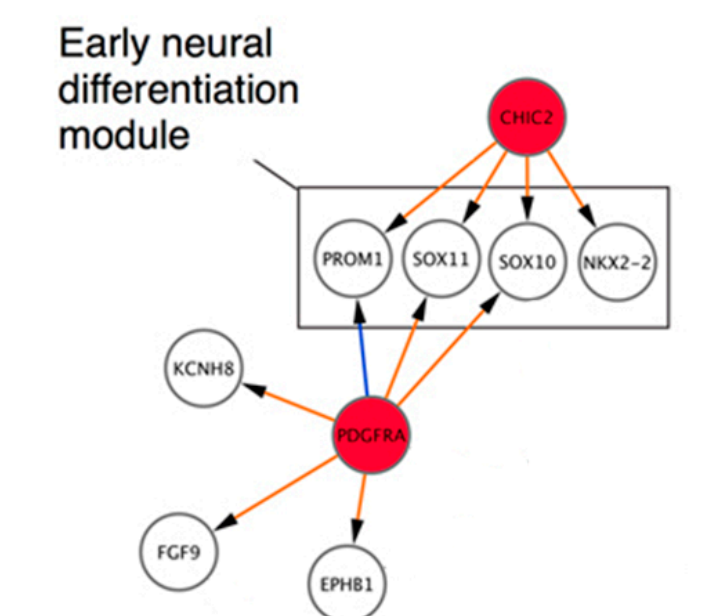
SAMR analysis comparing Group I (overlap with prognostic region) and Group II (no overlap) identified genes amplified in Group I enriched in neural stem cell processes (platelet-derived growth factor receptor-alpha signaling pathway)

Gene ID	Gene name	FDR q-value	Chrom – Pos	GO functional enrichment/literature citations
GSX2	GS homeobox 2	0	-	Forebrain dorsal/ventral pattern formation; neuron fate specification(1)
CHIC2	Cysteine-rich hydrophobic domain 2	0	4	CHIC2 and PDGFR regulate GBM stem cell markers and other neural differentiation markers(2)
RPL21P44	ribosomal protein L21 pseudogene 44	0	-	-
KIT	Mast/stem cell growth factor receptor Kit	0	4	LNX1 and KIT amplification has been shown experimentally in CNS tumors (3)
PDGFRA	platelet-derived growth factor receptor, alpha polypeptide	0	4	PDGFRA and KIT are commonly amplified in GBM(4, 5)

Understanding the Temporal Trends of Breast Cancer Incidence in the United States: a Novel Approach to address Identifiability in Age-Period-Cohort models.

Diego F. Munoz, Sylvia K. Plevritis

iSiS
Information Sciences
in Imaging at Stanford

OBJECTIVES

To develop an age-period cohort model $(\mathcal{APC})$[1,2,3]:

$$\log \lambda(a,p,c,i) = \mu + \rho(i) + \alpha(a) + \pi(p) + \gamma(c)$$
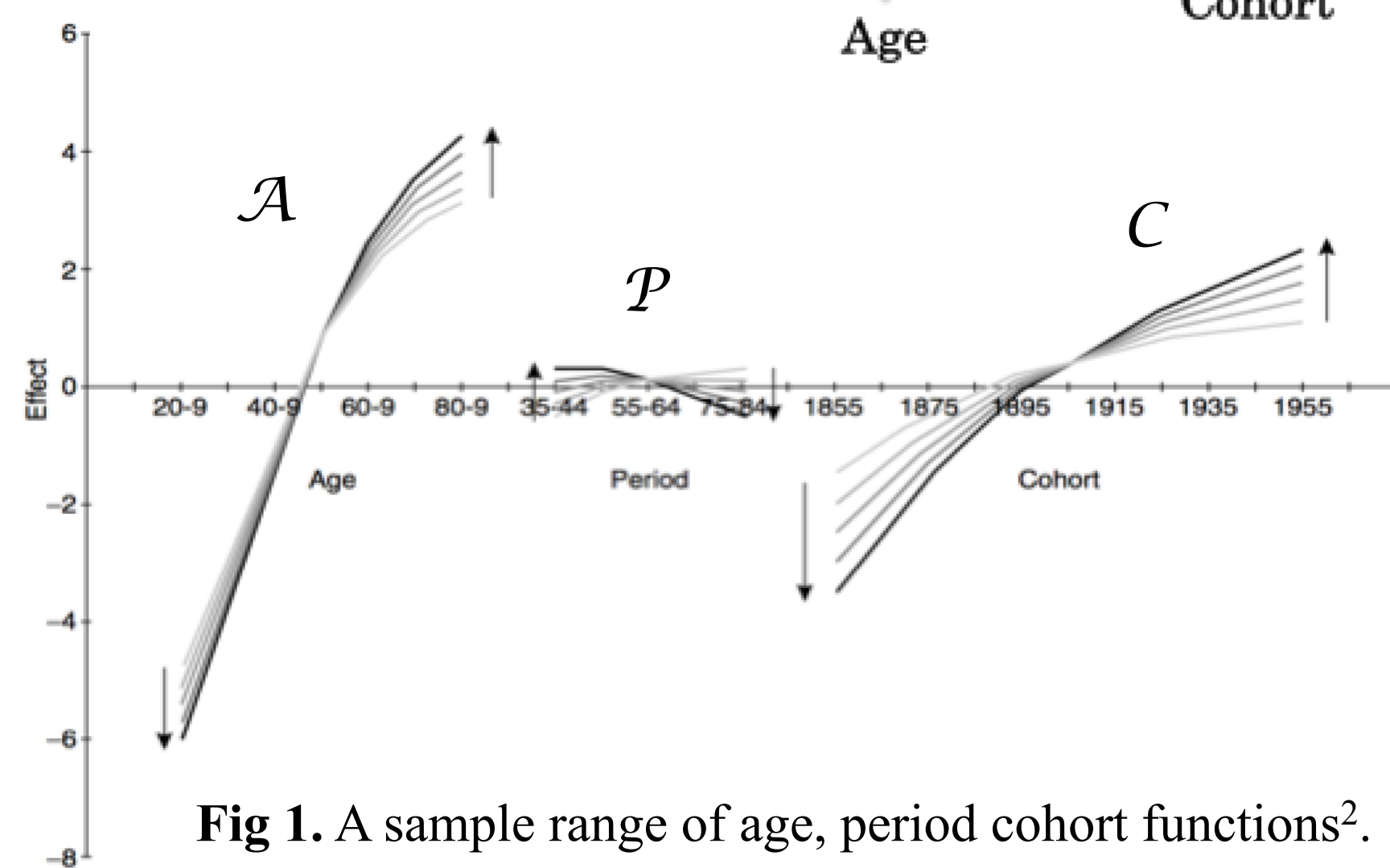
Age | Period | Cohort

Fig 1. A sample range of age, period cohort functions[2].

that accounts for the effects of screening mammography (SCR) and menopausal hormonal therapy (MHT) using breast cancer incidence data from SEER registries.
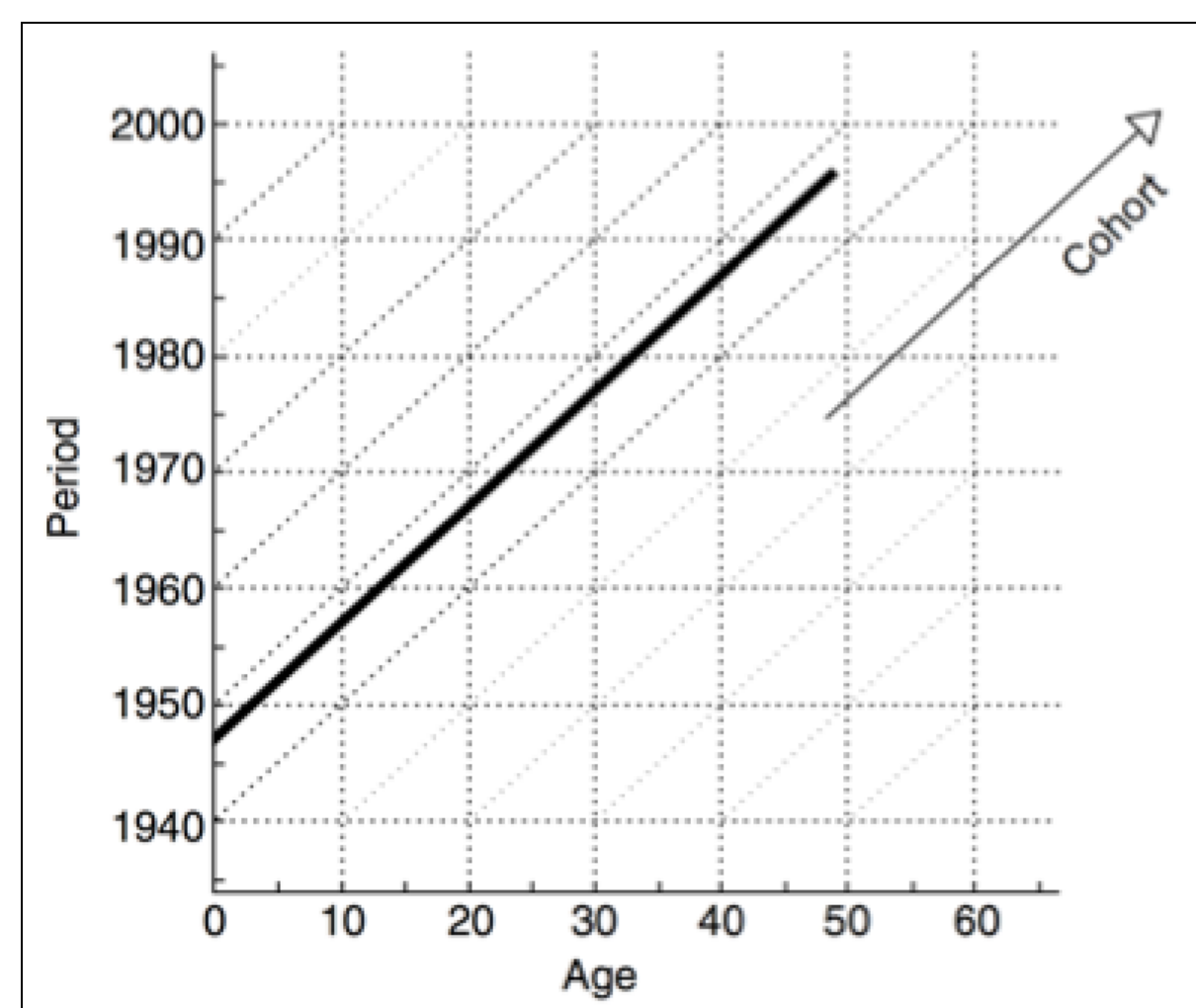
METHODS

APC model's identifiability problem:

Fig 2. Lexis diagram showing age, period, cohort relationship

Since: $c = p - a$

there is over-parameterization from the linear dependence of the parameters. Hence, the system cannot be uniquely and simultaneously estimated!!

Prior approaches to handle identifiability problem:

1. Add age-dependent constraints to the period and cohort effects specific to the problem[3].

2. Fit model assuming cohort or period effect to be zero on average with zero slope ($\mathcal{AC}$-$\mathcal{P}$ or $\mathcal{AP}$-$\mathcal{C}$ model, respectively)[4].
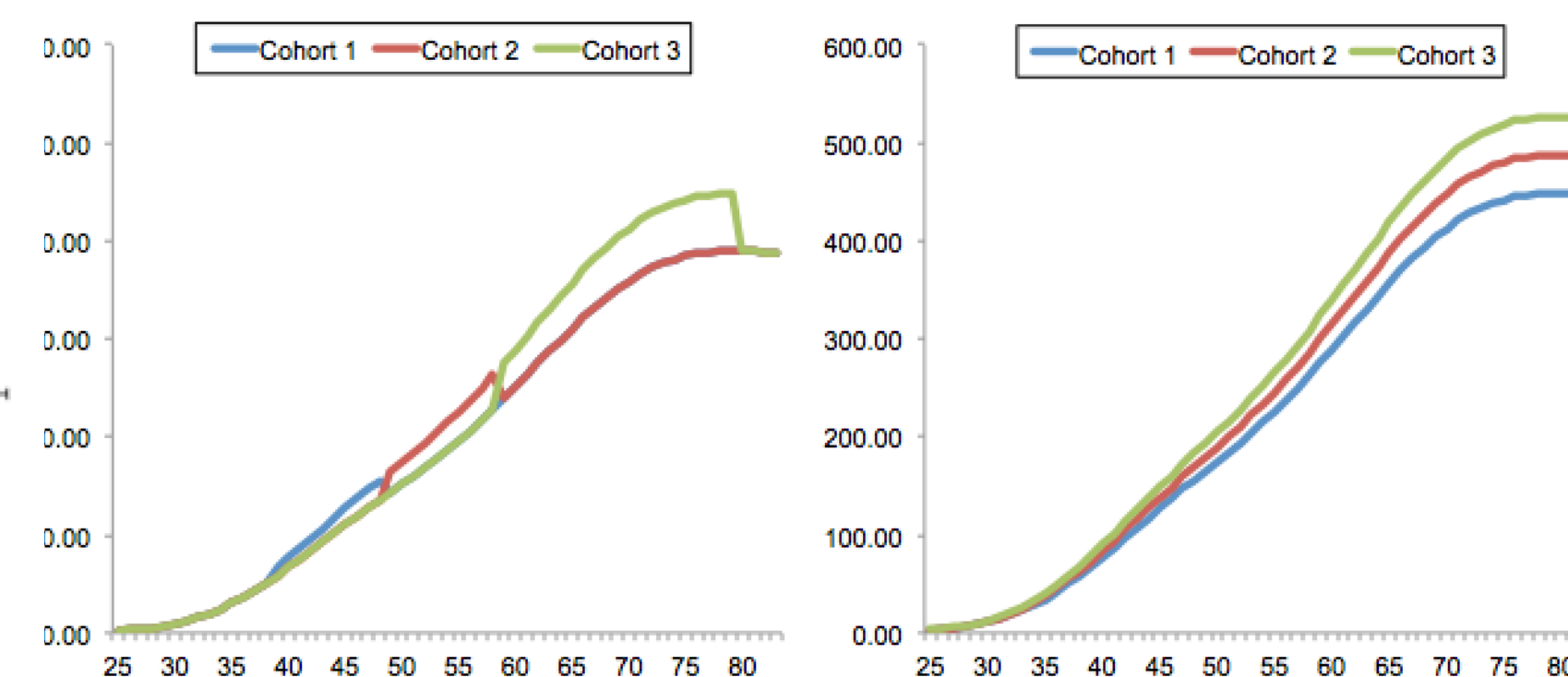

Fig 3. AP-C model with zero cohort effects (left panel)
AC-P model with zero period effects (right panel)

We present a novel approach to estimate temporal factors in breast cancer incidence by explicitly considering the effects of SCR and MHT.
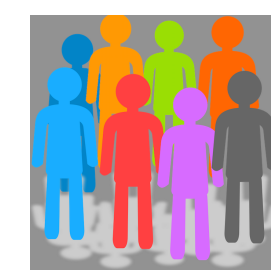
Let:

$$\mathcal{P} = \mathcal{P}_{SCR} + \mathcal{P}_{MHT} + \mathcal{P}_O$$
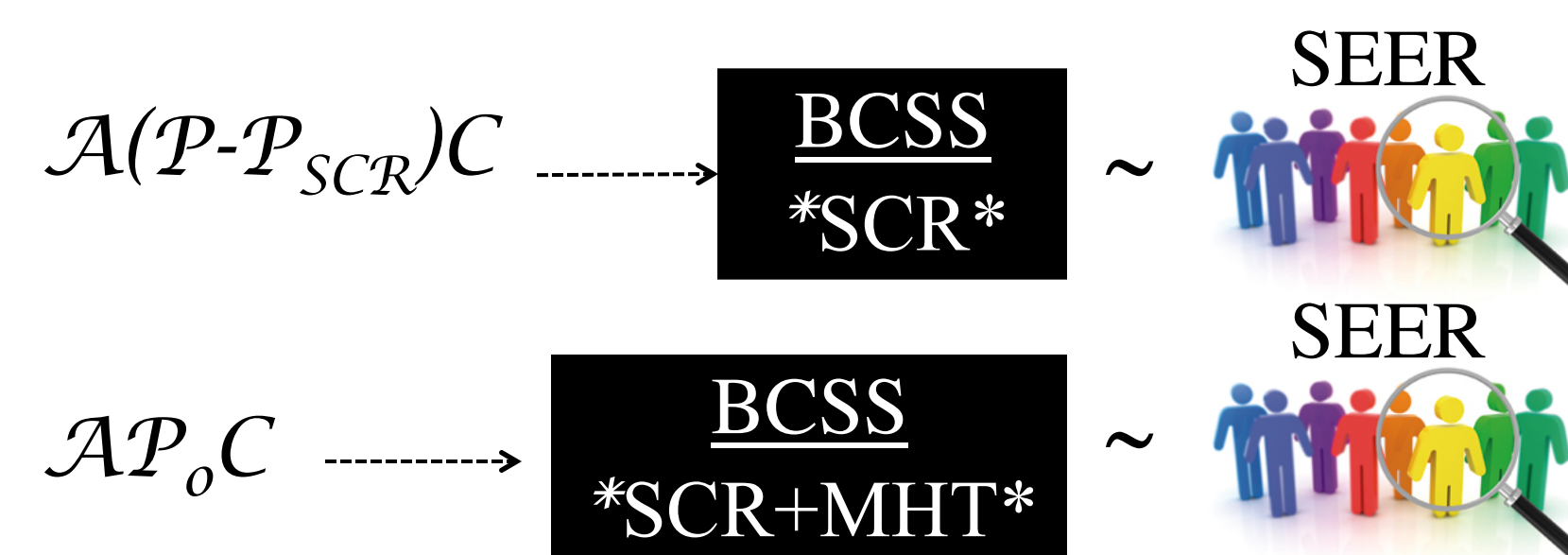
where $\mathcal{P}_O$ refers to all other period effects (non SCR or MHT).

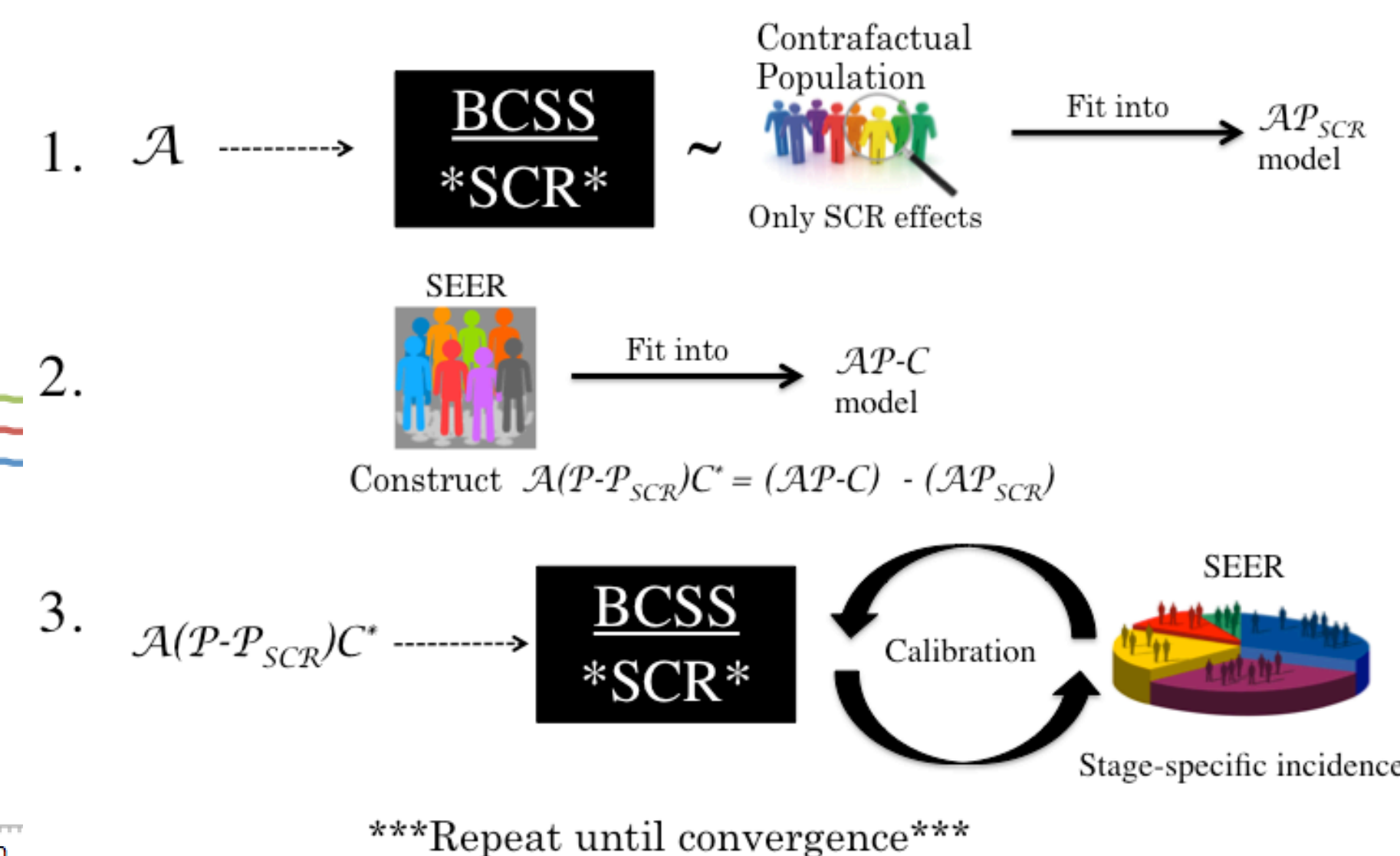And:

$$\mathcal{APC} \sim SEER$$

We use the previously developed Breast Cancer Screening Simulator (BCSS)[5] capable of reproducing SEER trends by modeling the effects of SCR and/or MHT.
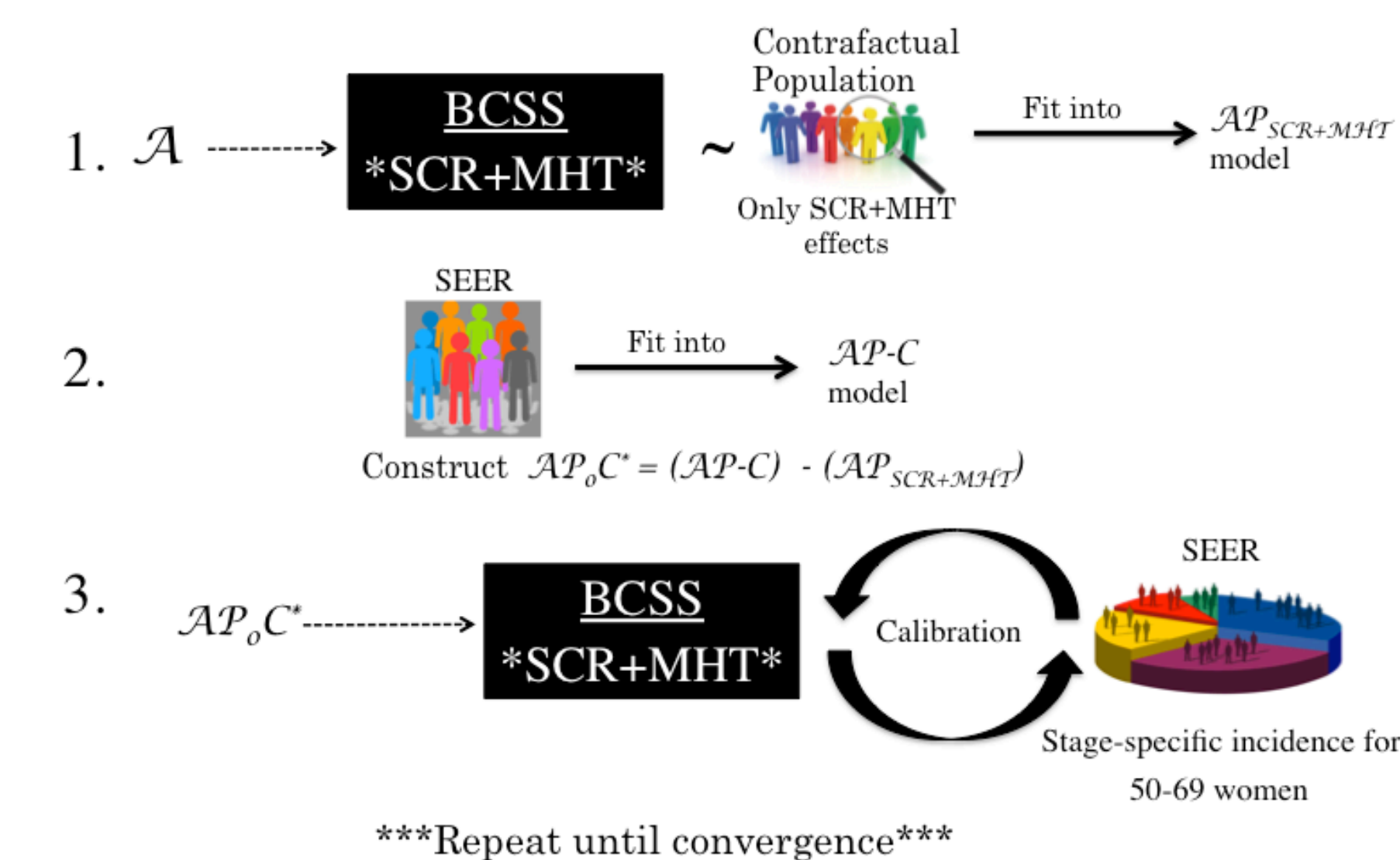
$$\mathcal{A}(\mathcal{P}\text{-}\mathcal{P}_{SCR})C \dashrightarrow \boxed{\text{BCSS *SCR*}} \sim SEER$$

$$\mathcal{AP}_oC \dashrightarrow \boxed{\text{BCSS *SCR+MHT*}} \sim SEER$$

By leveraging on this model, we estimate the individual temporal components iteratively.
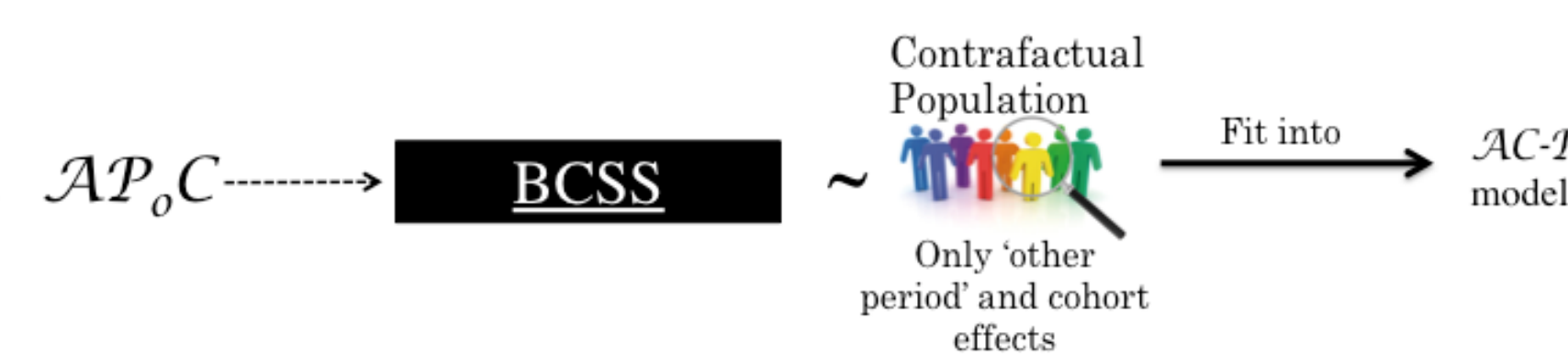

Estimating the effect of screening mammography (SCR)

1. $\mathcal{A} \dashrightarrow \boxed{\text{BCSS *SCR*}} \sim$ Contrafactual Population → Fit into $\mathcal{AP}_{SCR}$ model (Only SCR effects)

2. SEER → Fit into $\mathcal{AP\text{-}C}$ model
Construct $\mathcal{A}(P\text{-}P_{SCR})C^* = (\mathcal{AP\text{-}C}) - (\mathcal{AP}_{SCR})$

3. $\mathcal{A}(P\text{-}P_{SCR})C^* \dashrightarrow \boxed{\text{BCSS *SCR*}} \rightleftarrows$ Calibration → SEER, Stage-specific incidence

Repeat until convergence

Estimating the effect of menopausal therapy hormonal

1. $\mathcal{A} \dashrightarrow \boxed{\text{BCSS *SCR+MHT*}} \sim$ Contrafactual Population → Fit into $\mathcal{AP}_{SCR+MHT}$ model (Only SCR+MHT effects)

2. SEER → Fit into $\mathcal{AP\text{-}C}$ model
Construct $\mathcal{AP}_oC^* = (\mathcal{AP\text{-}C}) - (\mathcal{AP}_{SCR+MHT})$

3. $\mathcal{AP}_oC^* \dashrightarrow \boxed{\text{BCSS *SCR+MHT*}} \rightleftarrows$ Calibration → SEER, Stage-specific incidence for 50-69 women

Repeat until convergence

Estimating the 'others' period and cohort effects

Using the $\mathcal{AP}_oC$ derived from prior steps:

$$\mathcal{AP}_oC \dashrightarrow \boxed{\text{BCSS}} \sim \text{Contrafactual Population} \rightarrow \text{Fit into } \mathcal{AC\text{-}P} \text{ model (Only 'other period' and cohort effects)}$$

With this procedure, we re-allocate residual period into cohort effects.

RESULTS

Legend: 1891–1895, 1896–1900, 1901–1905, 1906–1910, 1911–1915, 1916–1920, 1921–1925, 1926–1930, 1931–1935, 1936–1940, 1941–1945, 1946–1950, 1951–1955, 1956–1960, 1961–1965, 1966–1970, 1971–1975
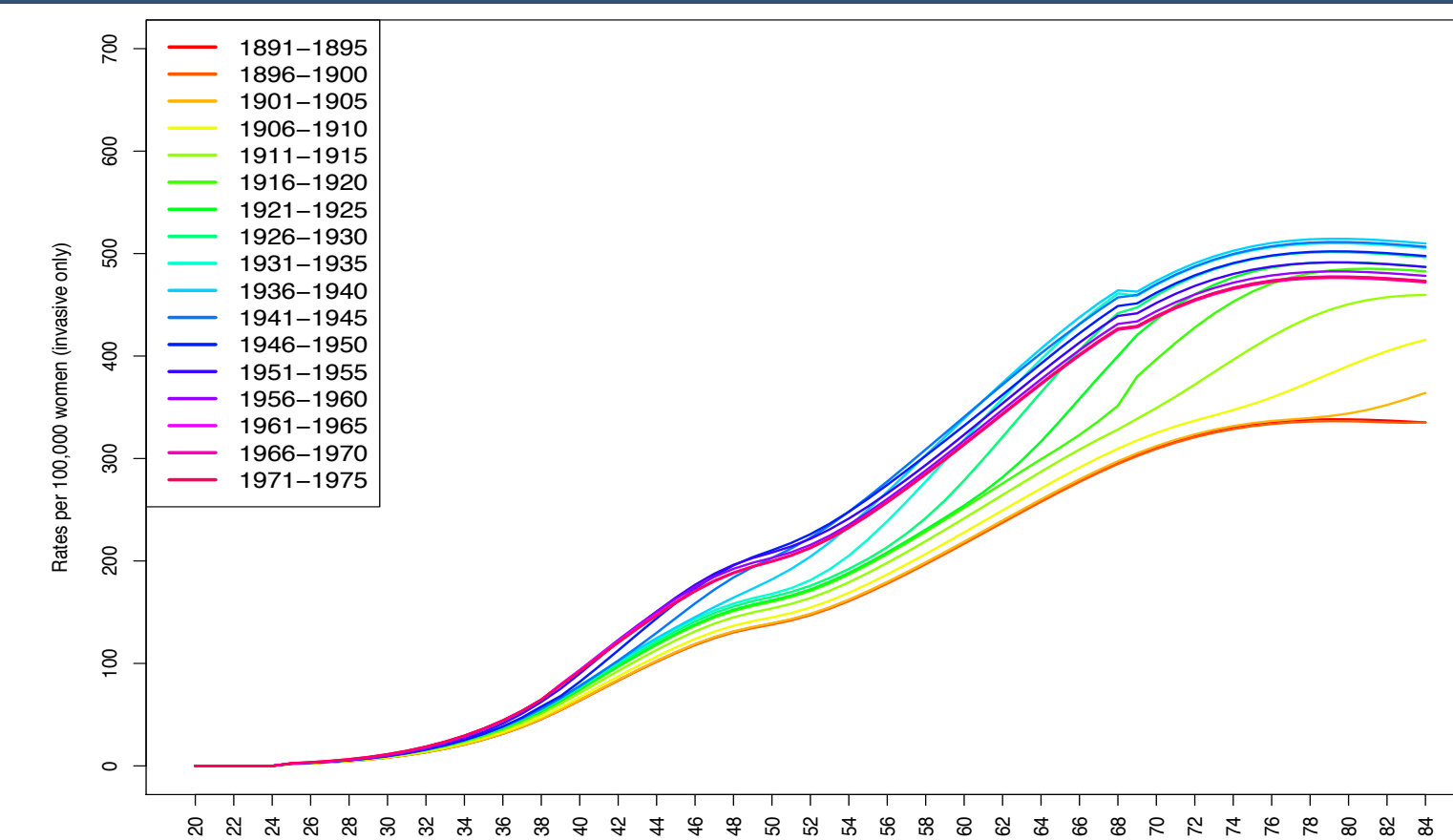
Fig 4. Background breast cancer incidence with no SCR and no MHT effects.

Legend: 1891–1895, 1896–1900, 1901–1905, 1906–1910, 1911–1915, 1916–1920, 1921–1925, 1926–1930, 1931–1935, 1936–1940, 1941–1945, 1946–1950, 1951–1955, 1956–1960, 1961–1965, 1966–1970, 1971–1975
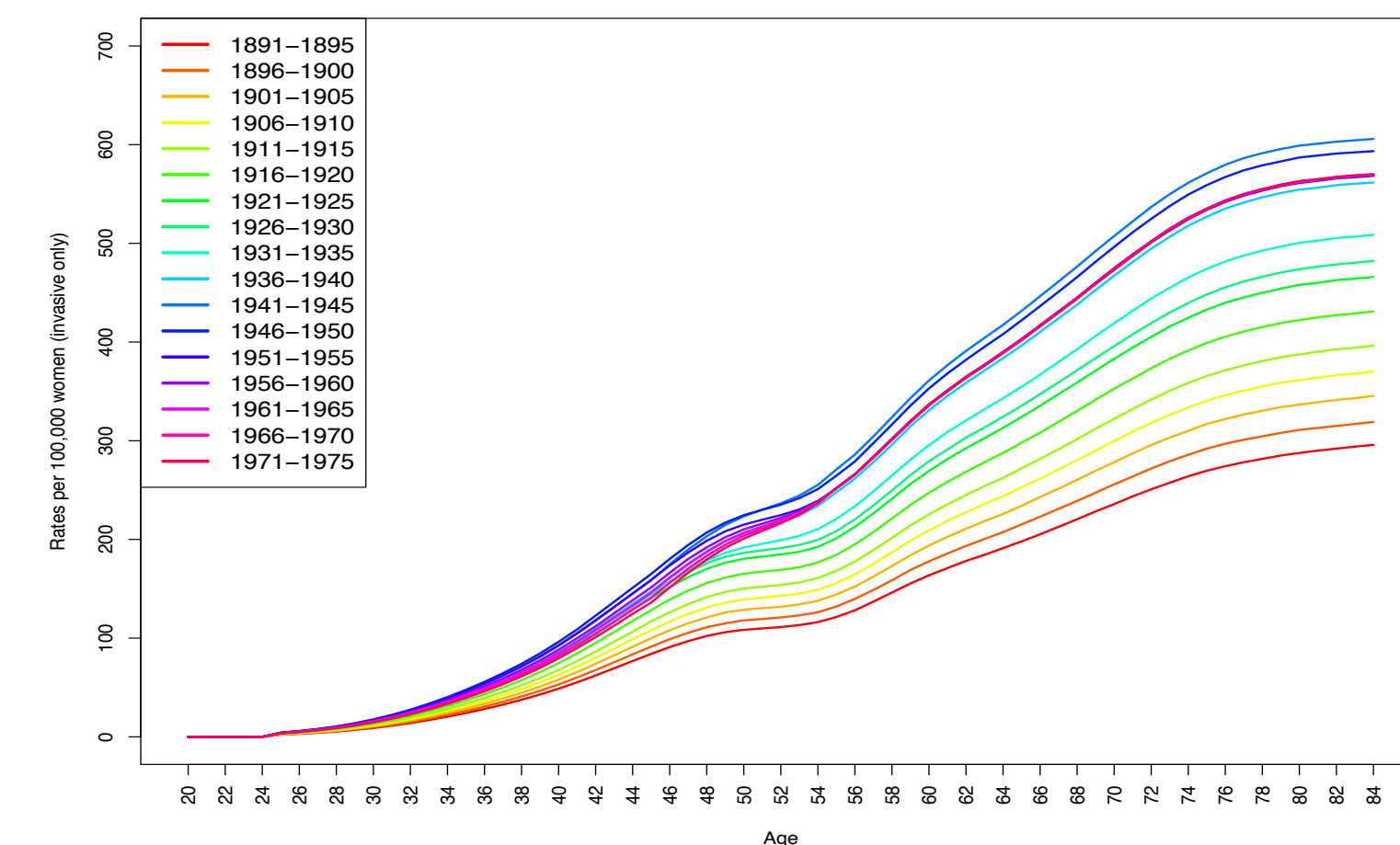
Fig 5. Holford's Background breast cancer incidence with no SCR effects[3].

Notably lower cohort effect and SCR effects. Our approach produces a residual period effect in younger cohorts that can be associated with increases in age at parity and obesity.

REFERENCES

1. Holford TR. *The estimation of age, period and cohort effects for vital rates*. Biometrics 1983; **39**:311–324.
2. Holford TR. *Age-period-cohort analysis*. In Armitage P, Colton T, editors. Encyclopedia of biostatistics. Chichester: John Wiley & Sons; 1998. pp. 82–99.
3. Holford TR, et. al. *Changing patterns in breast cancer incidence trends*. J Natl Cancer Inst Monogr. 2006(36): 19-25.
4. Carstensen B. *Age period-cohort models for the Lexis Diagram*. Stat Med 2007. Jul 10;26(15) 3018-45.
5. Plevritis, S.K., et al., *A stochastic simulation model of U.S. breast cancer mortality trends from 1975 to 2000*. J Natl Cancer Inst Monogr, 2006(36): p. 86-95.

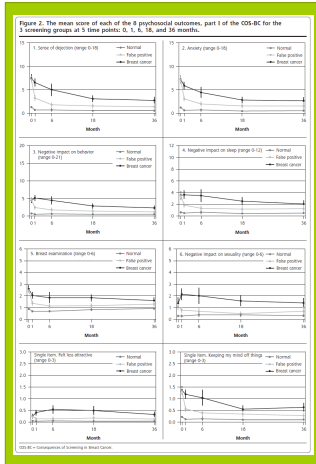# Computer-Aided Diagnosis of Breast Cancer Using Unsupervised Feature Learning

Rebecca L. Sawyer, Daniel Rubin

PROBLEM

Problem: Mammography is subject to reader variability and inaccuracy.

Breast Cancer is the most deadly cancer among women worldwide. Early detection greatly improves chance of survival, but currently only about 20% of biopsied lesions are actually cancerous [1]. This results in:

- Wasted resources
- Unnecessary invasive procedures
- Psychological damage to false positives [2]

Figure 2. The mean score of each of the 8 psychosocial outcomes, part 1 of the COS-BC for the 3 screening groups at 5 time points: 0, 1, 6, 18, and 36 months.

Solution: Computer-Aided Diagnosis (CADx)

Approach: Unsupervised feature learning

Specific Aims

- To develop methods of unsupervised feature learning for quantitative analysis and characterization of breast lesions and dense tissue
- To build a CADx system for decision support in mammography
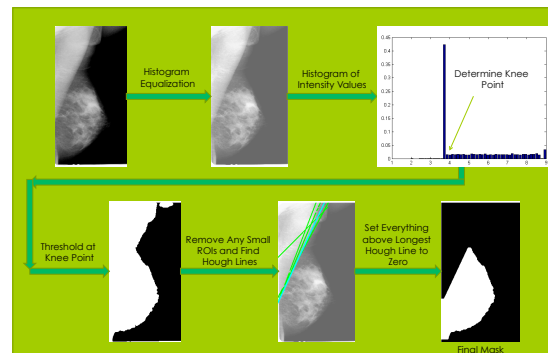- To evaluate accuracy of CADx predictions

Overall goal: To improve positive predictive value of mammography screening.

METHODS

Pipeline
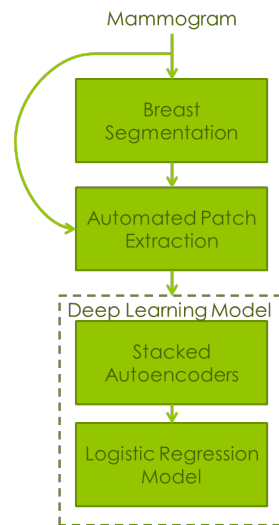
1. Breast and Pectoral Muscle Segmentation
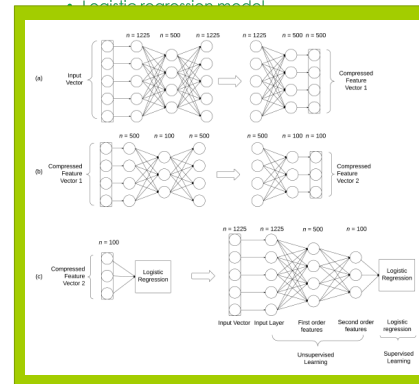

[3-4]

METHODS

2. Automated Patch Extraction

- Extract 10 random patches of 35x35 pixels within the masked area ($completeMask = breastMask \cap ROIMask$) of each training image.
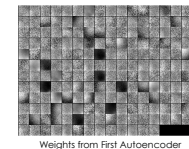- 35x35 patch ➜ 1x1225 feature vector

3. Deep Learning Model

- 2 stacked autoencoders
- Logistic regression model

Greedy Layer-wise Training

1. Train first autoencoder.
2. Train first autoencoder + additional layer.
3. Train (2) + additional layer, etc.
4. Fine-tune entire model.

Weights from First Autoencoder

RESULTS

Data

- DDSM
- Training Set
  - 1228 images (not including mirrored images)
  - 563 masses (355 benign, 208 malignant)
- Test Set
  - 404 images
  - 197 masses (130 benign, 67 malignant)

Analysis

- Hold-out validation
-

REFERENCES

[1] Herndon, Jaime. A Surgical Biopsy for Breast Cancer. Available at: http://www.livestrong.com/article/151292-a-surgical-biopsy-for-breast-cancer/.

[2] Brodersen, John and Siersma, Volkert Dirk. Long-Term Psychosocial Consequences of False-Positive Screening Mammography. Ann Fam Med March/April 2013 vol. 11 no. 2 106-115.

[3] Mirzaalian H, Ahmadzadeh M.R., Sadri S, Jafari M. Pre-processing Algorithms on Digital Mammograms. IAPR Conference on Machine Vision Applications, May 16-18, 2007.

[4] Karssemeijer N. Automated classification of parenchymal patterns in mammograms. Phys. Med. Biol. 43 365. 1998.

[5] Y. Bengio, P. Lamblin, D. Popovici, H. Larochelle et al., Greedy layer-wise training of deep networks, Advances in neural information processing systems, vol. 19, p. 153, 2007.

ACKNOWLEDGEMENTS

For additional information please contact:

Rebecca Sawyer
Biomedical Informatics
Stanford University
rlsawyer@stanford.edu